C.P. No. 435
(18,250)
A.R.C. Technical Report

C.P. No. 435
(18,250)
A.R.C. Technical Report

MINISTRY OF SUPPLY

AERONAUTICAL RESEARCH COUNCIL

CURRENT PAPERS

Preliminary Note on the Effect of Inertia Cross-coupling on Aircraft Response in Rolling Manoeuvres

by

W. J. G. Pinsker

LONDON: HER MAJESTY'S STATIONERY OFFICE

1959

PRICE 12s. 6d. NET

C.P. No.435

U.D.C. No. 533.6.013.153:533.6.013.63:533.6.013.4:

Technical Note No. Aero.2419

November, 1955.

ROYAL AIRCRAFT ESTABLISHMENT

Preliminary note on the effect of inertia cross-coupling on aircraft response in rolling manoeuvres

by

W. J. G. Pinsker

SUMMARY

Results from a systematic series of simulated responses to aileron manoeuvres are discussed. It is shown that large amplitudes in incidence and sideslip can occur on aircraft having large inertias in pitch and yaw when performing quite modest rolling manoeuvres. In general these amplitudes increase progressively with the duration of the rolling manoeuvre and with the incidence of the principal inertia axis. The aircraft response deteriorates rapidly as the rolling velocity approaches a value determined by the natural frequencies of the uncoupled lateral and pitching oscillation of the aircraft.

If the incidence of the principal inertia axis is below a critical value an autorotational rolling state exists towards which an aircraft tends to diverge once it has exceeded a certain critical rolling velocity. For aircraft with large inertia in pitch this critical value can be as low as about 20°/sec. The practical significance of this phenomenon to the pilot is not yet fully understood.

Various alternative schemes of autostabilization have been explored. They require generally very powerful control movements and may not necessarily relieve the tail loads as such.

LIST OF CONTENTS

LIST OF APPENDICES

LIST OF TABLES

LIST OF ILLUSTRATIONS

LIST OF ILLUSTRATIONS (Contd.)

LIST OF ILLUSTRATIONS (Contd.)

LIST OF ILLUSTRATIONS (Contd.)

1 Introduction

Recent flight incidents involving loss of control during rolling manoeuvres on some advanced American supersonic fighter and research aircraft[1] have revealed the existence of a coupled lateral-longitudinal motion which cannot be accounted for by classical stability theory.

Phillips[2] has pointed out that the equations of motion for the rigid aircraft contain product terms which couple the lateral and longitudinal motion of a rolling aircraft if it has extremely large inertias in pitch and yaw. This leads to a system of six simultaneous nonlinear differential equations for which no analytical solution exists. By suitable simplification Phillips has reduced these equations to a linear system and has predicted a combined lateral-longitudinal divergence for rates of roll beyond certain critical "resonance frequencies".

However, this attractively simple approach cannot predict the amplitudes in incidence and sideslip occurring during actual flight manoeuvres and is thus unable to assess the stress produced and the handling limitations of an actual aircraft design. With electronic computing aids it has, however, become possible to obtain solutions for nonlinear equations of motions and in particular to compute responses to aileron manoeuvres for any given aircraft. This has been done on a considerable scale in the U.S.A. without so far revealing sufficiently general criteria though it is indicated that the stability boundaries according to Phillips give a useful indication for the rates of roll, at which difficulties may arise.

In order to obtain a fairly general appreciation of the problem at first hand a series of computations have been undertaken on GEPUS, a general purpose simulator in RAE, which was made available for this investigation. The author wishes to express his gratitude and appreciation for the assistance received from Mr. T.R. Stretton, who suggested the circuit Fig.53 for computing sin and cos ϕ, and his Staff. Without them the results presented in this note could not possibly have been obtained in such a short time. The results of this investigation, which was mainly planned as a preliminary study to a more comprehensive further programme, are presented in this note. In support of this empirical work a theoretical study of the problem was begun in order to explore the possibilities of an analytical solution beyond the determination of the stability of an aircraft rolling with steady rates of roll as given in Ref.2. At the time of writing this theoretical work is still in progress, but as the results obtained to date appear encouraging they will be briefly summarized in Appendices E and F.

For the course of the computations on the simulator a tendency of certain aircraft configurations to develop a divergence in roll was observed - in addition to unstable motions predicted by Phillips - and a theoretical study has proved the existence of autorotational rolling states for aircraft with large inertias if the principal inertia axis is below a certain critical incidence.

Finally the possibilities of pilot's control and automatic stabilisation have been investigated. The equations for the ideal autostabiliser operating on rudder and elevator have been derived.

2 Stability equations

2.1 Euler equations

The Euler equations for the rigid aircraft when referred to a system of cartesian coordinates fixed in the body, (see Ref.3), are:

$$X = mV\left(\frac{\dot{u}}{V} - r\beta + q\alpha\right) \tag{1}$$

$$Y = mV\left(\dot{\beta} - p\alpha + r\right) \tag{2}$$

$$Z = mV\left(\dot{\alpha} - q + p\beta\right) \tag{3}$$

$$L = A\dot{p} - (B - C)\,qr + D\,(r^2 - q^2) - E\,(pq + \dot{r}) + F\,(pr - \dot{q}) \tag{4}$$

$$M = B\dot{q} - (C - A)\,rp + E\,(p^2 - r^2) - F\,(qr + \dot{p}) + D\,(qp - \dot{r}) \tag{5}$$

$$N = C\dot{r} - (A - B)\,pq + F\,(q^2 - p^2) - D\,(rp + \dot{q}) + E\,(rq - \dot{p}) \tag{6}$$

The forces and moments acting on the aircraft X, Y, Z, L, M, and N are aerodynamic gravitational and gyroscopic couples generated by the angular momentum of the engine. In order to introduce the gravity components into the force equations the orientation of the aircraft in the gravitational field had to be computed by the kinematic relations:

$$d\psi/dt = \sec\theta\,\{r\cos\phi + q\sin\phi\} \tag{7}$$

$$d\theta/dt = q\cos\phi - r_B\sin\phi \tag{8}$$

$$d\phi/dt = p_B + \tan\theta\,(r\cos\phi + q\sin\phi)\quad . \tag{9}$$

Stability theory usually employs the concept of small disturbances from an equilibrium state, i.e. the variables p, q, r, u, β, α are assumed small so that the products of the variables in equations (1-6) become small of second order and negligible. This permits the system of six simultaneous differential equations (1-6) to be split into two independent groups, describing the lateral and longitudinal motion separately, if - as is usually permissible - aerodynamic coupling between these as well as the gyroscopic engine couples are assumed negligible.

However, in controlled flight rate of roll, p, at least, cannot generally be assumed small, rates of more than 3 radians/sec constituting quite legitimate manoeuvres, and consequently the products with p in equations (1-6) will have to be considered in the study of general rolling manoeuvres, in particular if the inertia differences (B - A) and (C - A) are large.

2.2 Choice of axes

The system of coordinates normally used in aircraft stability investigations is the so-called, "wind axes" system. This system is a body-fixed system of cartesian coordinates with the origin in the CG whose X axis coincides with the flight path in the equilibrium state. This choice is largely determined by two considerations:

(i) aerodynamic data are generally given in this system;

(ii) the pilot refers the aircraft motion to the flight path and the variables of motion should therefore be expressed as deviation from this natural datum and referred to this datum.

However, equations (1-6) are greatly simplified when referred to principal inertia axes thus eliminating product of inertia terms DEF.

Aerodynamic data must, of course, be transformed to this system of axes, (RAe.C. Data Sheet Aircraft 00.00.06), but such transformation becomes necessary generally when considering motion with large disturbances as the force and moment equations are expressed in body fixed "wind axes" which are true wind axes only for small departures from the equilibrium state, in the sense understood in the usual presentation of aerodynamic derivatives.

2.3 Equations of motion used in the present analysis

The notation used throughout this note is generally that of R & M 1801 with the exception that the angles α and β replace the incremental velocities w and v .

Principal inertia axes are used, thus product of inertias

$$D = E = F = 0 \quad .$$

In the theoretical analysis linear aerodynamic derivatives are assumed throughout and gravity is neglected. Further as shown in Fig.1:

$\Delta\alpha$ = incremental incidence

$\alpha = \alpha_o + \Delta\alpha$ = incidence of principal inertia axis

α_o = incidence of the principal inertia axis in equilibrium flight.

Forward speed is assumed constant eliminating the X-Force equation. Thus equations (2-6) become:

$$\frac{1}{mV}\left\{Y_\beta\beta + Y_r r + Y_p p\right\} = \dot{\beta} - p\,(\alpha_o + \Delta\alpha) + r \qquad (10)$$

$$\frac{1}{mV}\left\{Z_\alpha\Delta\alpha + Z_q q + Z_{\dot{\alpha}}\dot{\alpha}\right\} = \dot{\alpha} - q + p\beta \qquad (11)$$

$$L_\xi\xi + L_\beta\beta + L_p p + L_r r = A\dot{p} - (B - C)\,qr \qquad (12)$$

$$M_\eta\eta + M_\alpha\Delta\alpha + M_{\dot{\alpha}}\dot{\alpha} + M_q q = B\dot{q} - (C - A)\,rp \qquad (13)$$

$$N_\xi\xi + N_\zeta\zeta + N_\beta\beta + N_p p + N_r r = C\dot{r} - (A - B)\,pq \quad . \qquad (14)$$

On the simulator gravity was also represented and the most marked linear variations of the lateral derivatives with incidence where considered in the form e.g.:

$$L_\beta = L_{\beta_o} + \frac{dL_\beta}{d\alpha}\,\alpha = L_{\beta_o} + L_{\beta\,\alpha}\alpha \qquad (15)$$

where L_{β_o} is the value for L_β at a flight attitude where the incidence α of the principal axis would be zero. In this form the simulator computed automatically the changes of these derivatives with C_L.

With these terms the equations of motion used in the present series of simulations (rudder ζ and elevator η assumed fixed) where:

$$\frac{1}{mV}\left\{Y_\beta\beta + Y_r r + Y_p p\right\} - \frac{g}{V}\sin\phi - r + p\alpha_o = \dot{\beta} \qquad (16)$$

$$\frac{1}{mV}\left\{Z_\alpha\Delta\alpha + Z_q q + Z_{\dot{\alpha}}\dot{\alpha}\right\} - \frac{g}{V}(1 - \cos\phi) + q - p\beta = \dot{\alpha} \qquad (17)$$

$$L_\xi\xi + L_\beta\beta + L_{\beta\alpha}\,\alpha\beta + L_p p + L_r r + (B - C)\,qr = A\dot{p} \qquad (18)$$

$$M_\alpha\Delta\alpha + M_{\dot{\alpha}}\dot{\alpha} + M_q q + (C - A)\,rp = B\dot{q} \qquad (19)$$

$$N_{\xi\alpha}\xi\alpha + N_\beta\beta + N_{p_o}p + N_{p\alpha}p\alpha + N_r r + (A - B)\,pq = C\dot{r}\ . \qquad (20)$$

As gravity has been generally found to be of secondary importance its representation has been simplified to the above form by assuming θ to be small so that the kinematic relation equation (9) can be reduced to:

$$\phi = \int p\,dt\ . \qquad (21)$$

3 Brief discussion of existing work

3.1 Flight evidence

The present investigation has been prompted by a number of flight incidents involving loss of control reported from the U.S.A.[1] where large amplitudes in α and β have occurred on some occasions when advanced high speed aircraft executed prolonged rolling or rolling pull out manoeuvres in a flight condition where otherwise satisfactory stability characteristics exist. As an example a typical manoeuvre as recorded in flight is shown in Fig.2. It was found that this type of instability could be related

to a critical rolling velocity and that in general the magnitude of the divergence of the aircraft in α and β increases progressively with the duration of the manoeuvre and also in proportion to the load factor applied during the manoeuvre.

Simulator computations were carried out in many instances in support of this flight work. These have proved conclusively that the observed flight phenomena can be satisfactorily explained by the effects of the product terms in the Euler-equations.

Although recorded evidence of flight incidences or inertia cross-coupling is only available from very recent cases, there is no reason to assume that isolated cases of inertia cross-coupled instability have not happened before.

Based on flight experience pilots have also been advised to refrain from recovery action with rudder and elevator and to bring ailerons gently back to neutral once rolling instability is experienced. It should be noted that the terms instability and divergence are used here loosely to describe the occurrence of large peak values during a manoeuvre though it is not necessarily the result of instability of motion in the strict sense of the word.

3.2 Theory

Considering stability for constant values of rate of roll $p = p_o$ in Ref.2 the system of differential equations (10-14) has been linearised and as p is now a parameter the rolling moment equation (12) becomes redundant. The remaining four simultaneous differential equations have a quartic as the characteristic equation which is reduced to a biquadratic if all the damping terms are neglected, as shown in Appendix D. The solution given there in equation (D.11) is identical to that given by Phillips in Ref.2, but written in the notation adopted for this note. When damping is neglected the solution depends on the two uncoupled angular frequencies of the aircraft in yaw and in pitch

$$\omega_\psi = \sqrt{N_\beta / C} \qquad (22)$$

$$\omega_\theta = \sqrt{-M_\alpha / B} \qquad (23)$$

on p_o and on the ratio of the inertias A/B. For $A/B = 0$ this solution has been computed and plotted in Fig.3 against $(\omega_\theta / p_o)^2$ and $(\omega_\psi / p_o)^2$. The major region in the upper right hand corner represents stable motion with two neutrally stable oscillatory modes with the frequencies ω_1 and ω_2. As p_o increases, or either of the two uncoupled frequencies, i.e. m_w and n_v are reduced, one of the two oscillatory modes degenerates into a divergence. The stability boundaries are indicated in Fig.3 and show that the motion is stable if

$$p_o < \omega_\psi \quad \text{and} \quad p_o < \omega_\theta \ .$$

For very large values of p_o, i.e. if

$$p_o > \omega_\psi \quad \text{and} \quad p_o > \omega_\theta$$

the motion becomes again stable as indicated by the hatched region in Fig.3.

These boundaries apply for an aircraft with inertia in roll (A) small when compared with inertia in pitch and for negligible damping in pitch and in yaw. Generally with $A \neq 0$ but inertias concentrated in one plane, i.e. $C = B + A$ and negligible damping the two stability boundaries will lie at

$$\left(\frac{\omega_\theta}{p_o}\right)^2 = 1.0 \quad \text{and} \quad \left(\frac{\omega_{\psi o}}{p_o}\right)^2 = 1 = \left(\frac{\omega_\psi}{p_o}\right)^2 \frac{B + A}{B - A} \tag{24}$$

as shown in Fig.4. For increasing inertia in roll when compared with inertia in pitch the stability boundary in ω_ψ is moved towards the origin, with which it will coincide if $A = B$, but the aircraft will still be unstable for $p > \omega_\theta$.

The effect of damping in yaw and/or in pitch on the stability boundaries is shown schematically in Fig.5. The two stable regions are now connected by a trough and an aircraft with $\frac{\omega_\theta}{\omega_{\psi_o}} \approx 1.0$ should be stable for all values of p.

4 Phillips criterion and design trends

Following the work described in the previous section, Phillips has suggested as the primary stability criterion

$$p < \sqrt{\frac{N_\beta}{B - A}} = \omega_{\psi_o} \quad . \tag{25}$$

Though the adequacy of this expression as a reliable criterion may be disputed, it is useful for demonstrating the design trends which have led to the advent of the divergence in rolling manoeuvres in some present designs and to assess future developments.

For this purpose equation (25) will be rewritten

$$p^2 < \frac{n_v}{i_B\left(1 - \frac{A}{B}\right)} \frac{V_i^2}{W/S \; b/2} \; 0.0765 \quad . \tag{26}$$

This discloses readily the four principal features which combine to lower the critical rate of roll into the range required in normal aircraft handling, say below 3 radians/sec:

(i) increasing wing loading,

(ii) i_B, which in this note is referred to semispan $b/2$, increases as fuselages become more elongated and loads are distributed more evenly over the full volume of the fuselage.

(iii) A/B, i.e. the ratio between inertia in roll and in pitch decreases with the reduction in wing span in relation to the fuselage length and in general for the reasons quoted under (ii).

For a typical World War II fighter A/B was of the order of 0.8 whereas with modern supersonic projects ratios of $1/5$ and less are commonplace. It should be noted, however, that increasing inertia in roll will not necessarily be the ideal remedy, as it might easily create difficulties in basic aileron control as shown in Ref.4.

(iv) Increases in operational height will allow the achievement of high rates of roll at low indicated speed, i.e. at a flight condition with a low critical value of p.

The effect of the ratio A/B on the critical rate of roll $p = \omega_{\psi_o}$ is illustrated in Fig.6. Values for $p_{crit} = \omega_{\psi_o}$ for a representative range of aircraft are shown in Fig.7 where the effects of the design trends discussed above are clearly demonstrated.

This attractively simple analysis is, however, insufficient to predict fully the flight behaviour of an aircraft in practical rolling manoeuvres and in particular the peak values of incidence and sideslip occurring during such a motion.

The actual criterion for these may be dictated by structural limitations, pilots discomfort and fatigue, effects on navigational techniques etc.

These peak values of α and β can only be obtained by computing the response of an aircraft to a given aileron manoeuvre.

The work undertaken at RAE was largely directed to determine systematically these critical quantities.

5 Computations on a General Purpose Simulator (GEPUS)

5.1 Scope of the Investigation

An extensive programme of analogue computations was carried out on a general purpose simulator (GEPUS). Due to the large number of multipliers installed in this computer the equations of motion could be fully represented including the effect of gravity and non-constant aerodynamic derivatives.

The programme was divided into two main tasks:

(i) Investigation of individual aircraft designs in cooperation with the manufacturers. As none of the aircraft analysed showed any alarming characteristics it is not proposed to report on these investigations here.

(ii) A systematic investigation of the effect of all the relevant parameters both with respect to aircraft design and the execution of the flight manoeuvre. This programme was centred round a typical advanced supersonic fighter design, but in the course of the investigation considerable variations of all major coefficients were explored, so that the results cover a fairly wide range of aircraft configurations. The primary task of this preliminary series of computations was, however, to determine the predominant parameters so that the number of relevant parameters could be reduced to a manageable order and then to draw up a programme for a more comprehensive study. At the time of writing such a programme has already been started and it is hoped that the results of this work will give more general data than those presented here.

5.2 Representation of the equations of motion and the aerodynamic forces and moments

The equations of motion represented on the simulator have been derived in section 2.3 and are equations (16-21). The circuit representing these equations is shown in Fig.52 and has been so arranged that the aerodynamic derivatives are set independently from speed, inertias, μ_2 . This assisted in the procedure of varying individual parameters by reducing the number of coefficients to be reset for each variation to the absolute minimum. Furthermore, since all gains represent then numerically familiar quantities, errors in setting and resetting a problem are more readily spotted.

It should also be noted that a number of apparently superfluous amplifiers in series with integrators has to be used as the integrators on GEPUS can only be set for a limited number of widely spaced discreet values of time constants.

The circuit computing $\sin \phi$ and $\cos \phi$ as required to represent gravity in the force equation is shown in Fig.53.

The aerodynamic, inertia and geometric data for the supersonic fighter presented as the "standard aircraft" in the programme are given in Table 1. When the individual parameters were varied the flight condition $M = 0.8$ at 40,000 ft altitude was chosen as the reference throughout.

It may be interesting to note that in the process of transforming the original aerodynamic derivatives (in wind axes) to the values tabulated as referring to principal inertia axes, $n_{\dot{\alpha}}$ has changed sign and $n_{p\alpha}$ has been coonsiderably altered. Unfortunately n_v has been represented by a constant value, but it is realised now that even for a basically constant $n_v(C_L)$, n_v in body axes will vary considerably with incidence and this obviously important effect will be investigated at the earliest possible moment.

5.3 Simulated flight manoeuvres and method of analysis

In order to obtain repetitive results and to be able to separate the effects of design modification from irrelevant factors, it was necessary to specify a well defined input. At the same time this input had to bear a reasonable resemblance to realistic flight manoeuvres. For the first reason rudder and elevator had to be assumed fixed. Aileron was applied as a single square wave function to a preset value of ξ_0 . It was held until a desired angle of bank $\Delta\phi$, as computed on the simulator and displayed on a meter in front of the operator was reached. ξ_0 and $\Delta\phi$ were varied systematically to cover a representative range of flight manoeuvres. A typical record of such a manoeuvre is shown in Fig.8.

After the ailerons are returned to $\xi = 0$ the aircraft does not instantaneously cease to roll so that the angle of bank through which the aircraft finally rolls is considerably in excess of $\Delta\phi$.

In order to check whether the results obtained by these obviously not quite realistic manoeuvres are sufficiently representative of a roll where the aircraft is stopped at $\Delta\phi$, the latter case was frequently attempted by manually controlling ξ through the knob of a variable resistor. This rather arbitrary procedure was repeated several times and it was generally found that the peak values in α and β obtained thereby scattered within the band of $^{+50\%}_{-20\%}$ about the values obtained with the standard manoeuvre. An example of such a series of tests is shown in Fig.9. This was accepted

as reasonable correlation so that the nominal bank angle $\Delta\phi$ can be interpreted as approximately representing the angle of bank change of a corresponding actual flight manoeuvre. This interpretation is, however, not valid for a case where p diverges after ξ is returned to neutral and results obtained in this condition have generally been rejected.

It is perhaps significant that pilots' efforts to terminate the manoeuvre quickly (that is what the operator has actually tried to achieve in the above mentioned manoeuvre) are apparently more likely than not to worsen the response in α and β, as is borne out by the predominance of the scatter towards an increase in α and β. This would substantiate similar flight experience in the U.S.A.

Fig.8(b) illustrates the method of computing peak values of $\Delta\alpha$ and β, which were taken as the significant quantities describing the behaviour of the aircraft in roll. $\Delta\alpha_{max}$ and β_{max} are defined as the larger of the first two peaks recorded in α and β respectively. It was assumed that if the motion would continue to diverge further the pilot would have taken some corrective action.

5.4 Aircraft responses*

Typical time histories of responses computed on the simulator are shown in Figs.10 to 14. Fig.10(a) represents the supersonic fighter chosen as the principal example (Table 1) flying at a Mach No. = 0.8 and 40,000 ft altitude. This condition was selected because it represents approximately the greatest height at which subsonic speed will be practicable. This was expected to give the worst response because m_w is at a minimum before it rises to its substantially greater supersonic value. Ailerons are held at $\xi = 4^o$ until a bank angle $\Delta\phi = 90^o$ was reached.

If the principal inertia axis was inclined -5^o (nose down) as compared with the basic $+5^o$ the motion shown in Fig.10(b) was obtained.

Fig.11(a) shows the response to a manoeuvre with ξ held at 8^o until $\Delta\phi = 180^o$; the amplitudes in α and β are considerably larger when compared with the roll through $\Delta\phi = 90^o$ shown in Fig.10(a).

Figs.12 and 13 show the same rolling manoeuvres on an aircraft with m_w increased to four times the value of the "standard" configuration. The peak values in α are reduced, those in β increased.

If the basic value of $n_v(0.20)$ is reduced to one quarter of its value, the amplitudes in β are substantially increased, α being slightly smaller as seen in Fig.14(a).

The dominating influence of the inertia crosscoupling terms on the aircraft response in rolling is illustrated in Fig.15 where these terms:

$$pq\,(B - A)\ ; \quad pr\,(C - A) \quad \text{and} \quad qr\,(C - B)$$

have been omitted during two otherwise identical manoeuvres.

In addition to the yawing and pitching motions, which are the principal topic of this note, Figs.10(b) to 14(b) all display a new type of instability in roll itself. It can be seen that in these cases ($\alpha_o = -5^o$) the aircraft continues rolling after the ailerons are centralised and will finally settle down to an autorotational rolling state, which is independent of the original

---

* The results shown in Figs.10-14 are slightly in error. Although the conclusions drawn are not invalidated by these errors, the time histories cannot be taken as correct in detail.

aileron application. This steady state is seen particularly well established in Figs.11(b) and 13(b). This phenomenon will be discussed in detail in section 6.1 and Appendix A, where it is shown to occur for values of α_o below a certain critical value.

The actual significance to the pilot of this rolling instability cannot be deduced immediately from these simple computations, where the motion is allowed to develop unchecked. Further study will be devoted to this aspect by computing the control movements required to stabilise the motion.

5.5 Effect of various aircraft parameters and flight condition

The effects of varying the inertia and aerodynamic parameters of an aircraft and the flight condition are investigated by considering only the peak values in $\Delta\alpha$ and β reached during a given rolling manoeuvre. It must be strongly emphasized that the trends established here for the effects of varying individual parameters are strictly applicable only to the particular aircraft configuration and flight condition for which they were obtained and do not necessarily admit of generalisation. Some of the conclusions drawn here may have to be amplified as more results are accumulated in the course of the continuation of the present series of computations.

5.51 Duration of aileron application

For all the configurations investigated the duration of the aileron application and thus the angle of bank reached during that time (as defined in section 5.3 and illustrated in Fig.8) has been systematically varied.

Analysis of the variation of the peak amplitudes in $\Delta\alpha$ and β with $\Delta\phi$ shows already the difficulties in laying down sufficiently generalised rules, as three distinctly different trends have been observed for different combinations of inertia and/or aerodynamic derivatives.

(i) $\Delta\alpha_{max}$ and β_{max} increase progressively with the duration of the aileron application, i.e. with $\Delta\phi$ and reach a maximum after which no further deterioration occurs even if ξ is held on indefinitely. See Fig.16. It appears that as the aileron angle ξ and thus the rate of roll is increased this maximum is reached at larger bank angles.

(ii) $\Delta\alpha_{max}$ and β_{max} increase progressively with the duration of the aileron application up to a certain value of $\Delta\phi$. If ailerons are held on longer, the peaks in $\Delta\alpha$ and β become smaller, reach a minimum after which they start to increase again. For the example shown in Fig.17 for $\xi = 10^o$ rolling through $\Delta\phi = 90^o$ results in a peak value of $\Delta\alpha = 10^o$. If the manoeuvre were continued through $\Delta\phi = 180^o$ only $\Delta\alpha_{max} = 3^o$ would be recorded.

(iii) $\Delta\alpha_{max}$ and β_{max} increase progressively with $\Delta\phi$ indicating the presence of a divergent mode of motion. Examples for this condition are shown in Fig.18.

These trends are examined theoretically in more detail in section 6.3 where they are illustrated by the first results of the new series of simulations (see Figs.49 to 51).

5.52 Aileron angle and rate of roll

In Fig.20 $\Delta\alpha_{max}$ and β_{max} have been plotted against aileron angle (ξ) for various flight conditions. As an alternative to ξ the abscissa is scaled

in terms of p_∞ i.e. the steady rate of roll corresponding to ξ, if it were held on indefinitely. (The values of p_∞ were obtained by observing this condition on the simulator). The actual peak values of p reached in the computed manoeuvres are, however, only approximately $\frac{3}{4}$ of these values p_∞.

In all cases computed $\Delta\alpha_{max}$ and β_{max} increase progressively with ξ (or p_∞) and reach a maximum at a certain value of p_∞ beyond which the aircraft rolling characteristics are again improved.

This phenomenon can be explained by the results of the stability analysis of Ref.2. This is illustrated in Fig.19, showing schematically the stability boundaries of Fig.3. The radial line through the origin represents variation in p for a given aircraft flying at a given speed and height, i.e. with a given ω_θ and ω_ψ. Within the range $p_1 < p < p_2$ the lateral-longitudinal aircraft motion will be unstable. From equation (24):

$$p_1 = \omega_{\psi_o} \qquad p_2 = \omega_\theta \tag{27}$$

can be established, thus instability occurs between

$$\omega_{\psi_o} < p < \omega_\theta \quad \text{if} \quad \omega_\theta > \omega_{\psi_o}$$

or (28)

$$\omega_{\psi_o} > p > \omega_\theta \quad \text{if} \quad \omega_\theta < \omega_{\psi_o}$$

whichever applies.

These ranges are indicated in Fig.20. They lie at approximately 50% of the values of p_∞ at which $\Delta\alpha_{max}$ and β_{max} have their maxima. As mentioned above the actual peak values of p reached during these manoeuvres were roughly $\frac{3}{4}\, p_\infty$ and an average figure for p is approximately $0.5\, p_\infty$. If these values of p are taken as representative the range $p_1 < p < p_2$ will then coincide with the maxima in $\Delta\alpha_{max}$ and β_{max}.

5.53 Incidence of the principal inertia axis and pull-out manoeuvres

It was noticed early in the computations that the incidence of the principal inertia axis α_o (with respect to the flight path in the trimmed equilibrium condition) has a dominating influence on the values of the peak amplitudes in $\Delta\alpha$ and β recorded. Consequently α_o was treated as an independent parameter during the whole investigation and not taken as the incidence of the particular aircraft chosen for an example as it would apply to the various flight conditions examined. By discussing these effects of height, speed and incidence separately more generally applicable conclusions can be drawn.

Theoretical analysis (section 6.3 and Appendix E) shows that $\Delta\alpha_{max}$ and β_{max} are largely proportional to α_o, containing in addition a contribution proportional to n_p. This is well represented in the results obtained on the simulator as shown in an example for many similar results in Fig.21(a).

The steep rise of β_{max} and α_{max} towards negative values of α_o seen in Fig.21(b) is the result of the development of a divergent rolling motion as discussed in sections 5.4, 6.1 and Appendix A and is not directly a feature of the lateral-longitudinal motion discussed here.

From the influence of α_o on the aircraft response shown in Fig.21(a), the behaviour of an aircraft in rolling pull outs may also be assessed, though such manoeuvres have not so far been actually computed in the present series. The application of g will result in an increase in incidence and thus in α_o. This will worsen the aircraft response in the sense indicated in Fig.21(a) apart from so far unexplored effects of simultaneously applying rate of pitch.

5.54 Speed and height

Results obtained for the supersonic fighter aircraft described in Table 1 at 60,000 ft altitude have been plotted against Mach No. in Fig.22. The sharp drop in $\Delta\alpha_{max}$ and β_{max} through the transonic range is largely the result of the increase in m_w from the low subsonic value of 0.083 to 0.25 at M = 1.0. The more gentle progressive reduction in the supersonic range reflect pure speed effects more directly as the derivatives vary less.

These trends will be fairly representative for an aircraft in which, as has been assumed in the example chosen, n_v is maintained fairly constant up to high supersonic speeds. Should n_v drop substantially with Mach No, the aircraft response in α_{max} can be expected then to deteriorate.

Variations with altitude at a constant Mach No, i.e. with constant derivatives and almost constant true speed, are shown in Fig.23. For the fighter aircraft represented there is a very regular progressive deterioration with height, which can be expressed by the empirical law:

$$\Delta\alpha_{max} = \text{const}\sqrt{1/\sigma} \quad . \tag{29}$$

In this analysis α_o (i.e. incidence) has been assumed constant as $\alpha_o = +5^o$. If α_{oo} is the incidence of the principal inertia axis at zero lift and a_1 the lift slope of the complete aircraft, α_o can be computed as

$$\alpha_o = \alpha_{oo} + \frac{840}{a_1}\,\frac{W/S}{V_i^2}$$

or

$$\alpha_o = \alpha_{oo} + \frac{840}{a_1}\,\frac{W/S}{V^2\sigma} \quad . \tag{30}$$

Thus if $\alpha_{oo} \geq 0$, α_o will increase progressively with height and with the inverse of speed. If $\alpha_{oo} < 0$ α_o will be zero somewhere within the flight range and $|\alpha_o|$ will increase from there in both directions. With equation (30), the results shown in Figs.22 and 23 can be readily modified to apply to level flight incidence if it is assumed (see section 5.53) that $\Delta\alpha_{max}$ and β_{max} are directly proportional to α_o. As α_o will generally increase with height and $1/V$ the trends shown in Figs.22 and 23 will be further accentuated.

5.55 m_w, n_v and inertias

From the stability analysis of Ref.2 it would be expected that the static stabilities in pitch and in yaw, m_w and n_v respectively and the inertias

are the predominant parameters. Considering these individually cannot be expected to reveal generalised trends as the stability of the motion is determined as shown in Figs.3-4 by the combination of the three parameters. This is reflected in the results shown in Figs.24-26 where m_w , n_v and the inertias (maintaining A:B:C = const) are varied individually from the standard configuration of the aircraft chosen as an example.

Increasing m_w (Fig.24) improves $\Delta\alpha$ without materially altering the response in yaw (β).

Increasing n_v worsens the response in pitch, as expected but again β is little affected.

Proportional increases in the inertias appears to have little effect within the range covered; reductions from the assumed original values show the expected improvement. The argument advanced in the discussion of the effect of rate of roll in section 5.52 and demonstrated in Fig.19 can similarly be applied to variation of inertias and there is in fact an indication of a resonance region at approximately 1.2 × original inertias; this agrees well with the centre of the unstable range intersected in Phillips stability diagram when a representative average rate of roll of approximately 2/3 of the recorded peak value is taken.

It appears from the above discussion of the effects of variations in inertias and in m_w , that the aircraft chosen as an example represent a critical combination at least with respect to these parameters.

Inertia in roll was reduced independently of that in pitch, reducing the ratio A/B from the value of the standard aircraft = $\frac{1}{4}$ to $\frac{1}{8}$. Contrary to theoretical expectation this improved the aircraft response slightly, as can be seen by comparing Figs.16(a) and 17.

Contours of constant values of $\Delta\alpha_{max}$ and β_{max} have been evaluated for two rolling manoeuvres in Fig.27 (rolling with $\xi = 8^o$ through 180^o) and Fig.28 (rolling with $\xi = 4^o$ through 180^o). Again based on a representative $p = 2/3\ p_{max}$ the stability boundaries obtained from Ref.2 with aerodynamic damping neglected are represented. In this form, the curves should directly reflect the implications of the theory advanced in Ref.2. It will immediately be noticed that large peak values of $\Delta\alpha$ and β are obtained well within the stable region. However, there is a strong tendency (somewhat complicated by local distortions of the contours) for $\Delta\alpha$ and β to increase more rapidly as the stability boundaries are approached and a reasonable correlation between the Phillips criteria and the actual flight behaviour of an aircraft is indicated. With the limited number of available results the unstable region near the ordinate axis is not very well established and it is intended to explore this further in a future expansion of the present programme. Reduced to the nondimensional parameters $(\omega_\theta/p)^2$ and $(\omega_\psi/p)^2$ Figs.27 and 28 should be identical. There are however considerable discrepancies which can only be attributed to the difference in the execution of the respective rolling manoeuvres. These are illustrated in Fig.29. It can be seen that there are two essential differences. For $\xi = 4^o$ ailerons have to be held on longer (2.8 sec as compared with 1.8 secs) to roll through the same angle of bank $\Delta\phi = 180^o$. As the parameters affecting the response of the aircraft in roll have been unaltered, rate of roll has almost approached its asymptotic steady value and the time history in p is less peaked when compared with the manoeuvre with $\xi = 8^o$. Secondly, as the duration of the aileron application is altered, ailerons are taken off at a different instant in the motion of the aircraft in α and β and this is bound to

affect the eventual peak amplitudes as these almost universally occur after cessation of the aileron application.

5.56 m_q , n_r and autostabilisation

The effects of variation of m_q and n_r are shown in Figs.30 and 31. Changes in n_r have practically no effect; increasing m_q reduces the pitching amplitudes, but the values of m_q for which a substantial improvement would be obtained are completely outside the scope of practicable tailplane design limits, but there is reasonable scope for artificial pitch damping.

These conclusions appear to be well substantiated by the latest American results and can be taken as generally valid.

The yawing and pitching motions discussed above are largely generated by the two product terms in the yawing and pitching moment equations and their removal has been shown to substantially improve the aircraft response (see Fig.15). Consequently if rudder and elevator can be applied to counteract these terms:

$$N_\zeta \zeta = (B - A)\, pq \qquad (31)$$

$$M_\eta \eta = -(C - A)\, pr \qquad (32)$$

complete autostabilisation would be affected. As opposed to conventional methods of autostabilisation this technique would require the maintenance of the correct signal throughout the flight regime as, obviously, overcompensation would reintroduce the product terms; if the signal has more than twice the proper value the response will be worse than with the original aircraft. Undercompensation would be less disastrous as it can only be expected to reduce the effectiveness of the installation. It can be shown that the amount of control demanded by the stabiliser is requiring up to and perhaps more than full control and this puts entirely new problems to the designer both with respect to reliability and safety and performance of the installation.

In order to show whether autostabilisation either by conventional yaw and pitch damping or by perfect compensation of the product terms according to equations 31 and 32 would in effect relieve the fin and tail loads substantially these have been computed on the simulator. The results are presented in Table 2 giving comparable values for the load peaks experienced with and without stabilisation. The results are disappointing as the loads on the tailplane are actually increased by the perfect stabiliser. Only pitch and yaw damping brought substantial relief. Either method would of course be effective in relieving the wings, as the build up in incidence is suppressed. Either method also relieves fin loads.

An alternative method of autostabilisation is outlined in the theoretical analysis in section 6.2 and Appendix B.

5.57 Miscellaneous

The remaining aerodynamic derivatives were also checked for their influence on the aircraft response in rolling. These checks indicated the following trends:

z_w and y_v are mainly affecting damping in pitch and yaw respectively and can be included with the corresponding rotary damping terms in the familiar combinations:

$$\left(\frac{n_r}{i_C} + y_v\right) \quad \text{and} \quad \left(\frac{m_q}{i_B} + z_w\right) .$$

n_p and n_ξ are detrimental. These terms are responsible for the values of $\Delta\alpha_{max}$ and β_{max} obtained for $\alpha_o = 0$, where otherwise no pitching and yawing motion would occur. If α_o is increased these effects become, however, progressively less important.

ℓ_v affects the autorotational rolling divergence but has otherwise no significant influence on the yaw and pitch response. ℓ_r is unimportant. The effect of gravity was frequently checked and in no case was there any noticeable difference. In fact it was found impossible to select two corresponding records in which the effect of gravity would be greater than the accuracy of the computing and recording equipment used.

6 Theoretical analysis

6.1 Autorotational rolling instability

Prompted by the observation of autorotational rolling states during the computations on the simulator, the equations of motion (10-14) were examined for the existence of quasisteady equilibrium states apart from the trivial solution $p = q = r = \alpha = \beta = 0$. By postulating such a steady state with

$$\dot{p} = \dot{q} = \dot{r} = \dot{\alpha} = \dot{\beta} = 0 \tag{33}$$

the equations of motion are reduced to a system of five nonlinear algebraic equations which have been solved in Appendix A to give a biquadratic in p

$$\left(\frac{p}{\omega_{\psi_o}}\right)^2 = \frac{1}{2}\left\{1 + \left(\frac{\omega_\theta}{\omega_{\psi_o}}\right)^2 + \alpha_o \nu\right\} \pm \sqrt{\frac{1}{4}\left\{1 + \left(\frac{\omega_\theta}{\omega_{\psi_o}}\right)^2 + \alpha_o \nu\right\}^2 - \left(\frac{\omega_\theta}{\omega_{\psi_o}}\right)^2 - \kappa} \tag{34}$$

where

$$\nu = z_w \frac{\ell_v}{\ell_p} \frac{i_B' - i_A}{n_v} \tag{35}$$

$$\kappa = z_w \frac{m_q}{n_v}\left(1 - \frac{A}{B}\right)\frac{(\ell/b/2)^2}{\mu_2} \quad . \tag{36}$$

Equation (34) has real solutions if

$$\alpha_o \nu \geq -\left\{1 + \left(\frac{\omega_\theta}{\omega_{\psi_o}}\right)^2\right\} + 2\sqrt{\left(\frac{\omega_\theta}{\omega_{\psi_o}}\right)^2 + \kappa} \tag{37}$$

i.e. there exists an autorotational equilibrium state if α_o is below a certain critical value (since $\nu < 0$). These critical boundaries for α_o

are plotted against $\left(\frac{\omega_\theta}{\omega_{\psi_o}}\right)^2$ and κ as parameters in Fig.32. If $\left(\frac{\omega_\theta}{\omega_{\psi_o}}\right) \neq 1$ autorotational instability in roll exists even at positive α_o, i.e. with the principal inertia axis inclined nose up. Damping in pitch m_q (being the main factor in κ) shifts the stability boundary towards more negative α_o.

For $\alpha_o \leq \alpha_{o_{crit}}$ equation (34) predicts two pairs of equilibrium states $\pm p_1$ and $\pm p_2$ which have been computed and plotted in Figs.33-35 for the significant range of the relevant parameters. If

$$|p_1| < |p_2|$$

$|p_1|$ will be neutrally stable and thus never occur as a steady state in flight. The upper value of $|p_2|$ constitutes a steady state towards which the aircraft will diverge, once p_1 has been exceeded. This interpretation of the physical significance of these equilibrium rolling states is illustrated in Fig.36.

For the supersonic fighter aircraft used as an example throughout this note values of p_1 and p_2 have been estimated for a number of flight conditions for $\alpha_o = 0$ and $\alpha_o = -5^\circ$ and the results are given in Table 2. Autorotation exists for all conditions quoted apart from one case. The divergence boundary is well within the operational flight regime, p_1 varying between 50 and 150°/sec.

For a supersonic bomber project this boundary was found to be as low as 20°/sec and this condition would amount to practically complete loss of roll damping, as the roll-subsidence must be expected to deteriorate for rolling velocities $p \to p_1$.

6.2 Pilots' control and autostabilisation

In an attempt to assess the chances of a pilot to keep the aircraft laterally and longitudinally under control against the action of inertia forces in rolling manoeuvres, the rudder and elevator movements required to keep $\Delta\alpha = 0$ and $\beta = 0$ throughout where estimated in Appendix B. For this ideal control coordination the pilot would have to sense p^2 and $\dot{p}$, as the major terms obtained read:

$$\zeta(t) = \frac{C}{N_\zeta} \alpha_o \dot{p}(t) \tag{38}$$

$$\eta(t) = \frac{C - A}{M_\eta} \alpha_o p^2(t) \quad . \tag{39}$$

These control movements have been computed in Appendix C for two typical rolling manoeuvres, which were selected to give the smoothest possible movement so as not to exaggerate the already very violent control manipulations demanded from the pilot. These manoeuvres are shown as time histories $\zeta(t)$ and $\eta(t)$ in Fig.37.(rolling through $\Delta\phi = 180^\circ$ in 2 secs) and in Fig.38 (rolling through $\Delta\phi = 90^\circ$ in 1 sec). The manoeuvres appear beyond the scope of even a highly skilled pilot and are further complicated by the fact that he has to know the incidence of the principal inertia axis for any

particular flight condition, before he even knows in which direction he is to move his controls.

Equations (38) and (39) indicate, however, the signals required for a perfect autostabiliser, which operating as a demand system rather than a suppressor offers perfect stabilisation, provided it can technically be realised. The difficulties discussed in section 5.56 apply of course here as well.

6.3 Response calculation

The system of nonlinear differential equations (10-14) cannot be solved by conventional methods of differential calculus. In order to gain some understanding of the results obtained on the simulator an attempt was made to estimate the response in pitch and yaw in an idealised rolling manoeuvre. If $p = \text{const}$, the equations of motion become linear and the stability of the system can be analysed as suggested in Ref.2 and shown in Appendix D. If the investigation is restricted to rates of roll below the critical values as defined by

$$p < \omega_\theta \quad \text{and} \quad p < \omega_{\psi_o} \tag{40}$$

the aircraft will perform two coupled lateral-longitudinal oscillations with the frequencies ω_1 and ω_2 and zero damping. Neglecting damping in pitch and in yaw these frequencies have been computed from Ref.2 and are plotted in Fig.39.

The amplitude ratios between α and β has been derived in App.D and are plotted against $(\omega_\theta/p_o)^2$ in Fig.40 for the high frequency mode ω_1 and for the low frequency mode ω_2 in Fig.41. It has also been shown that the amplitude ratios are imaginary, i.e. β is 90^o phase advanced on α if $(\frac{\beta}{\alpha}) > 0$ and vice versa if $(\frac{\beta}{\alpha}) < 0$. Thus the aircraft motion in $\Delta\alpha$ and β in response to an instantaneously applied rate of roll p_o must be of the form

$$\Delta\alpha(t) = \alpha_\infty + \alpha_{11} \cos(\omega_1 t) + \alpha_{12} \sin(\omega_1 t) + \alpha_{21} \cos(\omega_2 t) + \alpha_{22} \sin(\omega_2 t) \tag{41}$$

$$\Delta\beta(t) = \beta_\infty - \alpha_{11}\left(\frac{\beta}{\alpha}\right)_1 \sin(\omega_1 t) + \alpha_{12}\left(\frac{\beta}{\alpha}\right)_1 \cos(\omega_1 t) - \alpha_{21}\left(\frac{\beta}{\alpha}\right)_2 \sin(\omega_2 t) + \alpha_{22}\left(\frac{\beta}{\alpha}\right)_2 \cos(\omega_2 t) . \tag{42}$$

Solutions for all the constants in these equations have been derived in Appendix E and it has been shown, that apart from some secondary contributions, they are all proportional to α_o, the incidence of the principal inertia axis. This explains the predominant influence of α_o on the amplitudes in α and β computed on the simulator.

If the frequencies of the two oscillatory modes of the coupled lateral-longitudinal motion are sufficiently apart, say

$$\omega_1/\omega_2 > 4 ,$$

the peaks in $\Delta\alpha$ and β reached during a given manoeuvre can be simply estimated by adding algebraically the amplitudes of the two harmonics:

$$\Delta\alpha_{max} \approx \alpha_\infty \pm (\alpha_1 + \alpha_2) \tag{43}$$

$$\beta_{max} \approx \beta_\infty \pm \left(\frac{\beta}{\alpha}\right)_1 \alpha_1 + \left(\frac{\beta}{\alpha}\right)_2 \alpha_2 \tag{44}$$

taking whichever sign gives the larger result, where

$$\alpha_1 = \sqrt{\alpha_{11}^2 + \alpha_{12}^2} \tag{45}$$

$$\alpha_2 = \sqrt{\alpha_{21}^2 + \alpha_{22}^2} \quad . \tag{46}$$

In Appendix F this analysis has been extended to the calculation of the response to a square wave in $p(t)$, i.e. p_o is applied instantaneously at $t = 0$ and held until $t = t_1$. The motion is computed in two steps covering

(i) $0 > t > t_1$ with $p = p_o$

(ii) $t_1 > t > \infty$ with $p = 0$.

In both regimes $p = \text{const}$, the differential equations are linear and an analytical solution is readily obtained. Range (i) is computed with the procedure outlined above and the values of the variables computed for $t = t_1$ are then introduced as initial conditions into the solution of the motion for range (ii) with $p = 0$. In this range the motion consists of the two uncoupled oscillations in pitch and in yaw.

In Figs.44 to 46 a number of such responses have been computed for two aircraft with the characteristics listed in Table 4. As $n_p = n_\xi = 0$ the response in α and β is proportional to α_o thus the results are presented in terms of $\frac{\Delta\alpha}{\alpha_o}$ and $\frac{\beta}{\alpha_o}$. Further it can be shown that the response is uniquely determined when introducing (p_o) as nondimensional time and are then applicable to all values of p_o, provided they satisfy the given values of $\left(\frac{\omega_\theta}{p_o}\right), \left(\frac{\omega_\psi}{p_o}\right)$ and $(t_1 p_o)$. Fig.44(a) and 46 show responses to a step function in p and the two oscillatory modes of motion can be easily recognised in both $\Delta\alpha(t)$ and $\beta(t)$.

It can be seen that the high frequency oscillation (amplitude α_1 with frequency ω_1) is less prominant in the case with $\left(\frac{\omega_\theta}{p}\right)^2 = \left(\frac{\omega_\psi}{p}\right)^2 = 2$ (Fig.46) when compared with the case $\left(\frac{\omega_\theta}{p_o}\right)^2 = \left(\frac{\omega_\psi}{p_o}\right)^2 = 4$ in Fig.44(a). It appears to

be a general trend - supported by more unpublished calculations - that the long period mode becomes dominant as the stability boundaries in $\left(\frac{\omega_\theta}{p}\right)$ and $\left(\frac{\omega_\psi}{p_o}\right)$ are approached.

In Figs.44(b) and 45 responses have been computed for the same aircraft configuration when p_o is terminated instantaneously after various bank angles have been reached.

The amplitudes of the "residual" pitching and yawing oscillations (after t_1, i.e. with $p = 0$) are plotted against bank angle $\Delta\phi = p_o t_1$ in Figs.47 and 48 for the two cases considered. Fig.46 shows clearly, how the duration of the rolling manoeuvre affects the aircraft response in a quite unsystematic manner, (see also Fig.17) and that by rolling through $\Delta\phi = 5$ radians the amplitudes of the residual yawing motion are less than $\frac{1}{4}$ of those obtained when rolling through only 3 radians.

For the case $\left(\frac{\omega_\theta}{p_o}\right)^2 = \left(\frac{\omega_\psi}{p_o}\right)^2 = 2$ this trend is much less pronounced and within the range covered ($0 < \Delta\phi < 8$ radians) the amplitudes increase practically progressively with $\Delta\phi$. This may be explained by the much smaller amplitudes of the high frequency mode ω_1 present when the aircraft was rolling and the much longer period of the low frequency mode ω_2.

Considering also the amplitudes in $\Delta\alpha$ and β occurring before t_1, the peak values $\Delta\alpha_{max}$ and β_{max} obtained anywhere during the whole motion $0 < t < \infty$ were calculated and are plotted in Fig.49.

The same results were obtained on the simulator during a latest series of computation where a time history in $p(t)$ as illustrated in Fig.50 was used as the input instead of $\xi(t)$ as used during the present series. $p(t)$ is applied as an exponentially rising function

$$p = p_o \left(1 - e^{-t/t_p}\right)$$

and followed at t_1 with an exponential decay with the same time constant t_p.

The values of β_{max} for a series in which both t_p and t_1 were varied systematically are shown in Fig.51. The case $t_p = 0.02$ sec represents practically a perfect square wave and the results are practically identical with those calculated in Fig.49. As t_p is increased, i.e. as rate of roll is applied and taken off more gently the response in β becomes much less violent and also the variation of β_{max} with $\Delta\phi$ is more progressive.

7 Conclusions

A systematic series of computations of responses of a supersonic fighter aircraft to aileron movements has been carried out on an electronic simulator representing aircraft motion in 5 degrees of freedom. It has been shown that the gyroscopic forces couple the pitching and yawing motion resulting in large peak amplitudes in incidence and sideslip when inertia in pitch is large. These peak amplitudes occur usually after the termination of the actual rolling manoeuvre. From systematic variations of flight conditions and aircraft data the following conclusions can be drawn.

Aircraft response deteriorates progressively with increasing inertia in pitch, (and therefore in yaw) and with rolling velocity.

Usually the peak values of α and β recorded are greater if ailerons are held on longer. In some cases, however, intolerable peaks are reached when rolling through only 90° bank angle and less and the response hardly deteriorates when the duration of the manoeuvre is increased. In some cases again the response is noticeably improved if ailerons are held on longer and the resulting motion depends in a rather unsystematic manner on the precise instant at which the manoeuvre is terminated. Rapid control movements are generally detrimental.

Simultaneous increases in m_w and n_v are generally beneficial, whereas increasing these stabilities individually tends to relieve the motion in the freedom directly concerned at the expense of the other freedom. This is in agreement with the general indications of theoretical analysis.

Simulated responses and simplified theoretical analysis has shown that the peak amplitudes in pitch and in yaw are largely proportional to the incidence of the principal inertia axis in steady flight α_o with an additional contribution due to n_p and n_ξ.

Damping in yaw is ineffective.

Damping in pitch is moderately beneficial. An autorotational rolling state has been shown to exist, which is provoked once an aircraft exceeds a given critical rolling velocity. This phenomenon is also generated by the effects of inertia coupling and will occur only if the trimmed incidence of the principal inertia axis is below a certain critical value. Numerical solutions for all the relevant quantities are given. For a typical advanced supersonic aircraft the critical rate of roll can be as low as 20°/sec. The practical implications of this phenomenon are not yet known.

Pilot's control coordination to suppress completely the pitch and yaw divergence requires very large elevator and rudder movement which appear unrelated to readily perceptible physical or visual sensations.

Autostabilisation has been studied in detail and three alternative techniques are discussed:

(i) Pure pitch or combined pitch and yaw damping are relatively efficient.

(ii) Elevator and rudder control to counteract the inertia cross-coupling effects:

$$\eta \propto pr$$

$$\zeta \propto pq$$

would almost completely suppress the pitching and yawing motion. As this technique does not operate on an error signal the derived control law must be precisely maintained, as e.g. overcompensation reintroduces the inertia effects with reversed sign.

(iii) Perfect rolling with $\Delta\alpha = 0$ and $\beta = 0$ would be achieved with an autostabiliser operating rudder and elevator according to:

$$\eta \propto p^2 \alpha_o$$

$$\zeta \propto \dot{p} \alpha_o$$

where α_o is the incidence of the principal inertia axis relating to equilibrium flight condition. This technique also requires precise operation of the stabiliser servo for the reasons discussed under (ii).

All three proposals demand very large control movements which may even exceed the physically available range.

A simple analytical method to compute the aircraft response in yaw and pitch to an idealised rolling manoeuvre has been outlined and the results obtained to date appear to predict some of the trends observed on the simulator.

8 Future work

An extension of the programme of analogue computations described herein is already under way with the particular aim to reproduce a closer approximation to realistic rolling manoeuvres and to explore the general effects of piloting technique. It is then intended to cover a wider range of inertia variations and to simulate rolling pull out manoeuvres.

LIST OF SYMBOLS

A	inertia in roll	in principal inertia axes
B	inertia in pitch	
C	inertia in yaw	
L	rolling moment	in principal inertia axes
M	pitching moment	
N	yawing moment	

S wing area

V speed of flight

W aircraft weight

Y side force

Z normal force

b span

d_{suffix} damping parameters (Appendix E)

g gravitational acceleration

$i_A = \frac{A}{m(b/2)^2}$ inertia coefficient in roll

$i_B' = \frac{B}{m(b/2)^2}$ inertia coefficient in pitch

$i_C = \frac{C}{m(b/2)^2}$ inertia coefficient in yaw

$m = W/g$ mass of aircraft

ℓ_{suffix} nondimensional rolling moment derivative

m_{suffix} pitching moment derivative

n_{suffix} yawing moment derivative

p_o	steady rate of roll	in principal inertia axes
p	rate of roll	
q	rate of pitch	
r	rate of yaw	
t	time	

y_{suffix} side force derivative

z_{suffix} normal force derivative

α incidence of the principal inertia axis

α_o inclination of the principal inertia axis to the flight path in steady flight

$\Delta\alpha$ incremental incidence

$\Delta\alpha_{max}$ peak amplitude in $\Delta\alpha$

β sideslip

β_{max} peak amplitude in β

λ root of a charactistic equation

$$\kappa = \frac{z_w}{\mu_2}\frac{m_q}{n_v}\left(1 - \frac{A}{B}\right)\left(\frac{\ell}{b/2}\right)^2$$

$$\mu_2 = \frac{m}{\rho S b/2}$$ relative density

$$\mu_{2o} = \frac{m}{\rho_o S b/2}$$ μ_2 at sea level

$$\nu = z_w \frac{\ell_v}{\ell_p}\frac{i'_B - i_A}{n_v}$$

ρ air density

$\sigma = \rho/\rho_o$ relative density

$\omega = \frac{2\pi}{T}$ angular frequency (T = Period)

ω_1, ω_2 frequencies of the coupled lateral longitudinal motion of the rolling aircraft

$\omega_\theta = \sqrt{-\frac{M_\alpha}{B}}$ frequency of the isolated pitching oscillation

$\omega_\psi = \sqrt{\frac{N_\beta}{C}}$ frequency of the isolated directional oscillation

$\omega_{\psi_o} = \omega_\psi\sqrt{\frac{B+A}{B-A}}$ modified directional frequency

ξ aileron angle

ζ rudder angle

η elevator angle

ϕ	angle of bank
$\Delta\phi$	change in bank during a rolling manoeuvre
θ	angle of pitch
ψ	angle of yaw

Suffices and quantities to which they relate:

α, w	incidence
β, v	sideslip
p	rate of roll
q	rate of pitch
r	rate of yaw

REFERENCES

No.	Author	Title, etc
1	-	NACA high speed flight section: flight experience with two high-speed airplanes having violent lateral-longitudinal coupling in aileron rolls. NACA RM H55A13 (1955)
2	William H. Phillips	Effect of steady rolling on longitudinal and directional stability. NACA T.N. 1627 June 1948
3	W.J. Duncan	The principles of the control and stability of aircraft. Cambridge University Press 1952
4	W.J.G. Pinsker	Aileron control of small aspect ratio aircraft in particular delta aircraft. ARC 16711. Oct. 1953

APPENDIX A

Autorotational rates of roll of an aircraft with inertia-coupling

Neglecting small terms

$$Y_\beta = L_r = Y_r = Y_p = Z_q = 0 \quad \text{and gravity}$$

and assuming a quasisteady motion with

$$\begin{aligned} p &= \text{const.}, & \dot{p} &= 0 \\ r &= \text{const.}, & \dot{r} &= 0 \\ q &= \text{const.}, & \dot{q} &= 0 \\ \alpha &= \text{const.}, & \dot{\alpha} &= 0 \\ \beta &= \text{const.}, & \dot{\beta} &= 0 \end{aligned}$$

the equations of motion of the aircraft in five degrees of freedom (equations 7-11) are reduced to

$$L_\beta \beta + L_p p = 0 \tag{A.1}$$

$$N_\beta \beta - pq(B - A) = 0 \tag{A.2}$$

$$M_\alpha \alpha - M_q q + prB = 0 \tag{A.3}$$

$$\frac{Z_\alpha}{m_V} \alpha + q - p\beta = 0 \tag{A.4}$$

$$-r + p(\alpha + \alpha_o) = 0 \tag{A.5}$$

If the variables q, r, α and β are eliminated by substitution the system of equations will give a biquadratic in p:

$$p^4 - p^2 \left(\omega_\theta^2 + \omega_{\psi_o}^2 + \alpha_o \nu \omega_{\psi_o}^2\right) + \omega_{\psi_o}^2 \left(\omega_\theta^2 + \kappa \omega_{\psi_o}^2\right) = 0 \tag{A.6}$$

where

$$\omega_\theta^2 = -\frac{M_\alpha}{B} = -\frac{m_w}{i'_B} \frac{(V_i/b/2)^2}{\mu_{2o}} \frac{\ell}{b/2}$$

$$\omega_{\psi_o}^2 = \omega_\psi^2 \frac{B + A}{B - A} = \frac{n_v}{i'_B - i_A} \frac{(V_i/b/2)^2}{\mu_{2o}}$$

$$\nu = z_w \frac{\ell_v}{\ell_p} \frac{i'_B - i_A}{n_v}$$

$$\kappa = z_w \frac{m_q}{n_v} \left(1 - \frac{A}{B}\right) \frac{(\ell/b/2)^2}{\mu_2}$$

Equation A.6 gives:

$$\left(\frac{p}{\omega_{\psi_o}}\right)^2 = \tfrac{1}{2}\left\{1 + \left(\frac{\omega_\theta}{\omega_{\psi_o}}\right)^2 + \alpha_o\,\nu\right\} \pm \sqrt{\tfrac{1}{4}\left\{1 + \left(\frac{\omega_\theta}{\omega_{\psi_o}}\right)^2 + \alpha_o\,\nu\right\}^2 - \left(\frac{\omega_\theta}{\omega_{\psi_o}}\right)^2 - \kappa} \qquad \text{(A.7)}$$

In addition to the trivial solution of equations (A.1-A.5) $p = 0$ equation A.7 gives for values of α_o less than or equal to a certain critical value, four real solutions in p, $\pm p_1$ and $\pm p_2$ which constitute equilibrium states of autorotational rolling.

This analysis gives no indication of the stability of these quasi-steady states, but from a number of observations on aircraft responses obtained on the simulator it appears that only the larger values of $\pm p_2$ are stable. The lower values $\pm p_1$ have never been observed as steady states and seem to constitute a stability boundary, i.e. whenever $\pm p_1$ has been exceeded the aircraft will tend to diverge (or converge) towards the true autorotational state $\pm p_2$. This interpretation is illustrated in Fig.36. The solutions of equation (A.7) have been plotted against a representative range of parameters in Figs.23-35.

Inspection of equation (A.1) shows that for $L_\beta = 0$ there is only one solution $p = 0$ and thus the solutions shown in Figs.33-34 for $\alpha_o\,\nu = 0$ are not valid for $\nu = \ell_v = 0$. Equation (A.1) can be used to obtain

$$\beta = -\,p\,\frac{\ell_p}{\ell_v}\,\frac{b/2}{V} \qquad \text{(A.8)}$$

which states that for all values of $p \neq 0$, $\beta = \infty$ for $\ell_v = 0$. Physically this may mean that there is instability in p but autorotational equilibrium at $p = \pm p_2$ will only be reached at $t = \infty$ when $\beta = \infty$.

Equations (A.2 - A.5) give corresponding steady values for the other variables

$$\alpha = -\,\frac{1 - \left(\frac{p}{\omega_{\psi_o}}\right)^2}{\nu} \qquad \text{(A.9)}$$

$$q = -\,\omega_{\psi_o}^2\,\frac{\ell_p}{\ell_v}\,\frac{b/2}{V} \qquad \text{(A.10)}$$

$$r = p\,(\alpha_o + \alpha) \qquad \text{(A.11)}$$

APPENDIX B

Control manoeuvres required to roll with $\Delta\alpha = 0$ and $\beta = 0$

Setting $\Delta\alpha = \beta = \dot{\alpha} = \dot{\beta} = 0$ and neglecting gravity equations 10 and 11 give

$$q = 0$$

$$r = p\,\alpha_o \quad \text{and} \quad \dot{r} = \dot{p}\,\alpha_o$$

Thus the equation of motion of the aircraft (equations 12-14) are reduced to

$$L_\xi\,\xi + L_p\,p - A\,\dot{p} = 0 \tag{B.1}$$

$$N_\xi\,\xi + N_p\,p + N_r\,\alpha_o\,p + N_\zeta\,\zeta - C\,\dot{p}\,\alpha_o = 0 \tag{B.2}$$

$$M_\eta\,\eta + (C - A)\,p^2\,\alpha_o = 0 \tag{B.3}$$

when $\ell_r = 0$.

If the aircraft is set to perform a rolling manoeuvre given by

$$\phi = \phi(t) \tag{B.4}$$

then

$$p = p(t) = \frac{d\,\phi(t)}{dt} \tag{B.5}$$

$$\dot{p} = \dot{p}(t) = \frac{d\,p(t)}{dt} \tag{B.6}$$

are also determined and equations (B.1-B.3) can be used to compute the control movements $\xi(t)$, $\zeta(t)$ and $\eta(t)$ required to perform this manoeuvre with zero incremental incidence and sideslip.

$$\xi(t) = \frac{A}{L_\xi}\,\dot{p}(t) - \frac{L_p}{L_\xi}\,p(t) \tag{B.7}$$

$$\zeta(t) = \frac{C}{N_\zeta}\,\alpha_o\,\dot{p}(t) - p(t)\left(\frac{N_p}{N_\zeta} + \alpha_o\,\frac{N_r}{N_\zeta}\right) - \frac{N_\xi}{N_\zeta}\,\xi(t) \tag{B.8}$$

$$\eta(t) = -\frac{C - A}{M_\eta}\,\alpha_o\,p^2(t) \tag{B.9}$$

Retaining only major terms equation (B.8) will simplify to

$$\zeta(t) = \frac{C}{N_\zeta}\,\alpha_o\,\dot{p}(t) \tag{B.10}$$

Equations (B.7 - B.9) can be rewritten as

$$\xi(t) = \frac{\mu_{2o}}{(V_i/b/2)^2} \frac{i_A}{\ell_\xi} \dot{p}(t) - \frac{\ell_p}{\ell_\xi} \frac{b/2}{V} p(t) \qquad \text{(B.11)}$$

$$\zeta(t) = \frac{\mu_{2o}}{(V_i/b/2)^2} \frac{i_C}{n_\zeta} \alpha_o \dot{p}(t) - \frac{b/2}{V} \left(\frac{n_p}{n_\zeta} + \frac{n_r}{n_\zeta} \alpha_o \right) p(t) - \frac{n_\xi}{n_\zeta} \xi(t) \qquad \text{(B.12)}$$

$$\eta(t) = -\frac{\mu_{2o}}{(V_i/b/2)^2} \frac{i_C - i_A}{m_\eta} \frac{b/2}{\ell} p^2(t) \alpha_o \qquad \text{(B.13)}$$

APPENDIX C

Numerical example for ideal control coordination in rolling manoeuvres

So as not to exaggerate the control demands the smoothest possible manoeuvre will be chosen, as used in Ref.4:

$$\phi(t) = \Delta\phi \left\{ \frac{t}{t_m} - \frac{1}{\pi} \sin\left(\pi \frac{t}{t_m}\right) \cos\left(\pi \frac{t}{t_m}\right) \right\} \qquad (C.1)$$

Differentiation gives:

$$p(t) = \frac{\Delta\phi}{t_m} \left\{ 1 - \cos^2\left(\pi \frac{t}{t_m} + \sin^2\left(\pi \frac{t}{t_m}\right) \right\} \qquad (C.2)$$

$$\dot{p}(t) = \frac{\Delta\phi}{t_m^2} 2\pi \cos\left(\pi \frac{t}{t_m}\right) \sin\left(\pi \frac{t}{t_m}\right) \qquad (C.3)$$

where $\Delta\phi$ is the total change in bank angle and t_m the duration of the manoeuvre. Assuming:

$\Delta\phi$ = 3 radians = 172°

t_m = 2 secs

μ_{2o} = 40	H = 40,000 ft	α_o = 0.1 ≡ 5.7°
V = 800 ft/sec	V_i = 400 ft/sec	ℓ = 20 ft
b/2 = 20 ft	i_A = 0.05	ℓ_p = -0.20
i_C = 0.5	n_ζ = -0.10	n_p = 0 $\quad$ n_r = -0.4
n_ξ = 0.02	m_η = -0.09	

The manoeuvre illustrated in Fig.37a has been computed from equations (B.11-B.13). For the same aircraft rolling through $\Delta\phi$ = 86° in t_m = 1 sec has been computed and the control movements obtained are plotted in Figs. 37 and 38.

APPENDIX D

Aircraft motion with constant rate of roll

If rate of roll is assumed to be constant i.e. $p = p_o$ and gravity neglected the equation of motion of the aircraft become linear:

$$L_\xi \xi + L_\beta \beta + L_r r = -L_p p_o \qquad (D.1)$$

$$N_\xi \xi + N_\beta \beta + N_r r - (B - A) p_o q - C\dot{r} = -N_p p_o \qquad (D.2)$$

$$M_\alpha \Delta\alpha + M_q q + M_{\dot{\alpha}} \dot{\alpha} + (C - A) r p_o - B \dot{q} = 0 \qquad (D.3)$$

$$\frac{Y_\beta}{mV} \beta + p_o \Delta\alpha - r - \dot{\beta} = - p_o \alpha_o \qquad (D.4)$$

$$\frac{Z_\alpha}{mV} \Delta\alpha - p_o \beta + q - \dot{\alpha} = 0 \qquad (D.5)$$

By postulating $p = p_o$, ξ becomes one of the five variables in this system of five simultaneous equations and its solution would determine the aileron movements required to achieve the postulated value of p analogeous to the procedure applied in Appendices B and C. Knowledge of this control manoeuvre is, however, irrelevant to specific problem posed in this chapter, consequently equation (D.1) becomes redundant and will be omitted from the remainder of the analysis. This leaves the term $N_\xi \xi$ in equation D.2 undetermined and it has to be neglected though this may constitute a serious omission.

Introducing:

$$\frac{N_\beta}{C} = \omega_\psi^2 \; ; \quad - \frac{M_\alpha}{B} = \omega_\theta^2 \quad \text{and using } C = B + A \text{ the}$$

remaining four equations are now

$$\omega_\psi^2 \beta + \frac{N_r}{C} r - \frac{B - A}{B + A} p_o q - \dot{r} = - \frac{N_p}{C} p_o \qquad (D.6)$$

$$- \omega_\theta^2 \Delta\alpha + \frac{M_q}{B} q + \frac{M_{\dot{\alpha}}}{B} \dot{\alpha} + p_o r - \dot{q} = 0 \qquad (D.7)$$

$$\frac{Y_\beta}{mV} \beta + p_o \Delta\alpha - r - \dot{\beta} = - p_o \alpha_o \qquad (D.8)$$

$$\frac{Z_\alpha}{mV} \Delta\alpha - p_o \beta + q - \dot{\alpha} = 0 \qquad (D.9)$$

For the present simplified analysis damping terms N_r, M_q, $M_{\dot{\alpha}}$, Y_β and z_α are neglected and the above equations are then reduced to

$$\begin{array}{cccc} \Delta\alpha & \beta & q & r \\ \left|\begin{array}{cccc} 0 & \omega_\psi^2 & -\frac{B-A}{B+A}p_o & -\lambda \\ -\omega_\theta^2 & 0 & -\lambda & p_o \\ p_o & -\lambda & 0 & -1 \\ -\lambda & -p_o & 1 & 0 \end{array}\right| & = & \left|\begin{array}{c} -\frac{N_p}{C}P_o \\ 0 \\ -p_o\,\alpha_o \\ 0 \end{array}\right| \end{array} \qquad \text{(D.10)}$$

The determinant on the left hand side equated to zero gives as the characteristic equation a biquadratic in λ with the solution in terms of λ/p_o:

$$\left(\frac{\lambda}{p_o}\right)^2 = -\tfrac{1}{2}\left\{\left(\frac{\omega_\psi}{p_o}\right)^2 + \left(\frac{\omega_\theta}{p_o}\right)^2 + 1 + \frac{B-A}{B+A}\right\}$$

$$\pm\sqrt{\tfrac{1}{4}\left\{\left(\frac{\omega_\psi}{p_o}\right)^2 + \left(\frac{\omega_\theta}{p_o}\right)^2 + 1 + \frac{B-A}{B+A}\right\}^2 - \left(\frac{\omega_\psi}{p_o}\right)^2\left(\frac{\omega_\psi}{p_o}\right)^2 + \left(\frac{\omega_\psi}{p_o}\right)^2 - \frac{B-A}{B+A}\left\{1-\left(\frac{\omega_\theta}{p_o}\right)^2\right\}} \qquad \text{(D.11)}$$

This corresponds to the solution given in Ref.2. There it has been shown that for values of $p_o < p_{crit}$ equation 11 will have two pairs of conjugate imaginary solutions

$$\lambda_{1,2} = \pm i\omega_1 \quad \text{and} \quad \lambda_{3,4} = \pm i\omega_2$$

and the present analysis will be confined to this condition, i.e. to the regime where the aircraft motion is described by two neutrally stable oscillatory modes.

Equation (D.10) can be used to obtain a solution for the ratio between the amplitudes in β and α pertaining to these two oscillations:

$$\frac{\beta}{\alpha} = \frac{\left|\begin{array}{ccc} -\omega_\theta^2 & -\lambda & p_o \\ p_o & 0 & -1 \\ -\lambda & +1 & 0 \end{array}\right|}{\left|\begin{array}{ccc} 0 & -\lambda & p_o \\ -\lambda & 0 & -1 \\ -p_o & +1 & 0 \end{array}\right|}$$

giving

$$\left\{\frac{\beta}{\alpha}\right\}_1 = -\frac{1-\left(\frac{\omega_\theta}{p_o}\right)^2+\left(\frac{\omega_1}{p_o}\right)^2}{i\,2\left(\frac{\omega_1}{p_o}\right)} = i\left(\frac{\beta}{\alpha}\right)_1 \qquad (D.12)$$

and

$$\left\{\frac{\beta}{\alpha}\right\}_2 = -\frac{1-\left(\frac{\omega_\theta}{p_o}\right)^2+\left(\frac{\omega_2}{p_o}\right)^2}{i\,2\left(\frac{\omega_2}{p_o}\right)} = i\left(\frac{\beta}{\alpha}\right)_2 \qquad (D.13)$$

These amplitude ratios are imaginary, thus if $\left(\frac{\beta}{\alpha}\right) > 0$ β will be advanced 90^o in phase with respect to α and vice versa. Using values for ω_1 and ω_2 as given for an aircraft with A = 0 (or generally A << B) in Ref.2 and plotted in Fig.1 the amplitude ratios $\left(\frac{\beta}{\alpha}\right)_1$, and $\left(\frac{\beta}{\alpha}\right)_2$ corresponding to the high frequency and low frequency modes respectively have been computed and are plotted in Fig.40 and 41. It can be seen from Figs. 40 and 41 that for values of p_o not too close to the stability boundary these amplitude ratios are practically independent of p_o. Further $\left(\frac{\beta}{\alpha}\right)_2$, the amplitude ratio of the low frequency mode and thus of the generally more predominant motion is approximately determined by:

$$\left(\frac{\beta}{\alpha}\right)_2 \propto \left(\frac{\omega_\theta}{\omega_\psi}\right)^2 \qquad (D.14)$$

This expression explains why generally increasing m_w, i.e. ω_θ relieves the amplitudes in pitch at the expense of β and vice versa, as has been observed in flight and in simulated responses: The stability boundaries are determined by putting in equation D.11 $\lambda = 0$. Equation D.11 will then be satisfied if

$$-\left(\frac{\omega_\theta}{p_o}\right)^2\left(\frac{\omega_\psi}{p_o}\right)^2+\left(\frac{\omega_\psi}{p_o}\right)^2-\frac{B-A}{B+A}\left\{1-\left(\frac{\omega_\theta}{p_o}\right)^2\right\} = 0$$

or

$$\left(\frac{\omega_\psi}{p_o}\right)^2\frac{B+A}{B-A} = \frac{1-\left(\frac{\omega_\theta}{p_o}\right)^2}{1-\left(\frac{\omega_\theta}{p_o}\right)^2} \qquad (D.15)$$

This equation is satisfied for all values of

$$\left(\frac{\omega_{\psi_o}}{p_o}\right) = \left(\frac{\omega_\psi}{p_o}\right)\frac{B+A}{B-A}$$

If

$$\left(\frac{\omega_\theta}{p_o}\right)^2 = 1.0 \qquad \text{(D.16)}$$

and for all values of $\left(\frac{\omega_\theta}{p_o}\right)^2$ if

$$\left(\frac{\omega_{\psi_o}}{p_o}\right)^2 = 1.0 \qquad \text{(D.17)}$$

APPENDIX E

Aircraft response to instantaneously applied p

Using the results obtained in Appendix D , the response of an aircraft to an instantaneously applied rate of roll p_o can now be estimated.

Considering again only values of p_o for which the aircraft motion consists of oscillatory modes the general solution of equations (D.6-9) is

$$\Delta\alpha = \alpha_\infty + \alpha_{11} \cos(\omega_1 t) + \alpha_{12} \sin(\omega_1 t) + \alpha_{21} \cos(\omega_2 t) + \alpha_{22} \sin(\omega_2 t) \qquad (E.1)$$

It has been shown in Appendix D that the amplitude ratios $(\beta/\alpha)_1$ and $(\beta/\alpha)_2$ corresponding to ω_1 and ω_2 are imaginary, β being advanced 90° in phase with respect to α. Consequently the solution for β corresponding to equation (E.1) can be expressed in terms of α_{11}, α_{12} etc:

$$\beta = \beta_\infty - \left(\frac{\beta}{\alpha}\right)_1 \alpha_{11} \sin(\omega_1 t) + \alpha_{12} \left(\frac{\beta}{\alpha}\right)_1 \cos(\omega_1 t) - \alpha_{21} \left(\frac{\beta}{\alpha}\right)_2 \sin(\omega_2 t) + \alpha_{22} \left(\frac{\beta}{\alpha}\right)_2 \cos(\omega_2 t) \qquad (E.2)$$

Differentiation gives

$$\dot{\alpha} = -\alpha_{11} \omega_1 \sin(\omega_1 t) + \alpha_{12} \omega_1 \cos(\omega_1 t) - \alpha_{21} \omega_2 \sin(\omega_2 t) + \alpha_{22} \omega_2 \cos(\omega_2 t) \qquad (E.3)$$

$$\dot{\beta} = -\alpha_{11} \left(\frac{\beta}{\alpha}\right)_1 \omega_1 \cos(\omega_1 t) - \alpha_{12} \omega_1 \left(\frac{\beta}{\alpha}\right)_1 \sin(\omega_1 t) - \alpha_{21} \left(\frac{\beta}{\alpha}\right)_2 \omega_2 \cos(\omega_2 t) - \alpha_{22} \left(\frac{\beta}{\alpha}\right)_2 \sin(\omega_2 t) \qquad (E.4)$$

At $t = 0$ we have the initial conditions:

$$\Delta\alpha = 0 \qquad \beta = 0 \qquad q = 0 \qquad r = 0$$

and from equations (D.8) and (D.9)

$$\dot{\alpha} = 0 \qquad \dot{\beta} = \alpha_o p_o \qquad (E.5)$$

Substituted in equations (E.1-4) this leaves:

$$\left.\begin{aligned} 0 &= +\alpha_\infty + \alpha_{11} + \alpha_{21} \\ 0 &= +\beta_\infty + \alpha_{12}\left(\frac{\beta}{\alpha}\right)_1 + \alpha_{22}\left(\frac{\beta}{\alpha}\right)_2 \\ 0 &= \alpha_{12}\,\omega_1 + \alpha_{22}\,\omega_2 \\ \alpha_o p_o &= -\alpha_{11}\left(\frac{\beta}{\alpha}\right)_1 \omega_1 - \alpha_{21}\left(\frac{\beta}{\alpha}\right)_2 \omega_2 \end{aligned}\right\} \qquad \text{(E.6)}$$

α_∞ and β_∞ are the quasisteady values for α and β, which will be determined later in this Appendix.

In determinant form equations (E.6)

$$\Delta = \begin{vmatrix} \alpha_{11} & \alpha_{12} & \alpha_{21} & \alpha_{22} \\ +1 & 0 & +1 & 0 \\ 0 & \left(\frac{\beta}{\alpha}\right)_1 & 0 & \left(\frac{\beta}{\alpha}\right)_2 \\ 0 & \omega_1 & 0 & \omega_2 \\ -\left(\frac{\beta}{\alpha}\right)_1 \omega_1 & 0 & -\left(\frac{\beta}{\alpha}\right)_2 \omega_2 & 0 \end{vmatrix} = \begin{vmatrix} -\alpha_\infty \\ -\beta_\infty \\ 0 \\ \alpha_o p_o \end{vmatrix} \qquad \text{(E.7)}$$

can be solved for α_{11}, α_{12}, α_{21} and α_{22}. The amplitudes in α of the two oscillatory modes are then given as

$$\alpha_1 = \sqrt{\alpha_{11}^2 + \alpha_{12}^2} \qquad \text{(E.8)}$$

$$\alpha_2 = \sqrt{\alpha_{21}^2 + \alpha_{22}^2} \qquad \text{(E.9)}$$

The respective amplitudes of the yawing motion are then given as:

$$\beta_1 = \alpha_1' \left(\frac{\beta}{\alpha}\right)_1 \qquad \text{(E.10)}$$

$$\beta_2 = \alpha_2 \left(\frac{\beta}{\alpha}\right)_2 \qquad \text{(E.11)}$$

The response in $\Delta\alpha$ and β can now be computed from equations (E.1) and (E.2).

A quick assessment of the peak values of $\Delta\alpha_{max}$ and β_{max} is possible if $\omega_1 >> \omega_2$, say $\omega_1/\omega_2 > 4$. It can be shown that in superimposing two such oscillatory functions, the absolute maximum will be reasonably well approximated by the algebraic sum of the amplitudes of the two harmonics. If the above quoted condition applies then:

$$\Delta\alpha_{max} \propto \alpha_\infty \pm (\alpha_1 + \alpha_2) \tag{E.12}$$

and

$$\beta_{max} \propto \beta_\infty \pm (\beta_1 + \beta_2) \tag{E.13}$$

taking whichever sign gives the larger values.

Equation (E.7) gives the constants $\alpha_{11} \ldots \alpha_{22}$ as

$$\alpha_{11} = \frac{\alpha_o p_o - \alpha_\infty \left(\frac{\beta}{\alpha}\right)_2 \omega_2}{\left(\frac{\beta}{\alpha}\right)_2 \omega_2 - \left(\frac{\beta}{\alpha}\right)_1 \omega_1} \tag{E.14}$$

$$\alpha_{12} = -\frac{\beta_\infty \omega_2}{\left(\frac{\beta}{\alpha}\right)_1 \omega_2 - \left(\frac{\beta}{\alpha}\right)_2 \omega_1} \tag{E.15}$$

$$\alpha_{21} = \frac{\alpha_\infty \left(\frac{\beta}{\alpha}\right)_1 \omega_1 - \alpha_o p_o}{\left(\frac{\beta}{\alpha}\right)_2 \omega_2 - \left(\frac{\beta}{\alpha}\right)_1 \omega_1} \tag{E.16}$$

$$\alpha_{22} = \frac{\beta_\infty \omega_1}{\left(\frac{\beta}{\alpha}\right)_1 \omega_2 - \left(\frac{\beta}{\alpha}\right)_2 \omega_1} \tag{E.17}$$

As shown later (Equations E.28 to E.31) $\alpha_\infty \propto \alpha_o$ and $\beta_\infty \propto \alpha_o$ if $n_p = 0$. Then for $n_p = 0$ all the constants α_{11} to α_{22} are proportional to α_o, i.e. the response of the aircraft in pitch and in yaw to rolling is directly proportional to the incidence of the inertia axis (in equilibrium flight). Further with negligible aircraft damping β_∞ will be zero (equation E.30). This will simplify equations (E.8) and (E.9) to

$$\alpha_1 = \alpha_{11} \propto \alpha_o \tag{E.18}$$

$$\alpha_2 = \alpha_{21} \propto \alpha_o \tag{E.19}$$

The values of α_∞ and β_∞ represent the trim change in pitch and in yaw and can be estimated by equating steady terms in the equations of motion.

$$N_\beta \beta_\infty + N_r r_\infty - (B - A) p_o q_\infty = - N_p p_o \qquad (E.20)$$

$$M_\alpha \alpha_\infty + M_q q_\infty + (C - A) p_o r_\infty = 0 \qquad (E.21)$$

$$\frac{Y_\beta}{mV} \beta_\infty + p_o \alpha_\infty - r_\infty = - p_o \alpha_o \qquad (E.23)$$

$$\frac{Z_\alpha}{mV} \alpha_\infty - p_o \beta_\infty + q_\infty = 0 \qquad (E.24)$$

Setting

$$\alpha_\infty = \alpha_{\alpha_o} + \alpha_N \qquad (E.25)$$

$$\beta_\infty = \beta_{\alpha_o} + \beta_N \qquad (E.26)$$

where α_{α_o} and β_{α_o} are the contributions proportional to $(\alpha_o\ p_o)$ and α_N and β_N the contributions proportional to $(N_p\ p_o)$, these values can then be obtained as solutions of the determinant:

$$\begin{vmatrix} \alpha_\infty & \beta_\infty & q_\infty & r_\infty \\ 0 & \frac{N_\beta}{B} & -\left(1 - \frac{A}{B}\right) p_o & \frac{N_r}{B} \\ \frac{M_\alpha}{C} & 0 & \frac{M_q}{C} & \left(1 - \frac{A}{C}\right) p_o \\ p_o & \frac{Y_\beta}{mV} & 0 & -1 \\ \frac{Z_\alpha}{mV} & -p_o & 1 & 0 \end{vmatrix} = \begin{vmatrix} - \frac{N_p}{B} p_o \\ 0 \\ - p_o \alpha_o \\ 0 \end{vmatrix} \qquad (E.27)$$

as:

$$\frac{\alpha_{\alpha_o}}{\alpha_o} = \frac{1}{1 - \left(\frac{\omega_\theta}{p_o}\right)^2 + \frac{d_\beta}{p_o}\frac{d_\alpha}{p_o} + \frac{\left\{\frac{d_\beta}{p_o} - \frac{d_q}{p_o}\right\}\left\{\left(\frac{\omega_{\psi_o}}{p_o}\right)^2 \frac{d_\alpha}{p_o} - \left(\frac{\omega_\theta}{p_o}\right)^2 \frac{d_r}{p_o}\right\}}{1 - \left(\frac{\omega_{\psi_o}}{p_o}\right)^2 + \frac{d_r}{p_o}\ \frac{d_q}{p_o}}} \qquad (E.28)$$

$$\frac{\alpha_N}{\frac{N_p}{B-A}\frac{d_q}{p_o^2}} = \frac{-\left(1+\frac{d_\beta}{d_q}\right)}{\left\{1+\frac{d_q}{p_o}\frac{d_r}{p_o}\right\}\left\{1+\frac{d_\beta}{p_o}\frac{d_\alpha}{p_o}\right\}+\left(\frac{\omega_{\psi_o}}{p_o}\right)^2\left(\frac{\omega_\theta}{p_o}\right)^2-\left(\frac{\omega_{\psi_o}}{p_o}\right)^2\left\{1-\frac{d_\alpha}{p_o}\frac{d_q}{p_o}\right\}-\left(\frac{\omega_\theta}{p_o}\right)^2\left\{1-\frac{d_\beta}{p_o}\frac{d_r}{p_o}\right\}} \qquad \text{(E.29)}$$

$$\frac{\beta_\alpha}{\alpha_o} = -\frac{\left(\frac{\omega_\theta}{p_o}\right)^2\frac{d_r}{p_o}+\frac{d_\alpha}{p_o}\left\{1+\frac{d_q}{p_o}\frac{d_r}{p_o}\right\}}{\left\{1+\frac{d_q}{p_o}\frac{d_r}{p_o}\right\}\left\{1+\frac{d_\beta}{p_o}\frac{d_\alpha}{p_o}\right\}-\left(\frac{\omega_{\psi_o}}{p_o}\right)^2\left\{1-\left(\frac{\omega_\theta}{p_o}\right)^2-\frac{d_\alpha}{p_o}\frac{d_q}{p_o}\right\}-\left(\frac{\omega_\theta}{p_o}\right)^2\left\{1-\frac{d_\beta}{p_o}\frac{d_r}{p_o}\right\}} \qquad \text{(E.30)}$$

$$\frac{\beta_N}{\frac{n_p}{n_v}\frac{b/2}{V}p_o} = -\frac{1}{1-\frac{-\left(\frac{\omega_\theta}{\omega_{\psi_o}}\right)^2\left\{1-\frac{d_\beta}{p_o}\frac{d_r}{p_o}\right\}+\left(\frac{p_o}{\omega_{\psi_o}}\right)^2\left\{1+\frac{d_q}{p_o}\frac{d_r}{p_o}\right\}\left\{1-\frac{d_\beta}{p_o}\frac{d_\alpha}{p_o}\right\}}{1-\left(\frac{\omega_\theta}{p_o}\right)^2-\frac{d_q}{p_o}\frac{d_\alpha}{p_o}}} \qquad \text{(E.31)}$$

where

$$\omega_{\psi_o}^2 = \frac{N_\beta}{B-A}$$

$$\omega_\theta^2 = -\frac{M_\alpha}{B}$$

and d_α, d_β, d_r, d_q represent damping terms:

$$d_\alpha = \frac{Z_\alpha}{mV}$$

$$d_\beta = \frac{Y_\beta}{mV}$$

$$d_r = \frac{N_r}{B - A}$$

$$d_q = \frac{M_q}{B}$$

α_N and β_α are directly proportional to damping terms and should therefore be negligible.

α_{α_o} and β_N have been computed for a limited range of parameters and are plotted in Figs. 42 and 43.

APPENDIX F

Aircraft response to a square wave function p(t)

If p_o is applied as a step at $t = 0$ and taken off instantaneously at $t = t_1$ the computation of the aircraft response to this simplified rolling manoeuvre can be carried out in two steps for the two regimes

$$\text{(a)} \quad 0 > t > t_1 \qquad p = p_o \tag{F.1}$$

$$\text{(b)} \quad t_1 > t > \infty \qquad p = 0 \tag{F.2}$$

This procedure will be outlined here for the simplified case where aircraft damping is neglected. In both regimes p = const. and consequently the equations of motion are linear. $\Delta\alpha$ and β for $0 > t > t_1$ will be computed by the method developed in Appendix E.

For $t > t_1$, $p = 0$ the cross-coupling terms disappear from the equations of motion (D.6 to D.9), which are thus reduced to:

$$\omega_\psi^2 \beta - \dot{r} = 0 \tag{F.3}$$

$$-\omega_\theta^2 \Delta\alpha - \dot{q} = 0 \tag{F.4}$$

$$-r - \dot{\beta} = 0 \tag{F.5}$$

$$q - \dot{\alpha} = 0 \tag{F.6}$$

This system will split up into two uncoupled second order equations

$$\omega_\psi^2 \beta - \ddot{\beta} = 0 \tag{F.7}$$

$$\omega_\theta^2 \Delta\alpha - \Delta\ddot{\alpha} = 0 \tag{F.8}$$

These describe the two uncoupled and - as assumed - undamped aircraft oscillations in pitch and in yaw with the frequencies ω_θ and ω_ψ respectively with the general solutions

$$\Delta\alpha = C_\alpha + a_{31} \cos(\omega_\theta t) + a_{32} \sin(\omega_\theta t) \tag{F.9}$$

$$\beta = C_\beta + b_{31} \cos(\omega_\psi t) + b_{32} \sin(\omega_\psi t) \tag{F.10}$$

As there is no external disturbance applied, the constants

$$C_\alpha = C_p = 0$$

If the values for $\Delta\alpha$, β, $\Delta\dot{\alpha}$ and $\dot{\beta}$ as computed for the step function with $p = p_o$ at $t = t_1$ are substituted as initial conditions into the solution F.9 and F.10, the constants a_{31} .... b_{32} can be calculated and the response computed for $t > t_1$. When reducing equations (D.6 to D.9) to equations (F.3 to F.6) the product terms with p_o disappeared which constitute discontinuities in $\dot{r}$, $\dot{q}$, $\dot{\beta}$ and $\dot{\alpha}$ at $t = t_1$.

Thus if $\dot{r}_1$ $\dot{q}_1$ $\dot{\beta}_1$ and $\dot{\alpha}_1$ are instantaneous values at $t = t_1 - \varepsilon$ where ε is infinitesimally small, the corresponding values at $t = t_1 + \varepsilon$ will be obtained by substracting the corresponding discontinuities:

$$\dot{r}\,(t_1 + \varepsilon) = \dot{r}\,(t_1 - \varepsilon) + \frac{B - A}{B + A}\, p_o\, q_1 \qquad \text{(F.11)}$$

$$\dot{q}\,(t_1 + \varepsilon) = \dot{q}\,(t_1 - \varepsilon) - p_o\, r_1 \qquad \text{(F.12)}$$

$$\dot{\beta}\,(t_1 + \varepsilon) = \dot{\beta}\,(t_1 - \varepsilon) - p_o\, \Delta\alpha_1 - p_o\, \alpha_o \qquad \text{(F.13)}$$

$$\dot{\alpha}\,(t_1 + \varepsilon) = \dot{\alpha}\,(t_1 - \varepsilon) + p_o\, \beta_1 \qquad \text{(F.14)}$$

If for $t < t_1$ we introduce

$$t' = t - t_1 \qquad \text{(F.15)}$$

Equations F.9 and F.10 can be rewritten and differentiated

$$\Delta\alpha = \alpha_{31} \cos(\omega_\theta t') + \alpha_{32} \sin(\omega_\theta t') \qquad \text{(F.16)}$$

$$\beta = \beta_{31} \cos(\omega_\psi t') + \beta_{32} \sin(\omega_\theta t') \qquad \text{(F.17)}$$

$$\dot{\alpha} = \omega_\theta \{-\alpha_{31} \sin(\omega_\theta t') + \alpha_{32} \cos(\omega_\theta t')\} \qquad \text{(F.18)}$$

$$\dot{\beta} = \omega_\psi \{-\beta_{31} \sin(\omega_\psi t') + \beta_{32} \cos(\omega_\psi t')\} \qquad \text{(F.19)}$$

Substituting the initial conditions at $t' = 0$ this gives

$$\Delta\alpha_1 = \alpha_{31} \qquad \text{(F.20)}$$

$$\beta_1 = \beta_{31} \qquad \text{(F.21)}$$

$$\dot{\alpha}\,(t_1 - \varepsilon) + p_o\, \beta_1 = \omega_\theta\, \alpha_{32} \qquad \text{(F.22)}$$

$$\dot{\beta}\,(t_1 - \varepsilon) - p_o\, \Delta\alpha_1 - p_o\, \alpha_o = \omega_\psi\, \beta_{32} \qquad \text{(F.23)}$$

This determines the constants α_{31} .... β_{32} and the amplitudes of the "residual" pitching and yawing oscillation for $t > t_1$ are then given by

$$\alpha_3 = \sqrt{\alpha_{31}^2 + \alpha_{32}^2} \qquad \text{(F.24)}$$

$$\beta_3 = \sqrt{\beta_{31}^2 + \beta_{32}^2} \qquad \text{(F.25)}$$

These values can be calculated without computing the responses $\alpha(t)$ and $\beta(t)$. Only the values at $t = t_1$ of $\Delta\alpha$, β, $\dot{\alpha}$ and $\dot{\beta}$ have to be computed from equations (E.1 ... E.4) and substituted into equations (F.20 ... F.23) to give the amplitudes α_3 and β_3 according to equations (F.24) and (F.25).

TABLE 1

Geometric, inertia and aerodynamic data of the supersonic fighter aircraft used as an example

$S = 400\ ft^2$ $\quad b = 35\ ft$ $\quad \ell = 28\ ft$

$W = 25,000\ lb$ $\quad A = 900,000\ lb\ ft^2$ $\quad i_A = 0.125$

$B = 4,100,000\ lb\ ft^2$ $\quad i_B' = 0.54$

$C = 5,000,000\ lb\ ft^2$ $\quad i_C = 0.65$

Mach No.	0.8			1.0	1.5	2.0
Height	0	40,000	60,000	60,000	60,000	60,000
V (ft/sec)	892	770	770	960	1,440	1,920
μ_2	47.3	186.2	492	492	492	492
ℓ_ξ		-0.25		-0.25	-0.12	-0.09
ℓ_p		-0.25		-0.27	-0.30	-0.25
ℓ_v		-0.10		-0.11	-0.09	-0.075
$dn_\xi/d\alpha$		-0.07		-0.07	-0.07	-0.07
n_{po}		0.05		0.05	0.05	0.05
$dn_p/d\alpha$		-0.3		-0.3	-0.3	-0.3
n_v		0.20		0.22	0.25	0.24
n_r		-0.46		-0.48	-0.52	-0.48
m_w		-0.083		-0.246	-0.335	-0.300
m_q		-0.376		-0.481	-0.295	-0.196
$m_{\dot{w}}$		0.218		0.292	0.070	-0.005
y_v		-0.32		-0.32	-0.32	-0.32
z_w		-2.175		-2.875	-1.77	-1.19

$$\ell_r = y_p = n_{\xi o} = d\ell_v/d\alpha = 0$$

TABLE 2

Effect of autostabilization on fin and tail loads experienced by an aircraft rolling through $\Delta\phi$ with $\xi = 8^{\circ}$

(a) Tail load peaks

Autostabilization term operating / $\Delta\phi$	Basic aircraft	$M_{(p \times r)}$	$M_{(p \times r)} + N_{(p \times q)}$	$8 \times M_q$	$8 \times M_q + 8 \times N_r$
90°	7.5	5	6	4	2.5
180°	10	12	13	7.5	5
270°	16	16	22	12	5
360°	17.5	16	28	12	5

(b) Fin load peaks

Autostabilization term / $\Delta\phi$	Basic aircraft	$M_{(p \times r)}$	$M_{(p \times r)} + N_{(p \times q)}$	$8 \times M_q$	$8 \times M_q + 8 \times N_r$	$8 \times n_r$
90°	12	9	9	10	7.5	7
180°	26	9	9	10	7.0	7
270°	30	9	9	11	7.0	9
360°	30	11	9	16	9.0	16

TABLE 3

Critical rolling velocity p_1 and autorotational rate of roll p_2 for the supersonic fighter aircraft of Table 1

Height ft	Mach No.	ω_θ^2	$\omega_{\psi_o}^2$	$\left\{ z_w \frac{\ell_v}{\ell_p} \frac{i_C - 2i_A}{n_v} \right\}$	$\left(\frac{\omega_\theta}{\omega_{\psi_o}}\right)^2$	ν
40,000	0.8	2.8	4.15	-2.18	0.675	0.083
60,000	0.8	1.1	1.3	-2.18	0.85	0.032
	1.0	5.0	2.85	-2.13	1.75	0.024
	1.5	11.2	6.25	-0.85	1.80	0.008

Height (ft)	Mach No.	$\alpha_o = 0$				$\alpha_o = -5^o$			
		$\left(\frac{p_1}{\omega_{\psi_o}}\right)$	$\left(\frac{p_2}{\omega_{\psi_o}}\right)$	p_1	p_2	$\left(\frac{p_1}{\omega_{\psi_o}}\right)$	$\left(\frac{p_2}{\omega_{\psi_o}}\right)$	p_1	p_2
40,000	0.8	0.8	1.0	94 °/sec	117	0.74	1.15	80 °/sec	125
60,000	0.8	–	–	–	–	0.81	1.17	53	86
	1.0	1.05	1.70	110	164	0.92	1.75	89	170
	1.5	1.04	1.75	149	250	0.98	1.80	140	258

TABLE 4

Data obtained in the computation of aircraft responses to a square-wave in p by the method of Appendices E and F

$\left(\frac{\omega_\theta}{p_o}\right)^2$	$\left(\frac{\omega_\psi}{p_o}\right)^2$	$\frac{A}{B}$	$\left(\frac{\omega_1}{p_o}\right)$	$\left(\frac{\omega_2}{p_o}\right)$	$\left(\frac{\beta}{\alpha}\right)_1$	$\left(\frac{\beta}{\alpha}\right)_2$	$\frac{\alpha_\infty}{\alpha_o}$	$\frac{\alpha_{11}}{\alpha_o}$	$\frac{\alpha_{21}}{\alpha_o}$
4	4	0.25	2.80	1.104	-0.960	0.806	0.20	0.230	-0.430
2	2	0	2.414	0.414	-1.000	+1.000	+1.000	0.207	-1.207

$$\left(\frac{\alpha_{12}}{\alpha_o}\right) = \left(\frac{\alpha_{22}}{\alpha_o}\right) = \left(\frac{\beta_\infty}{\alpha_o}\right) = 0$$

KT.2078.C.P.435.K3 - Printed in Great Britain

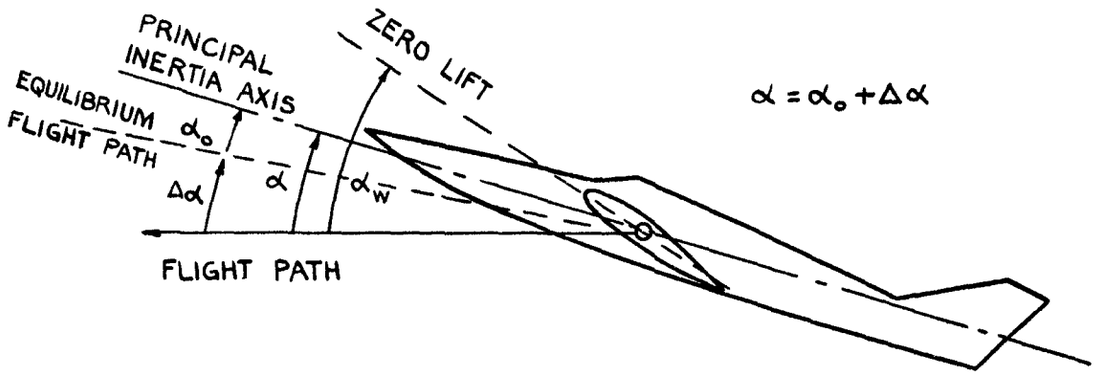

FIG.1. AIRCRAFT INCIDENCE IN DISTURBED FLIGHT.

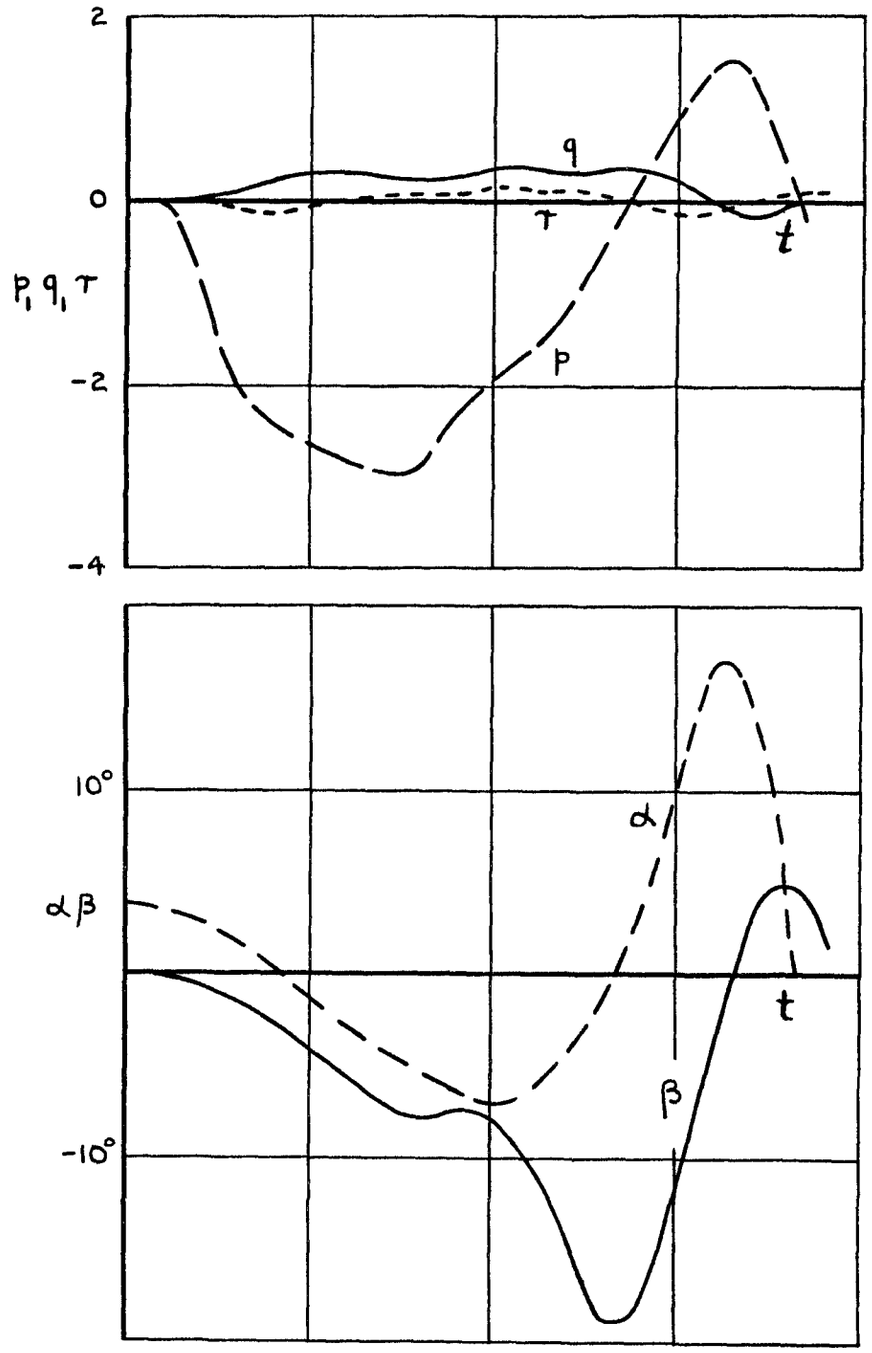

FIG. 2. TYPICAL FLIGHT RECORD OF A ROLLING MANOEUVRE OF A MODERN FIGHTER AEROPLANE AT 40,000 FT. ALTITUDE.

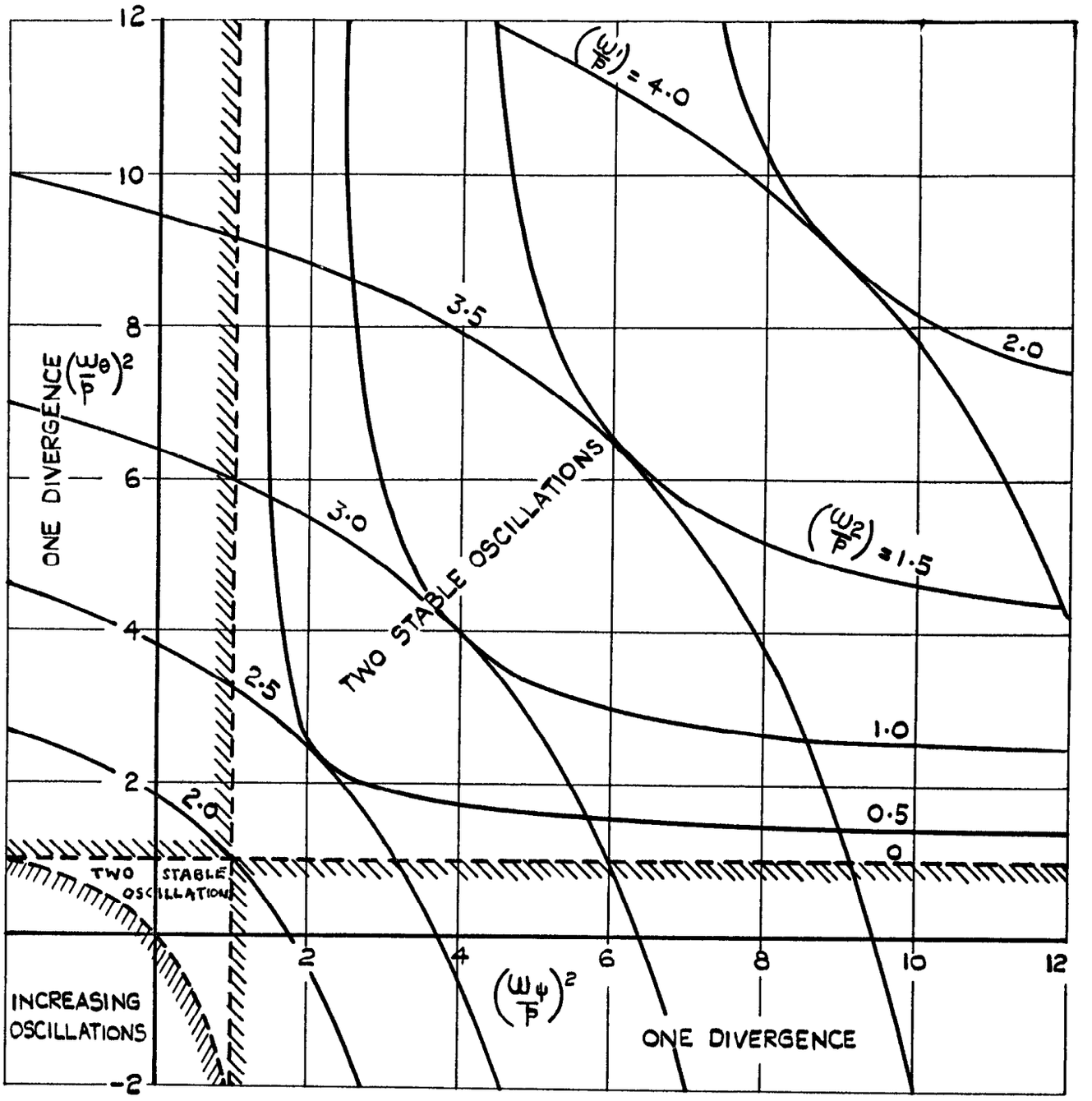

FIG. 3. STABILITY DIAGRAM FOR THE ROLLING AIRCRAFT.

(THE UNCOUPLED LATERAL AND LONGITUDINAL FREQUENCIES ω_1 AND ω_2 ARE THE FREQUENCIES OF THE OSCILLATORY MODES OF MOTION OF THE AIRCRAFT ROLLING AT RATE p) [FROM NACA T.N. 1627].

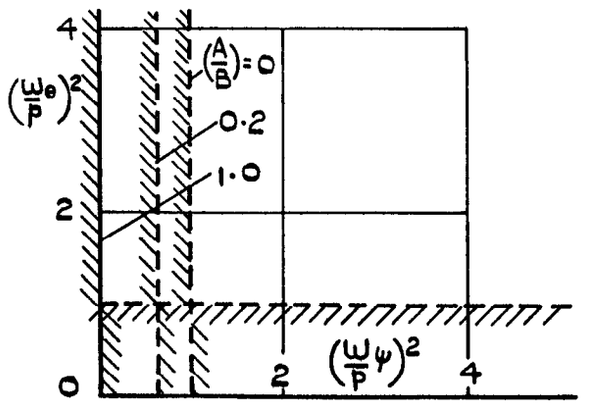

FIG. 4. EFFECT OF INERTIA DISTRIBUTION ON STABILITY BOUNDARIES.

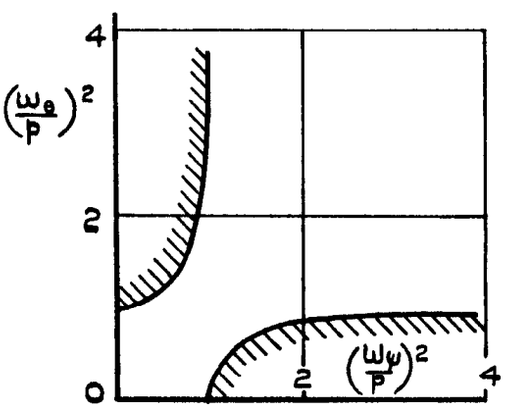

FIG. 5. EFFECT OF DAMPING IN PITCH OR/AND YAW ON STABILITY BOUNDARIES.

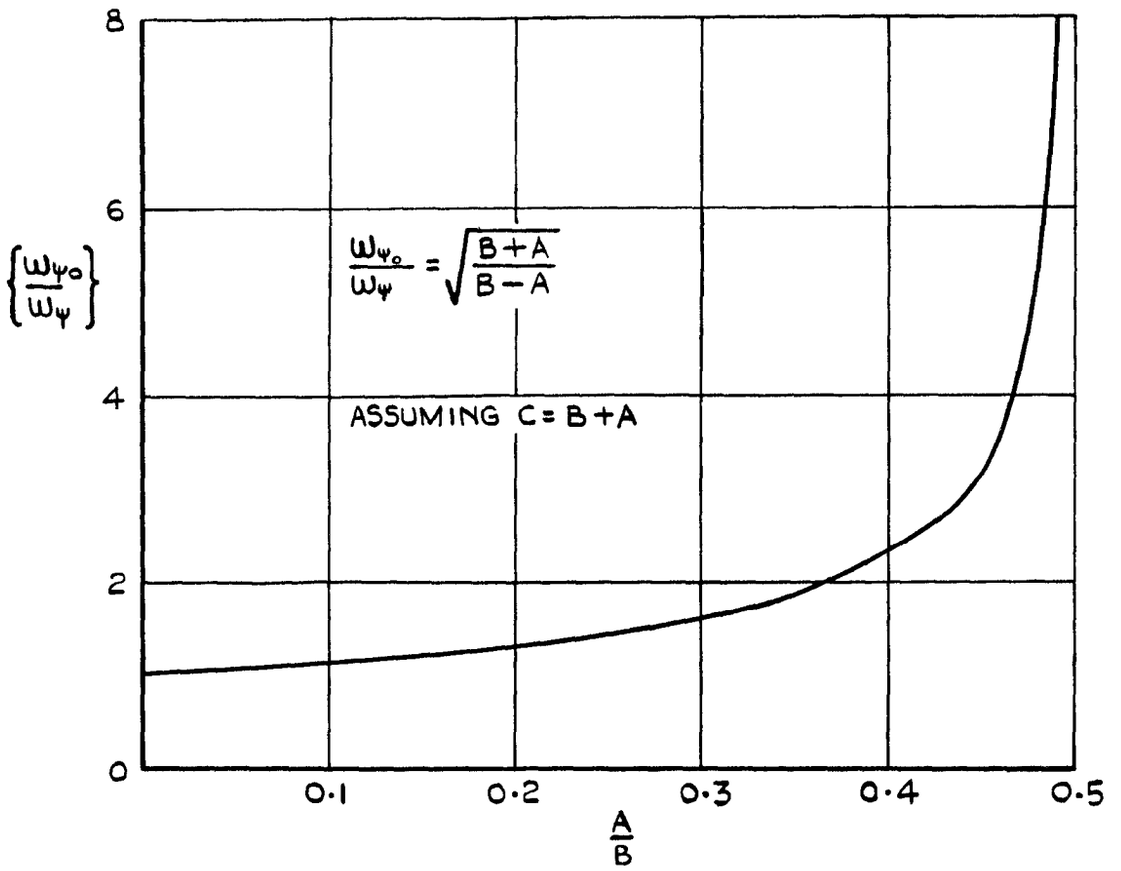

FIG. 6. EFFECT OF INERTIA DISTRIBUTION ON RESONANCE FREQUENCY IN YAW.

(ω_ψ = ANGULAR FREQUENCY OF THE UNCOUPLED PURE DIRECTIONAL OSCILLATION).

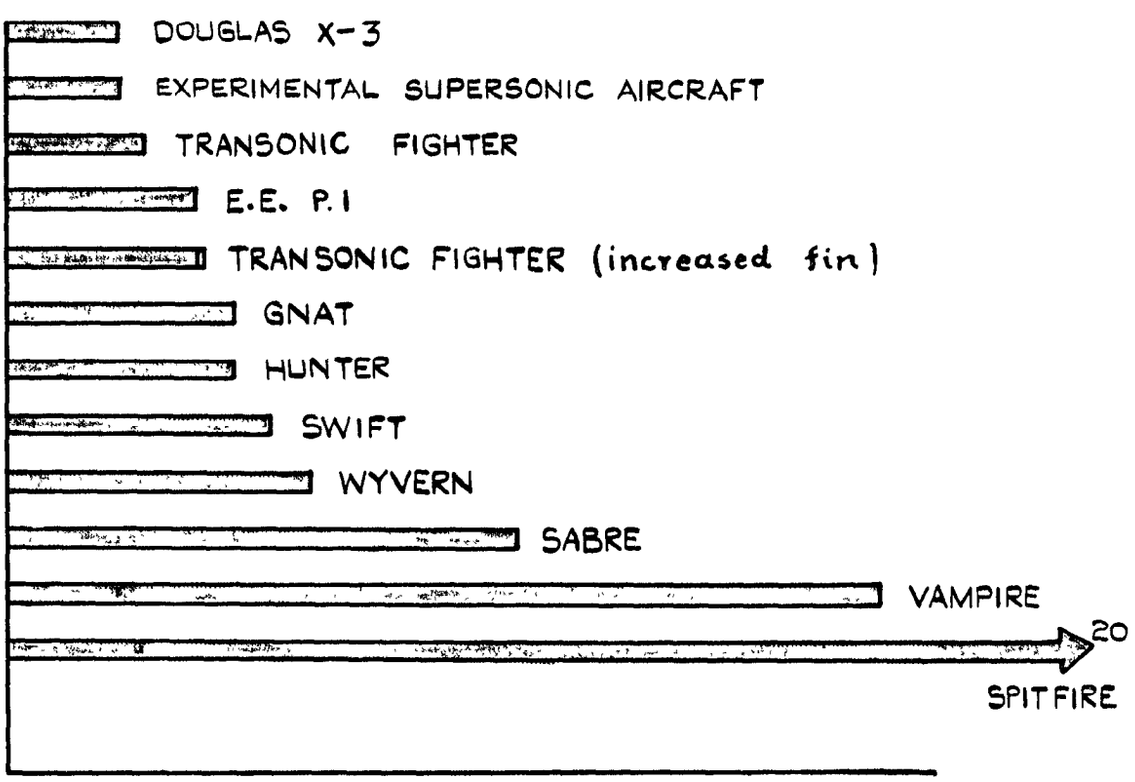

FIG. 7. CRITICAL RATE OF ROLL FOR A NUMBER OF AIRCRAFT FLYING AT V_i = 240 KNOTS.

(P_{CRIT} INCREASES PROPORTIONAL TO V_i).

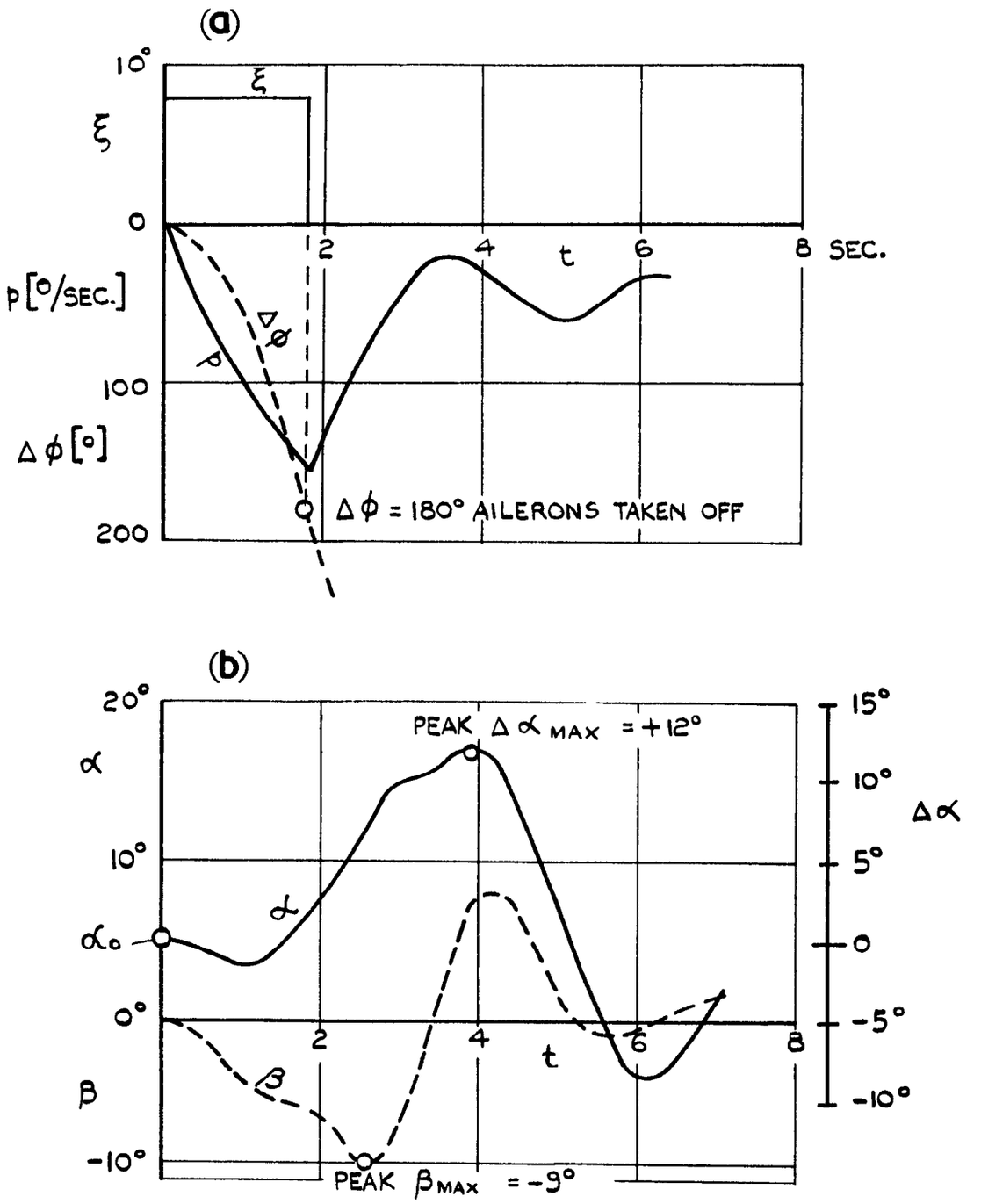

FIG.8.(a&b) ILLUSTRATION OF THE MANOEUVRE COMPUTED ON THE SIMULATOR.

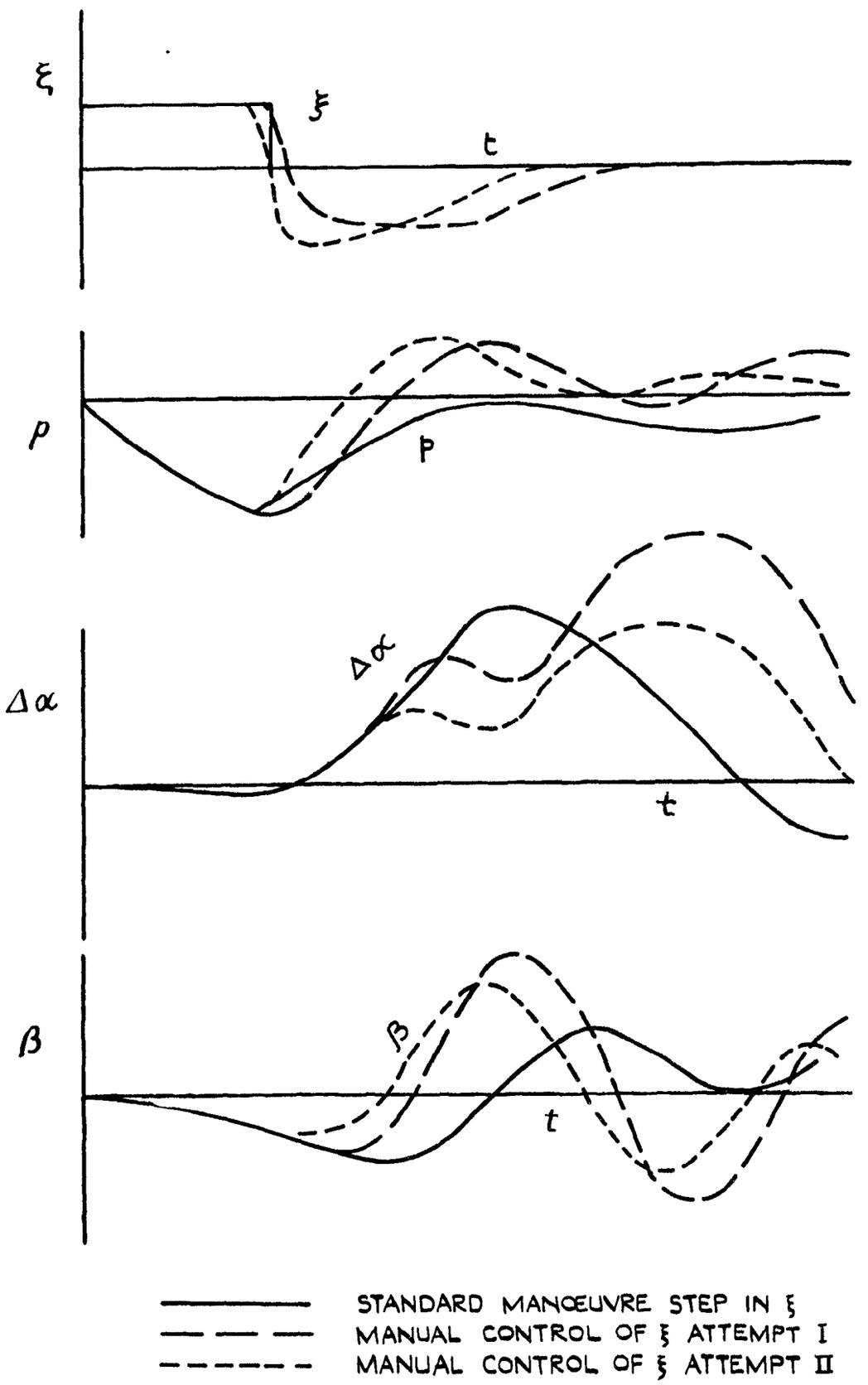

FIG. 9. EFFECT OF PILOTS CONTROL MOVEMENTS ON AIRCRAFT RESPONSE IN ROLLING MANOEUVRES WHEN COMPARED WITH THE "STANDARD MANOEUVRE."

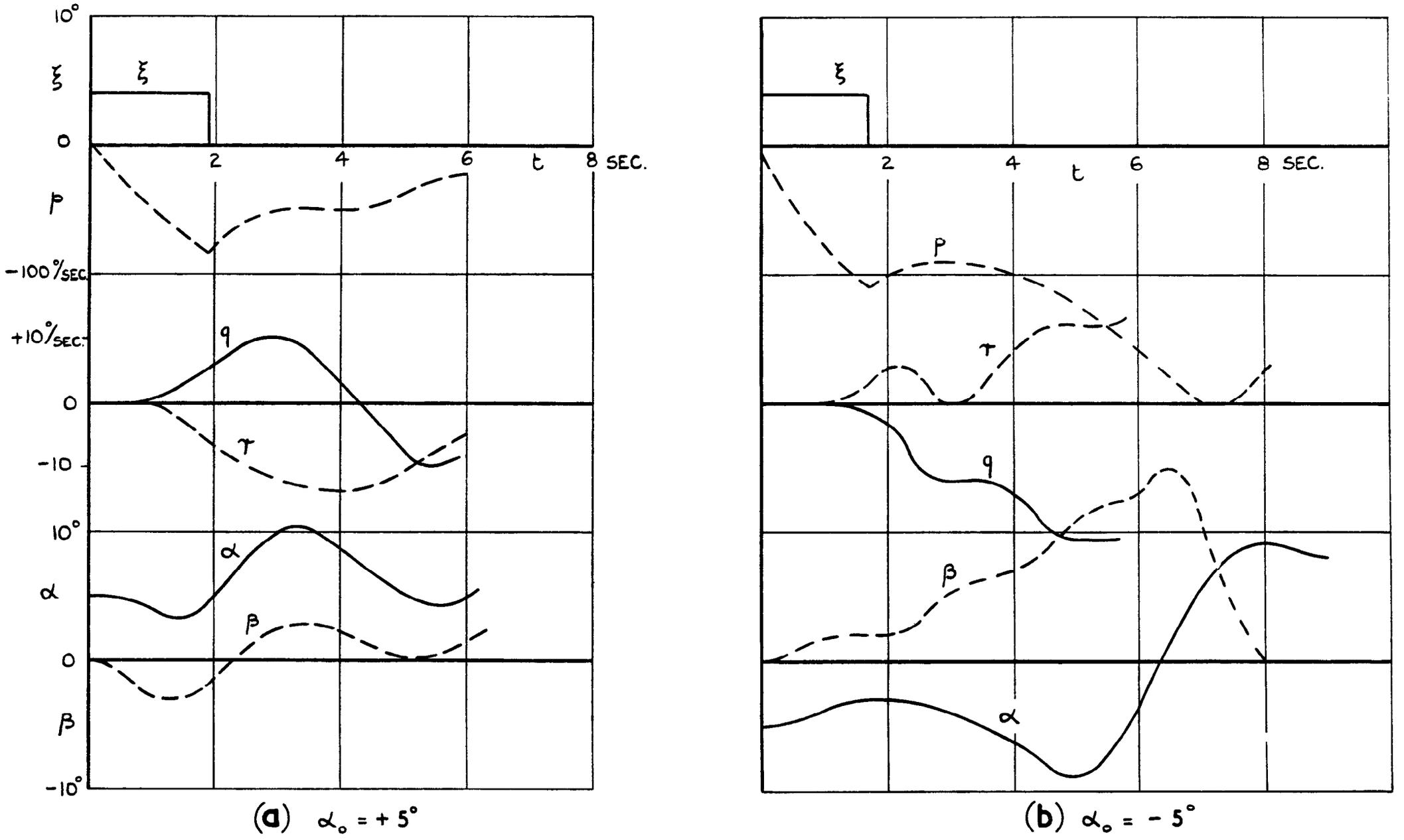

FIG.10(a & b). SIMULATED RESPONSES OF A SUPERSONIC FIGHTER AT 40,000FT. M=0·8 AILERONS TAKEN OFF WHEN THE AIRCRAFT HAS ROLLED THROUGH $\Delta\phi = 90°$.

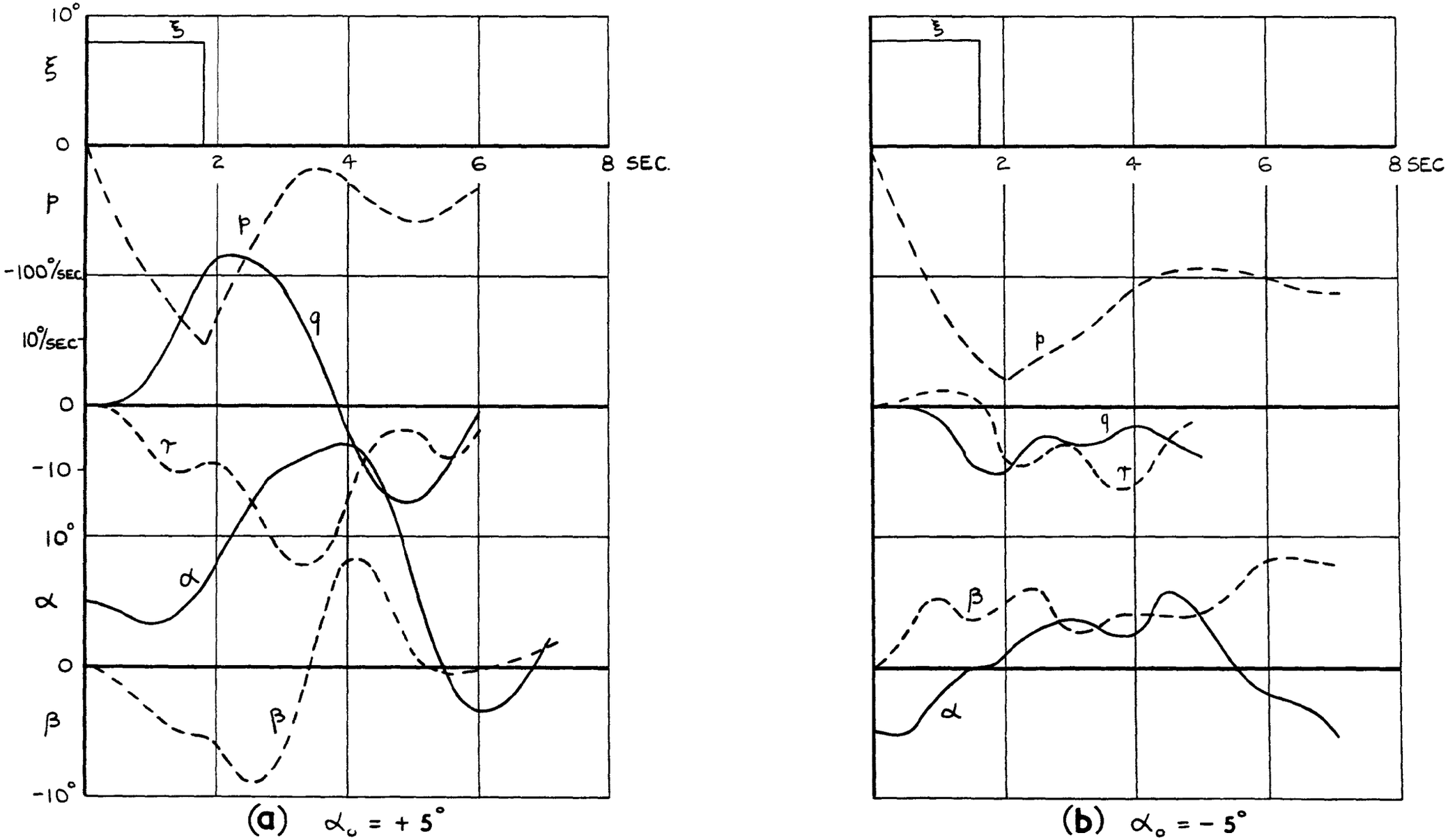

FIG.11(a&b). SIMULATED RESPONSES OF A SUPERSONIC FIGHTER AT 40,000FT. M=0·8 AILERONS TAKEN OFF WHEN THE AIRCRAFT ROLLED THROUGH $\Delta\phi = 180°$.

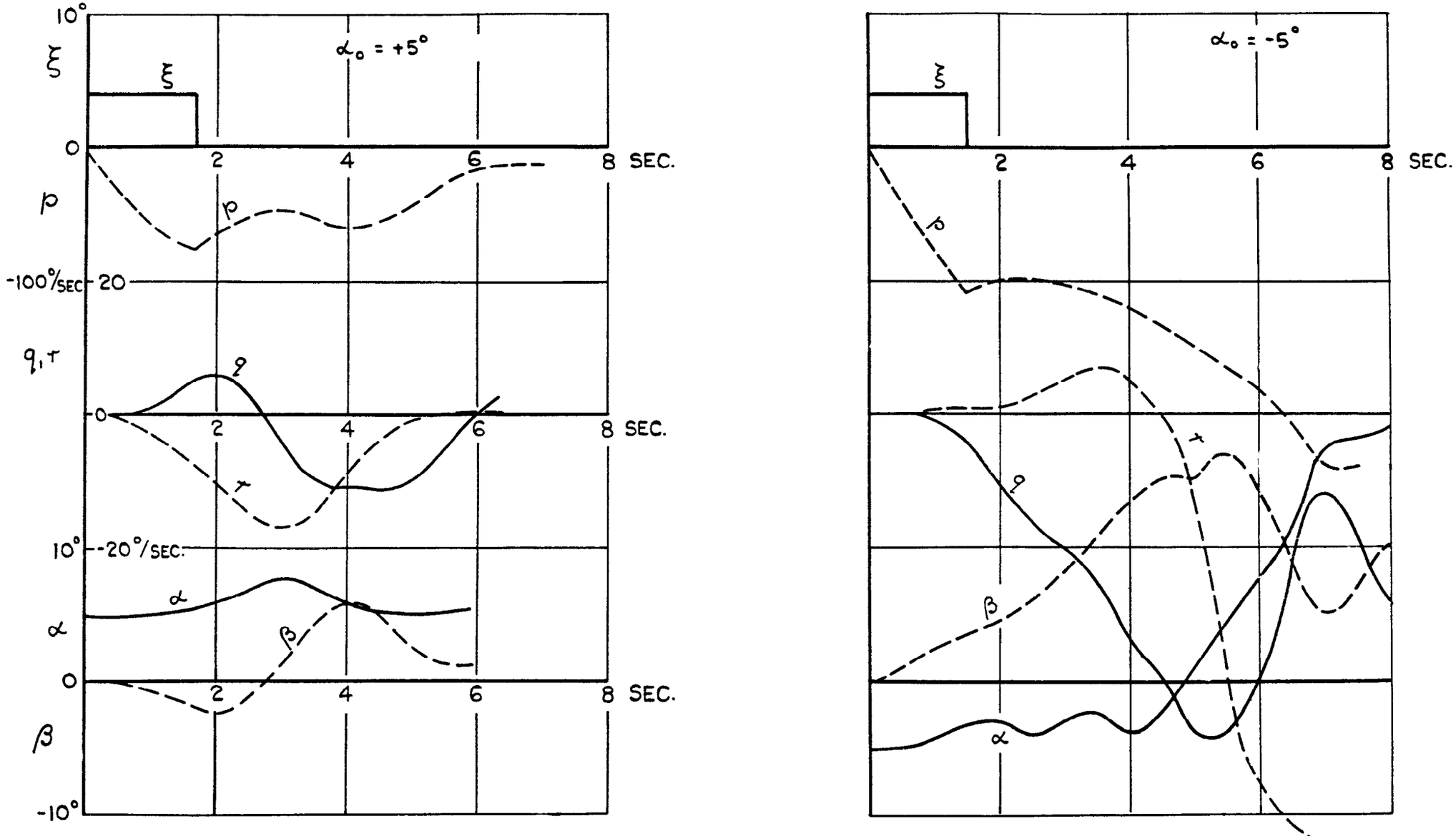

FIG. 12. SIMULATED RESPONSES OF A SUPERSONIC FIGHTER AT 40,000 FT. M = 0·8 WITH m_w INCREASED TO −0·32 AILERONS TAKEN OFF WHEN AIRCRAFT ROLLED THROUGH $\Delta\phi = 90°$

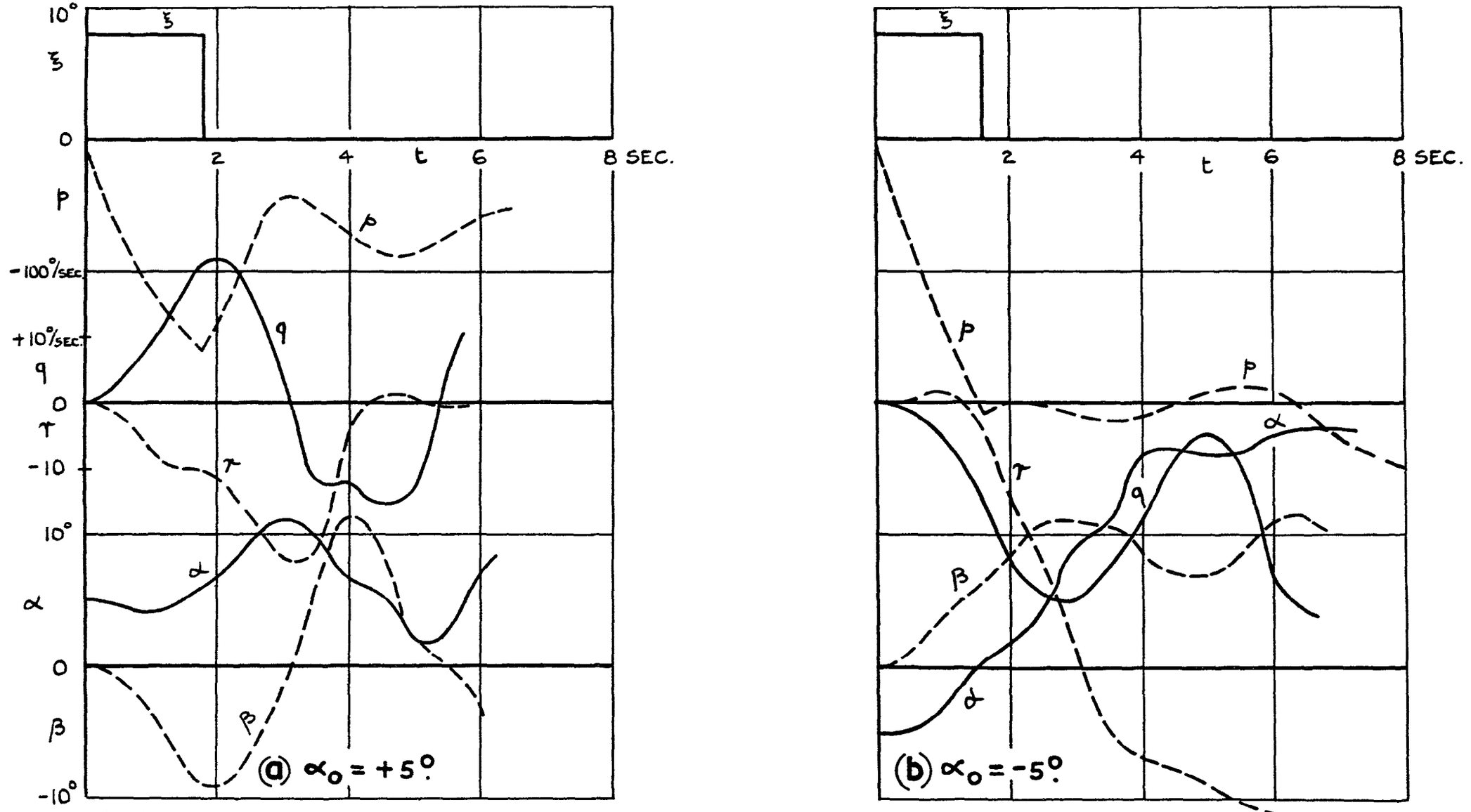

FIG. 13. (a&b) SIMULATED RESPONSES OF A SUPERSONIC FIGHTER AT 40,000 FT. M = 0·8 WITH m_w INCREASED TO −0·32 AILERONS TAKEN OFF WHEN THE AIRCRAFT ROLLED THROUGH $\Delta\phi = 180°$.

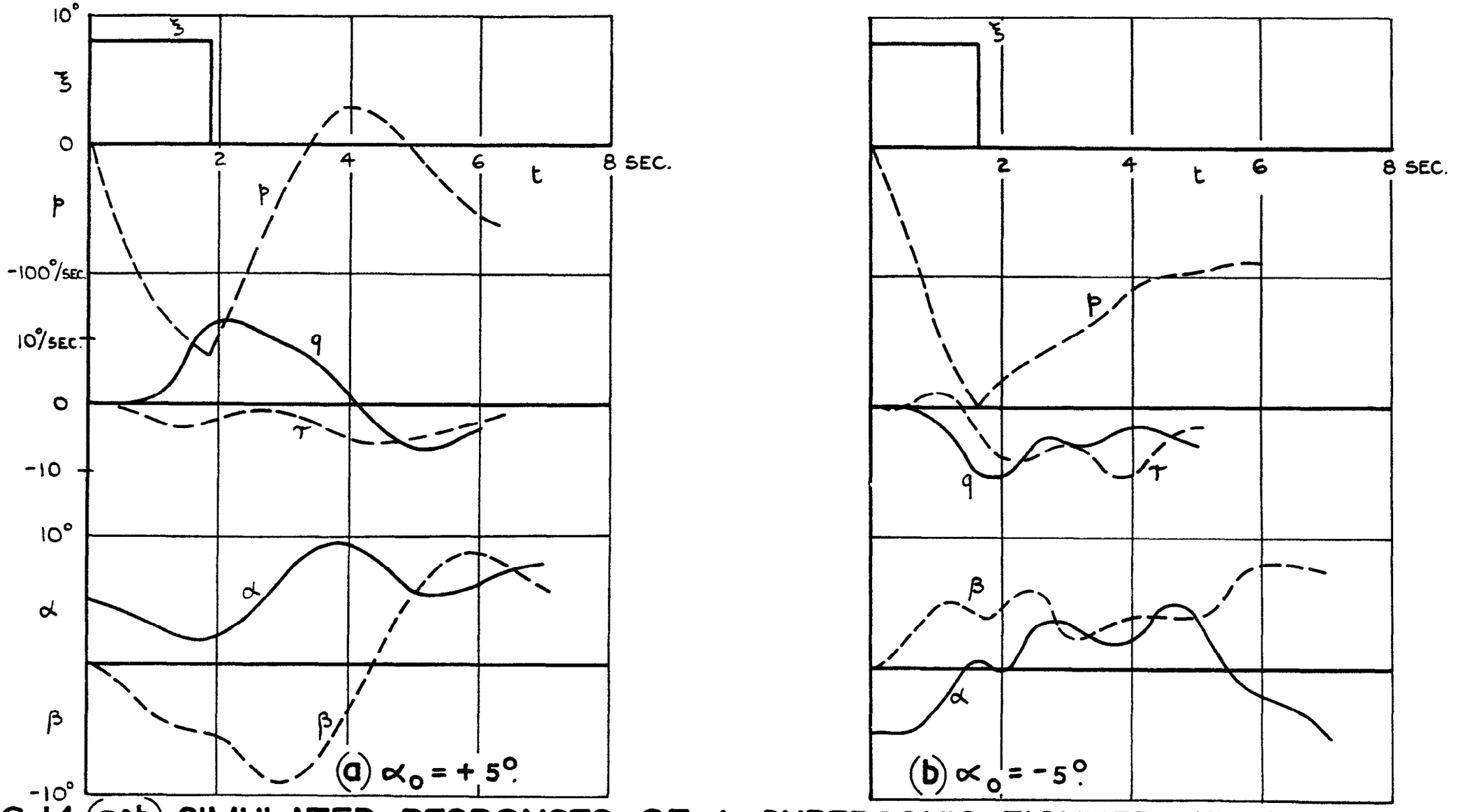

FIG. 14.(a&b) SIMULATED RESPONSES OF A SUPERSONIC FIGHTER AT 40,000 FT. M = 0·8 WITH n_v REDUCED TO 0·05 AILERONS TAKEN OFF WHEN AIRCRAFT HAS ROLLED THROUGH $\Delta\phi = 180°$

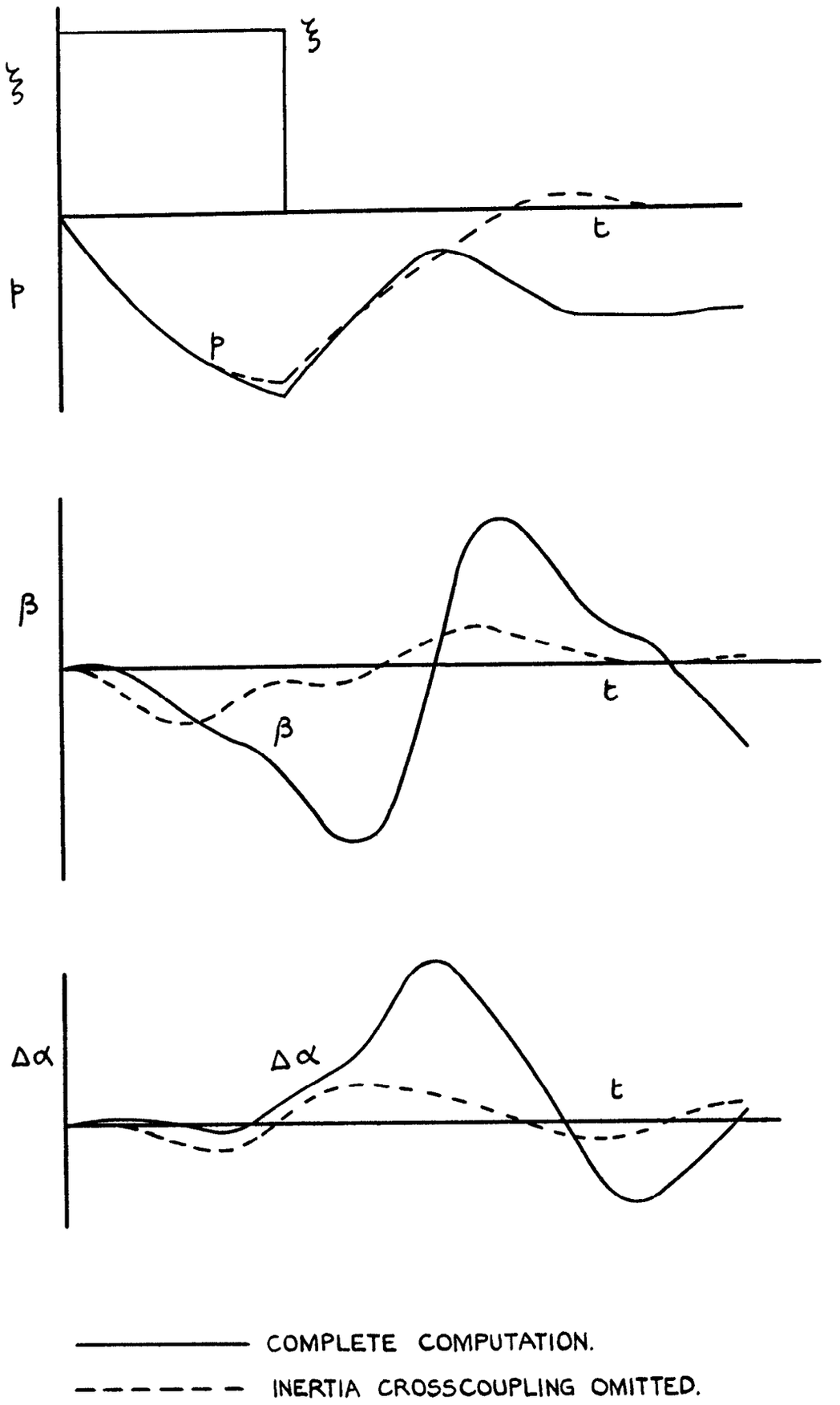

FIG.15. EFFECT OF INERTIA CROSSCOUPLING ON THE RESPONSE OF AN AIRCRAFT TO AILERON MANOEUVRES.

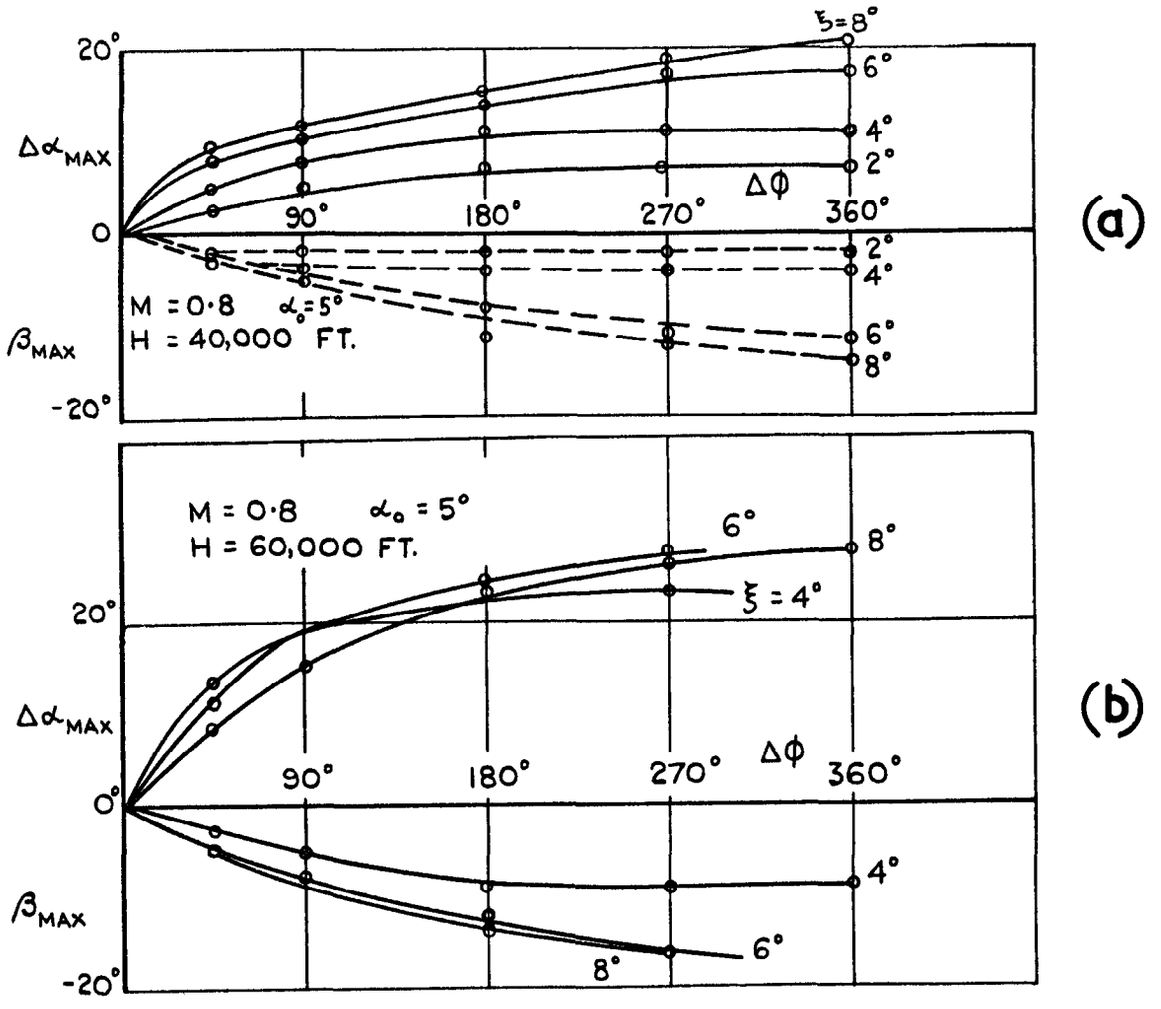

THE PEAKS REACHED INCREASE PROGRESSIVELY WITH THE DURATION OF THE AILERON APPLICATION & REACH A MAXIMUM AFTER WHICH NO FURTHER DETERIORATION IS OBSERVED. NO INSTABILTY.

FIG.16(a&b). VARIATION OF $\Delta\alpha_{max.}$ AND $\beta_{max.}$ WITH THE ANGLE OF BANK $\Delta\phi$ WHERE AILERON WAS CENTRALISED.

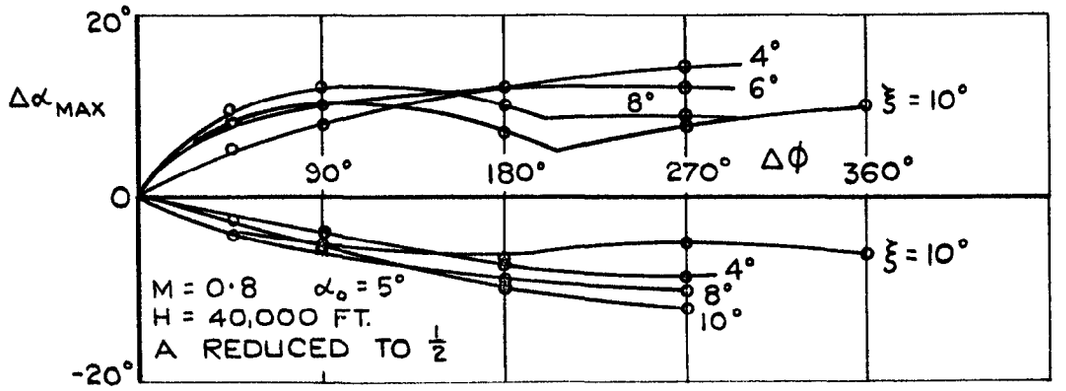

THE DURATION OF THE AILERON APPLICATION IS CRITICAL FOR THE RESPONSE IN α AND β. WORST PEAKS OCCUR WHEN AILERON IS TAKEN OFF AFTER $\Delta\phi = 90°$.

FIG.17. VARIATION OF $\Delta\alpha_{max.}$ WITH $\Delta\phi$ WHERE AILERON WAS CENTRALISED.

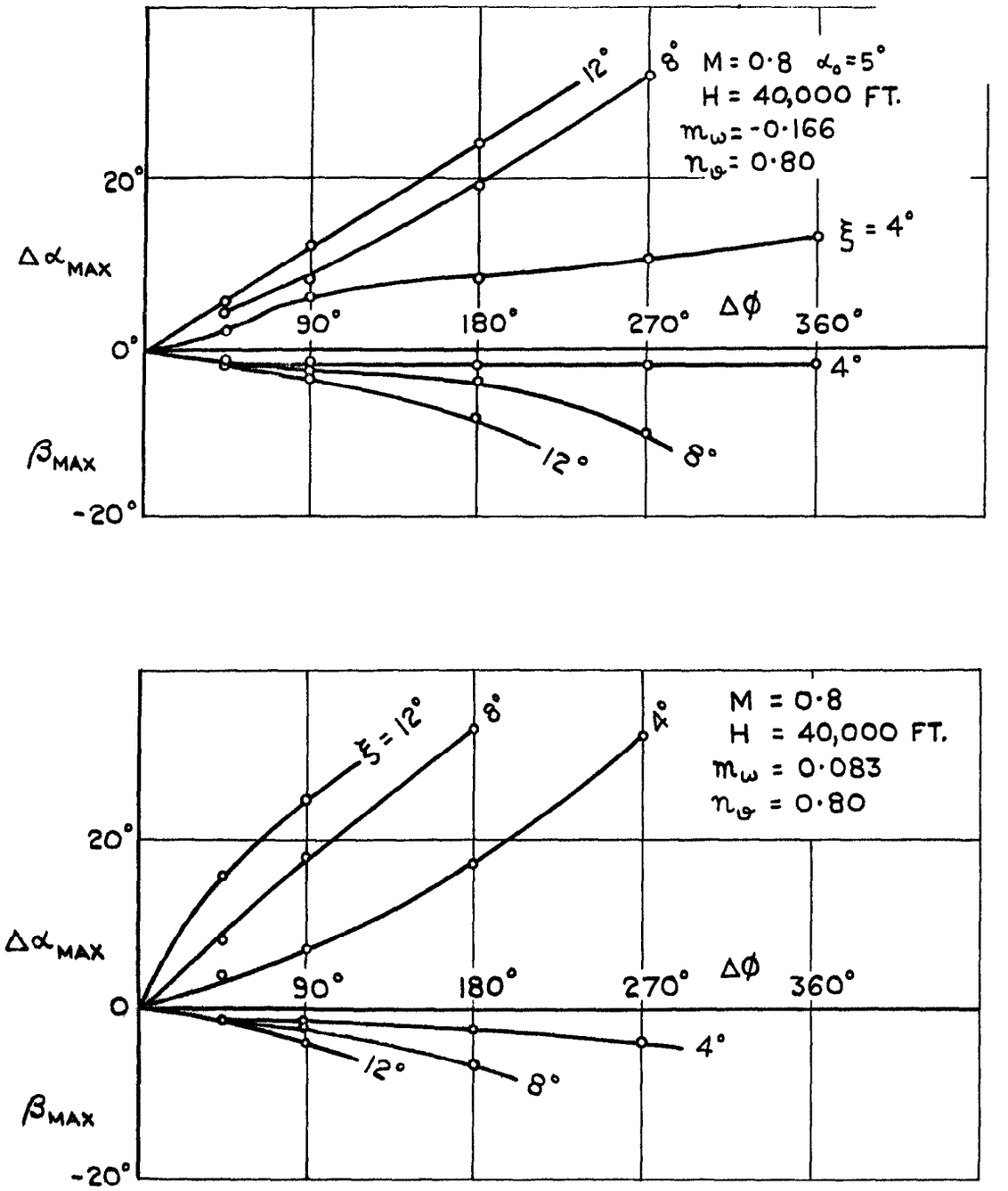

FIG. 18. $\Delta\alpha$ max. AND β max. IN ROLLS DIVERGENT CONDITION.

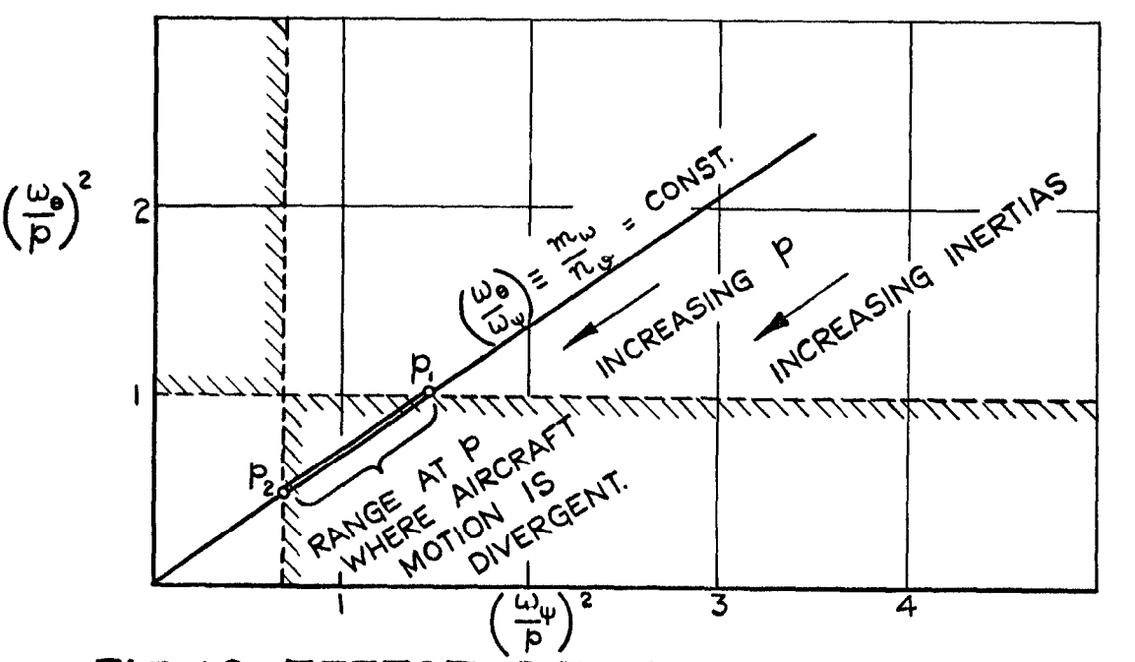

FIG. 19. EFFECT OF VARYING p ON THE STABILITY OF THE LATERAL-LONGITUDINAL MOTION.

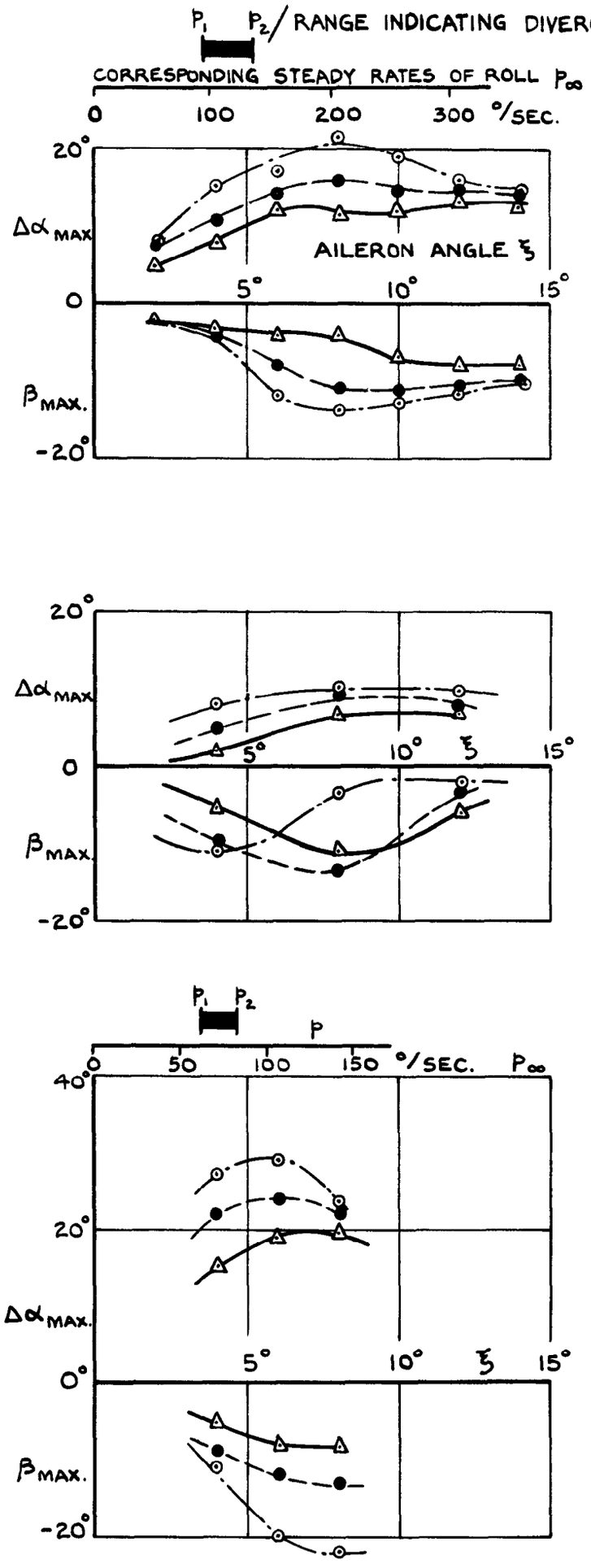

NOTE :- P_∞ IS THE STEADY RATE OF ROLL CORRESPONDING TO ξ.

FIG.20(a-c) EFFECT OF AILERON ANGLE OR RATE OF ROLL ON $\Delta\alpha_{max.}$ AND $\beta_{max.}$

α_o = INCIDENCE OF PRINCIPAL AXIS OF INERTIA

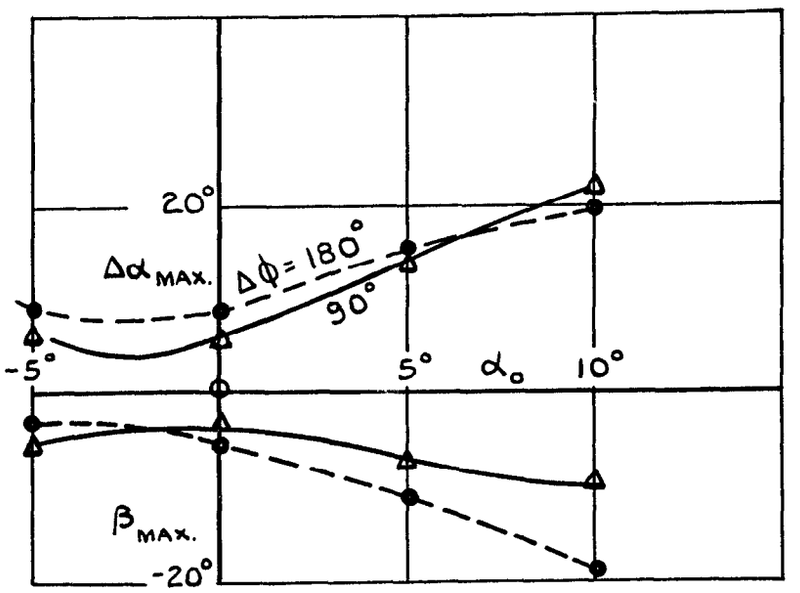

(a) $\Xi = 12°$
H = 40,000 FT.
M = 0·8

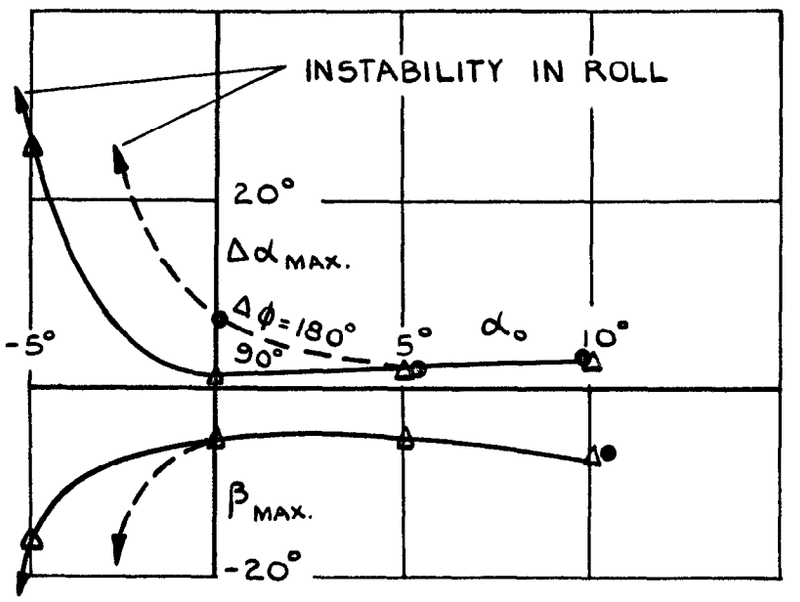

(b) $\Xi = 4°$
H = 60,000 FT.
M = 1·0

FIG. 21(a & b). EFFECT OF INCIDENCE ON $\Delta\alpha_{max.}$ AND $\beta_{max.}$

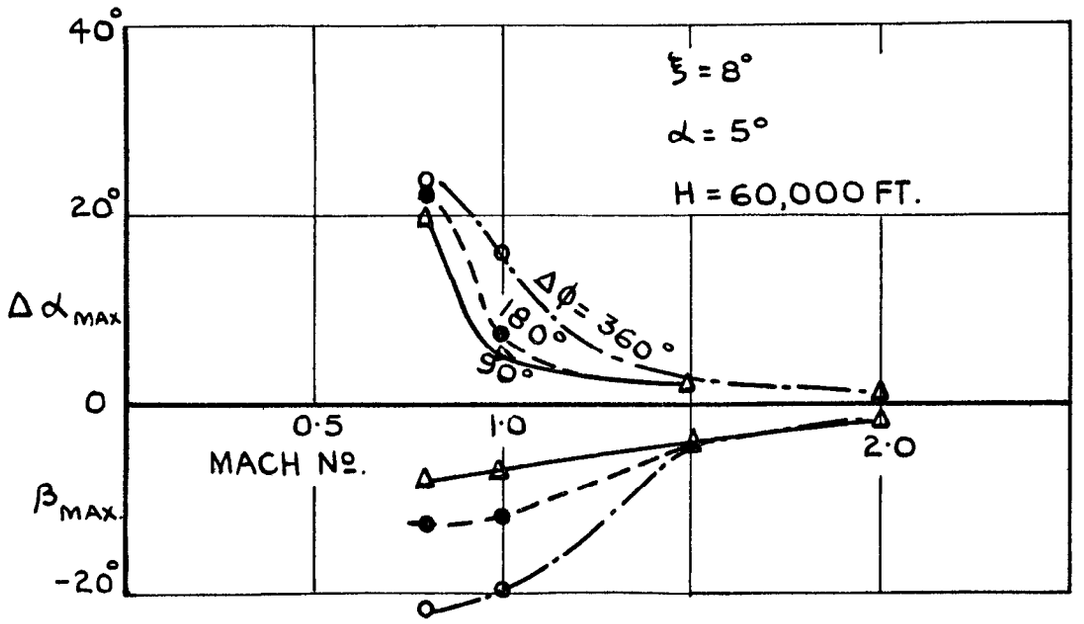

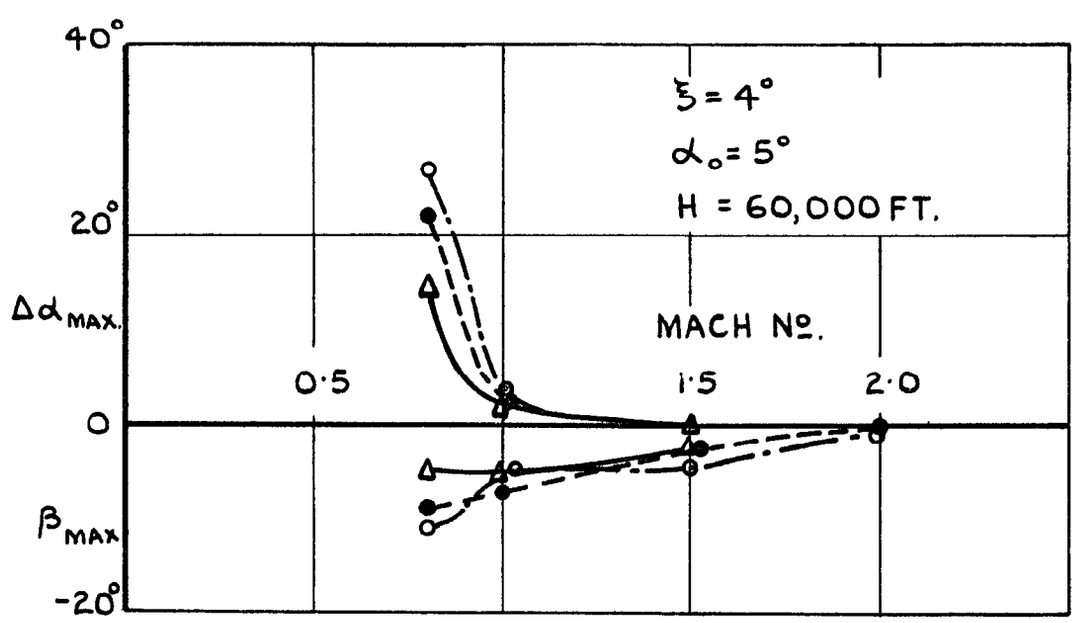

NOTE:- THE CHANGES IN THE AERODYNAMIC DERIVATIVES WITH MACH Nº. HAVE BEEN TAKEN INTO ACCOUNT, THUS THE TRENDS INDICATED ARE NOT PURE SPEED EFFECTS.

FIG. 22. VARIATION OF $\Delta\alpha_{max}$ AND β_{max} WITH MACH No. (AIRCRAFT OF TABLE I)

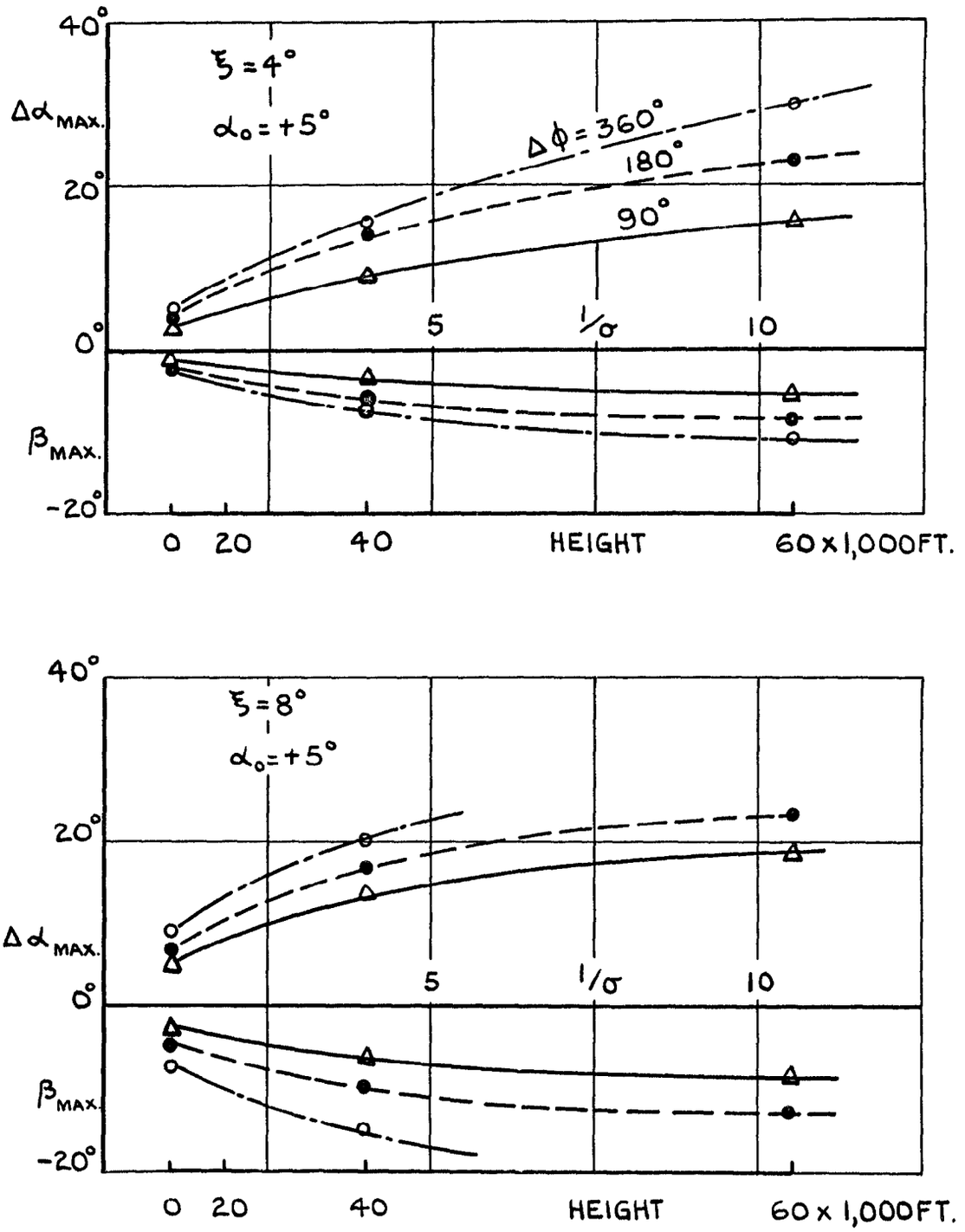

FIG. 23. EFFECT OF HEIGHT ON $\Delta\alpha_{max.}$ AND $\beta_{max.}$ IN ROLLS. (AIRCRAFT OF TABLE I M = 0.8)

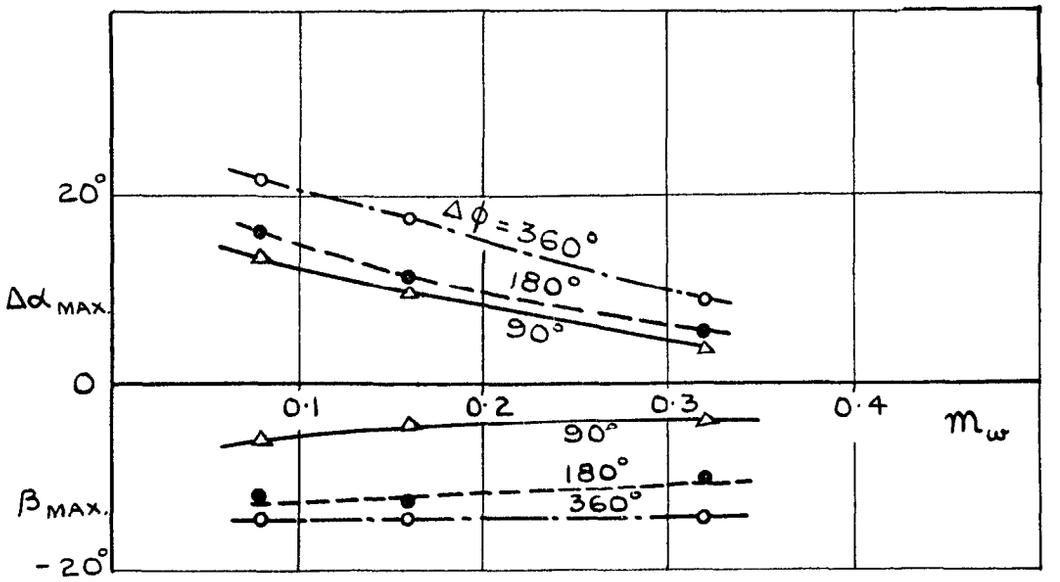

FIG.24. EFFECT OF m_w ON $\Delta\alpha_{max}$ AND β_{max}
(H=40,000FT. M=0·8 α_o=+5° n_v=0·22 ξ=8°)

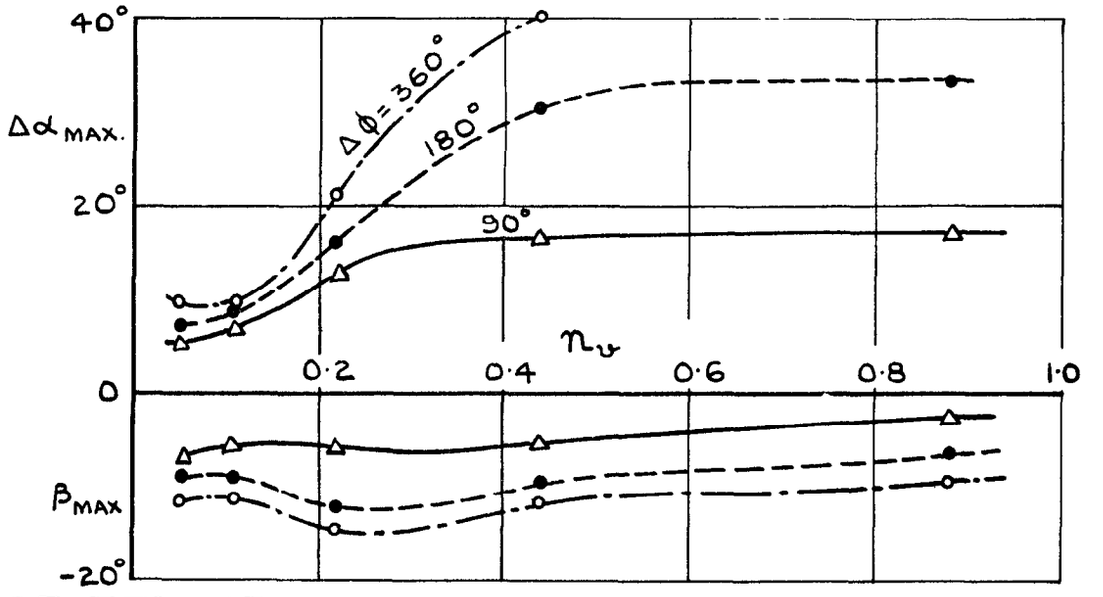

FIG.25. EFFECT OF n_v ON $\Delta\alpha_{max}$ AND β_{max}
(H=40,000FT. M=0·8 α_o=5° $m_{\dot{w}}$=0·08 ξ=8°)

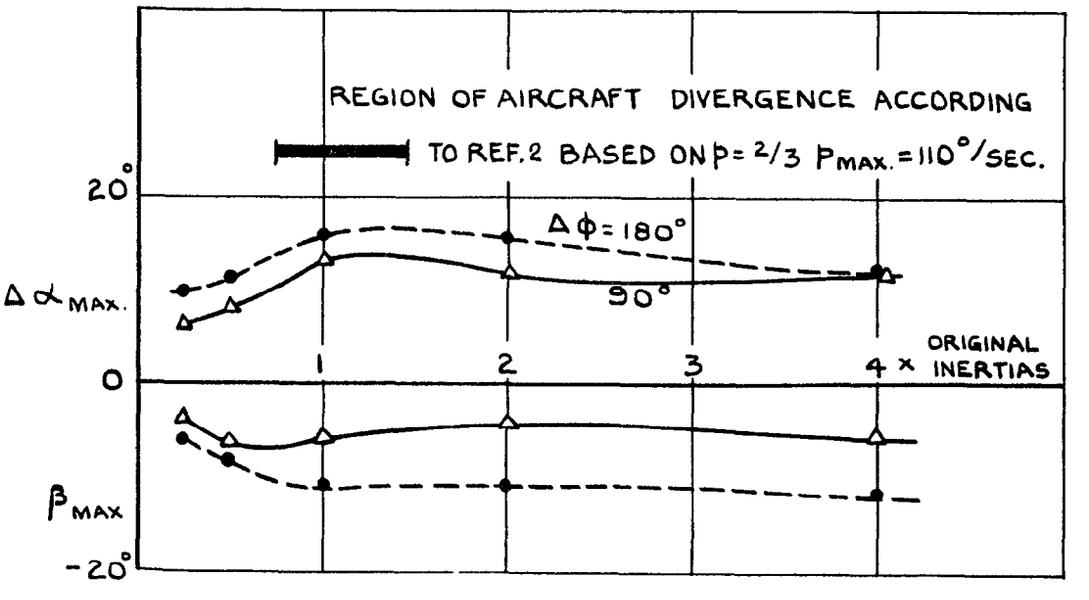

FIG. 26. EFFECT OF INERTIA VARIATIONS ON $\Delta\alpha_{max}$ AND β_{max}.
(H=40,000FT. M=0·8 α_o=5° ξ=8°)

CONDITIONS:
THE STANDARD AIRCRAFT
$A/B = \frac{1}{4}$ $\alpha_0 = 5°$
$\zeta = 8°$ $\Delta\phi = 180°$
PEAK $p \approx 150°/SEC.$
◎ H = 40,000 FT. M = 0·8
◉ H = 60,000 FT. M = 0·8
● H = 60,000 FT. M = 1·0
□ H = 60,000 FT. M = 1·5
ANGLES QUOTED BESIDE EACH POINT ARE: $\Delta\alpha_{max.}$, $\beta_{max.}$

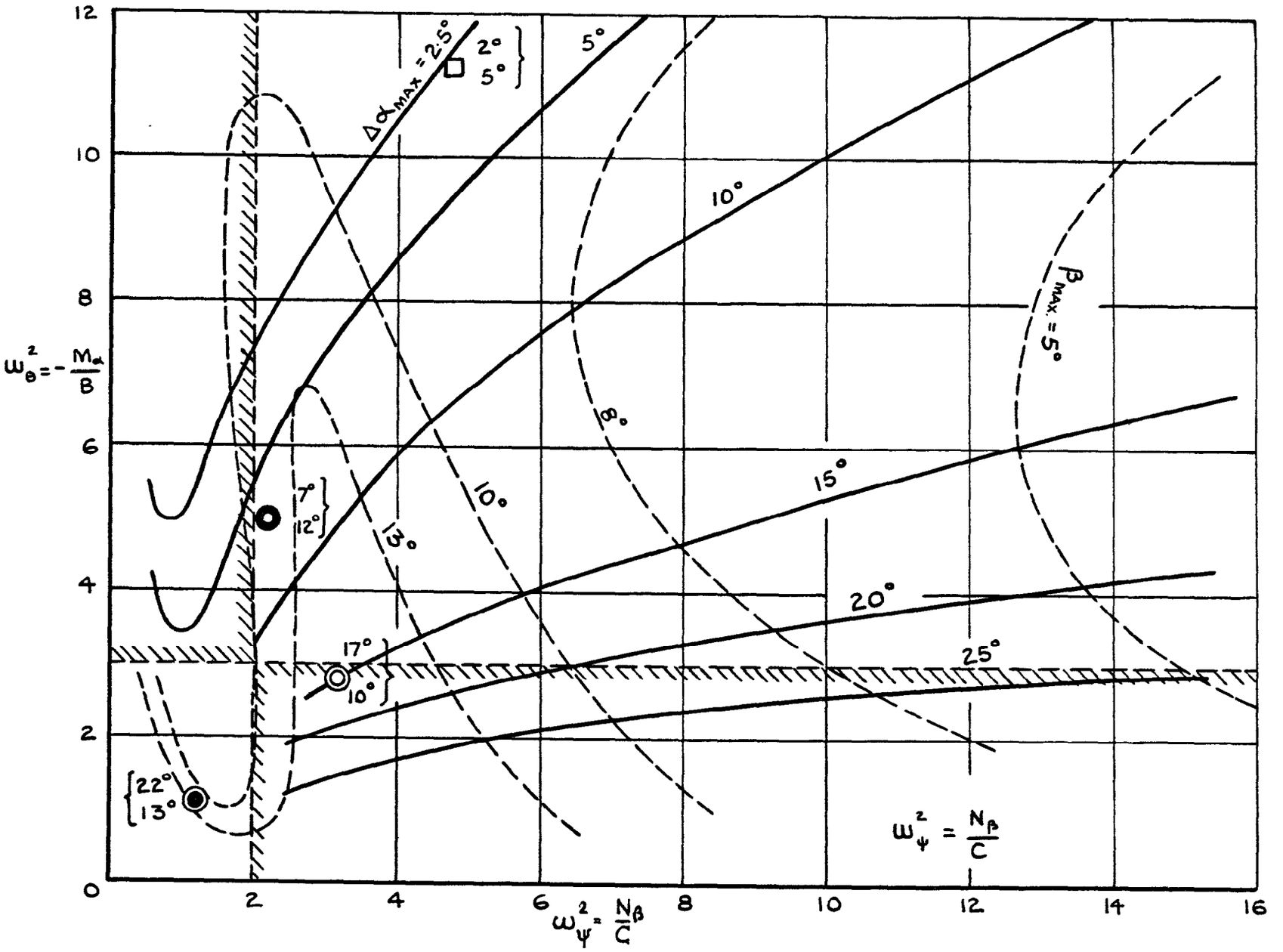

FIG. 27. PLOT OF $\Delta\alpha_{max.}$ AND $\beta_{max.}$ AGAINST ω_θ^2 AND ω_ψ^2.

CONDITIONS FOR THE STANDARD AIRCRAFT

$A/B = \frac{1}{4}$ $\alpha_0 = 5°$

$\zeta = 4°$ $\Delta\phi = 180°$

PEAK $p \approx 100°/\text{SEC.}$

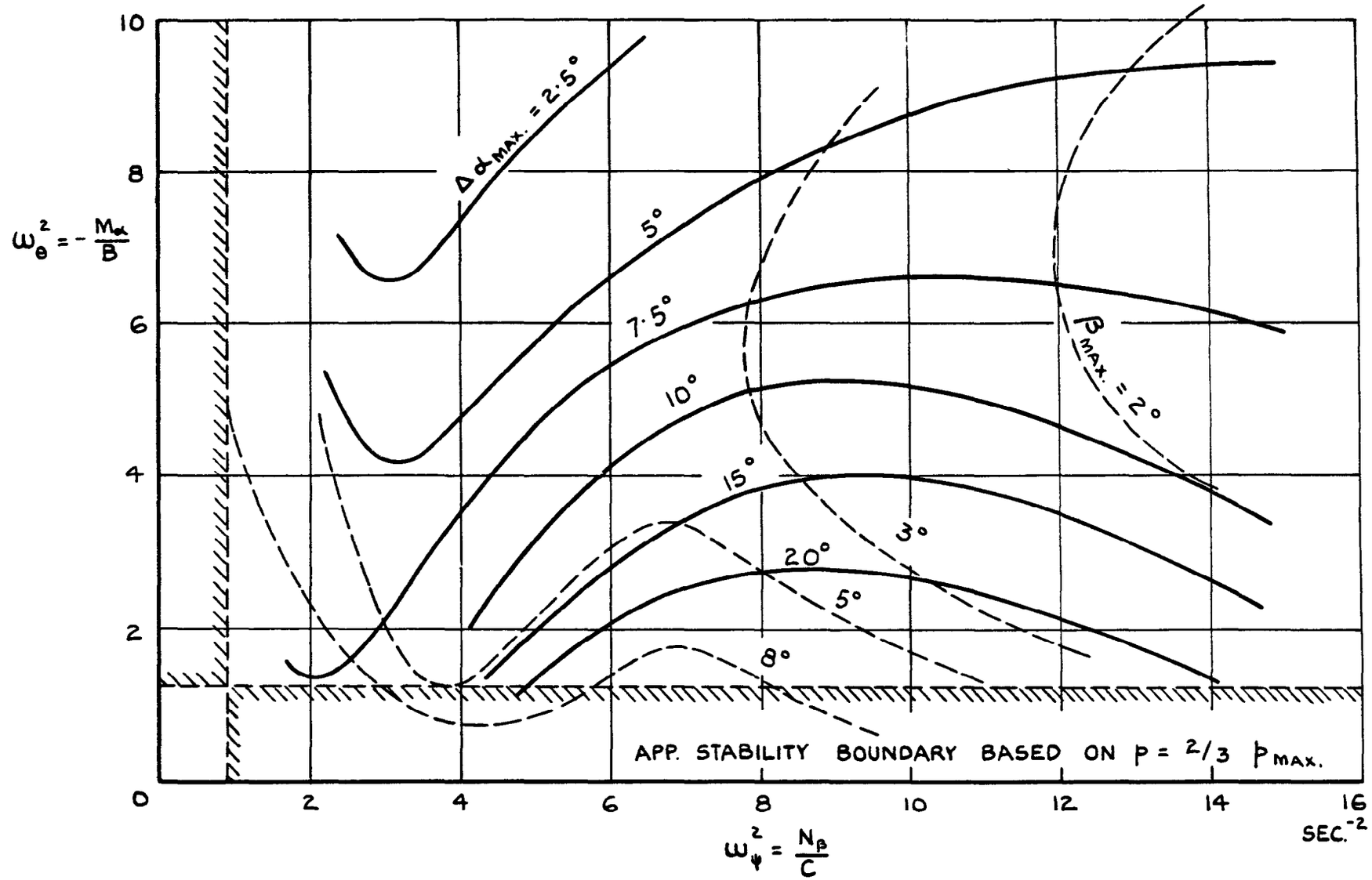

FIG.28. PLOT OF $\Delta\alpha_{max.}$ AND $\beta_{max.}$ AGAINST ω_θ^2 AND ω_ψ^2.

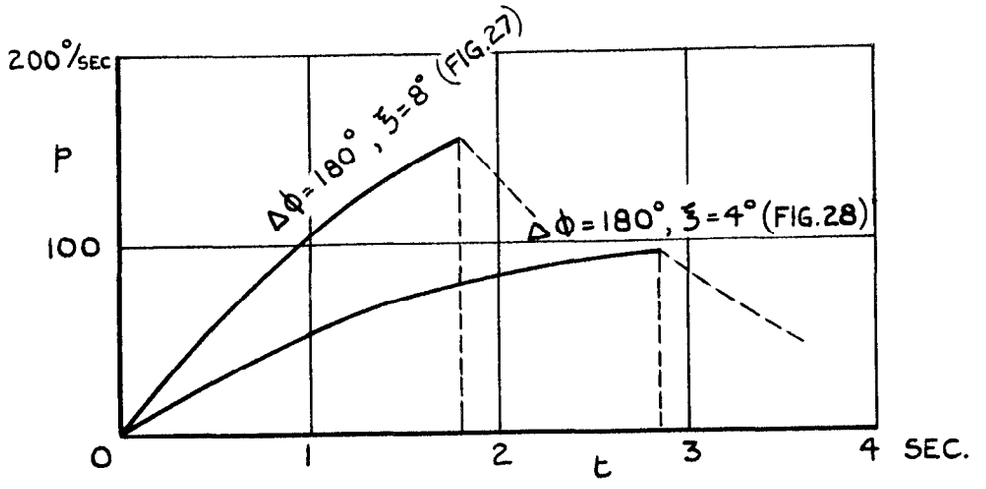

FIG.29. ROLLING MANOEUVRES SIMULATED FOR THE COMPUTATION OF THE DATA PRESENTED IN FIGS. 27 AND 28.

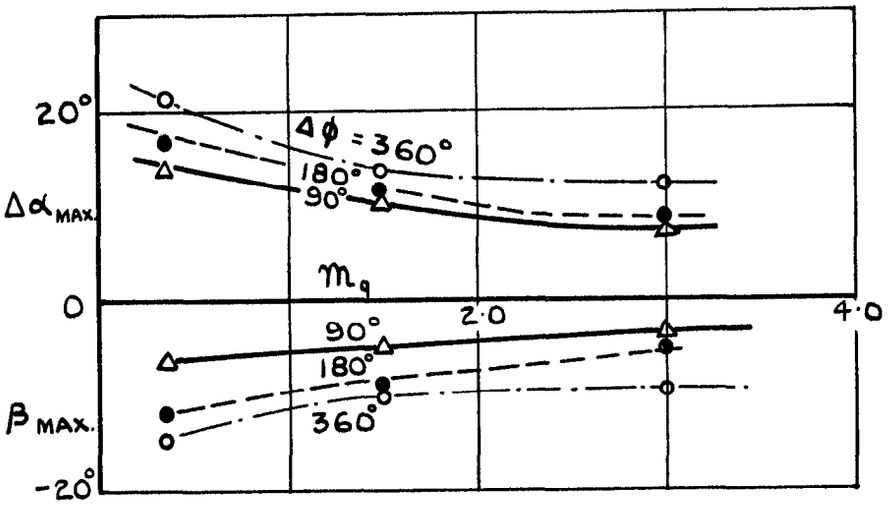

FIG.30. EFFECT OF M_q (PITCH STABILIZATION) ON $\Delta\alpha_{max.}$ AND $\beta_{max.}$. ($\xi = 8°$, AT 40,000 FT, $M = 0{\cdot}8$, $\alpha_0 = +5°$).

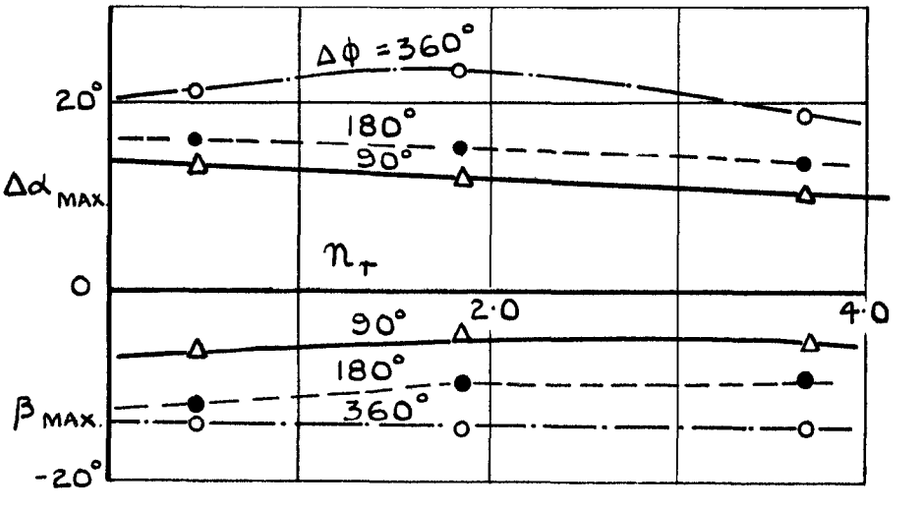

FIG. 31. EFFECT OF n_r (YAW STABILIZATION) $\Delta\alpha_{max.}$ AND $\beta_{max.}$ ($\xi = 8°$, AT 40,000 FT, $M = 0{\cdot}8$, $\alpha_0 = +5°$).

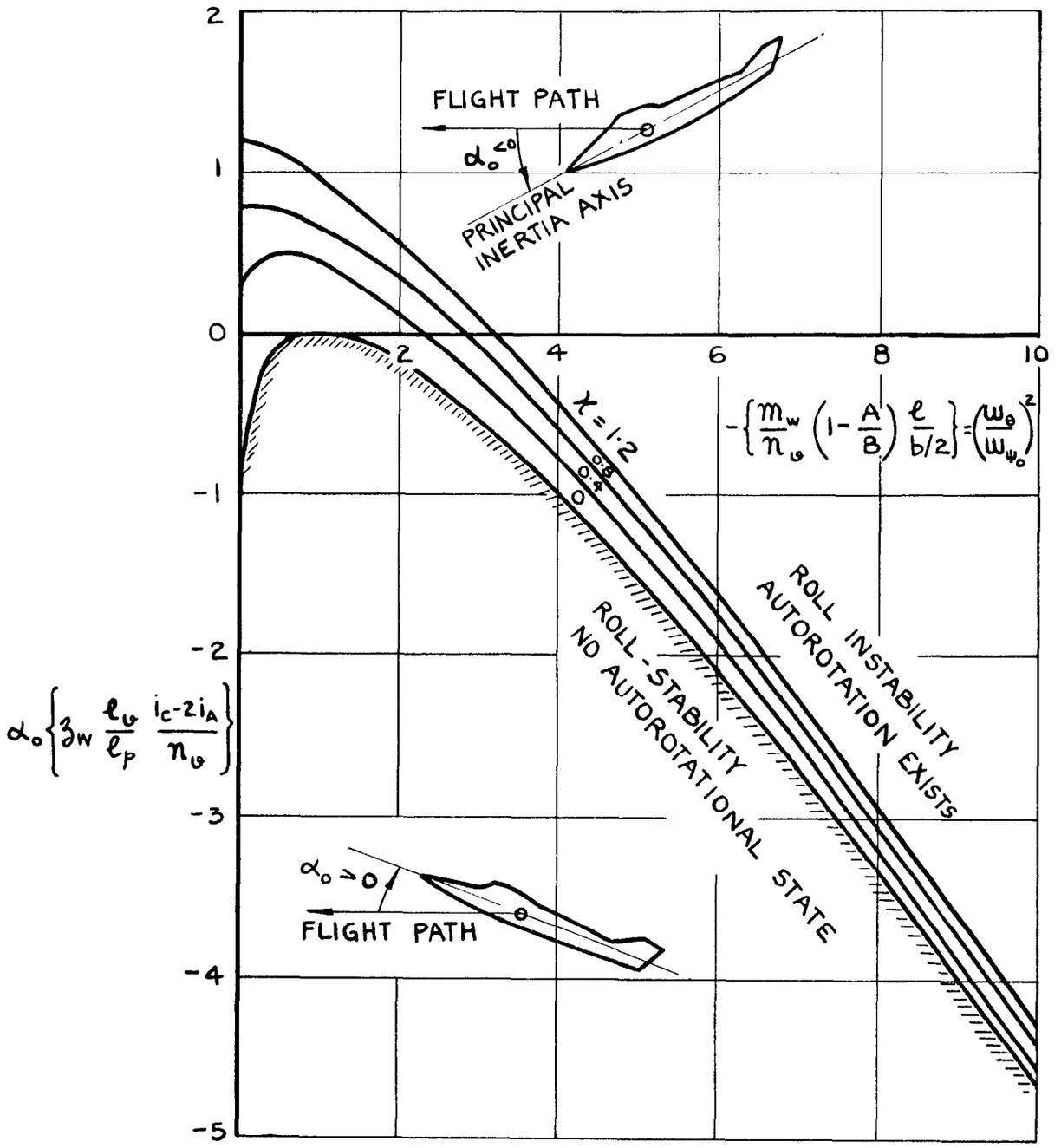

FIG. 32. BOUNDARIES OF CRITICAL VALUES OF α_o BELOW WHICH AUTORATIONAL INSTABILITY IN ROLL OCCURS.

$$\chi = \zeta_w \frac{m_q}{n_v}\left(1-\frac{A}{B}\right)\frac{\{\ell / b/2\}^2}{\mu_2}$$

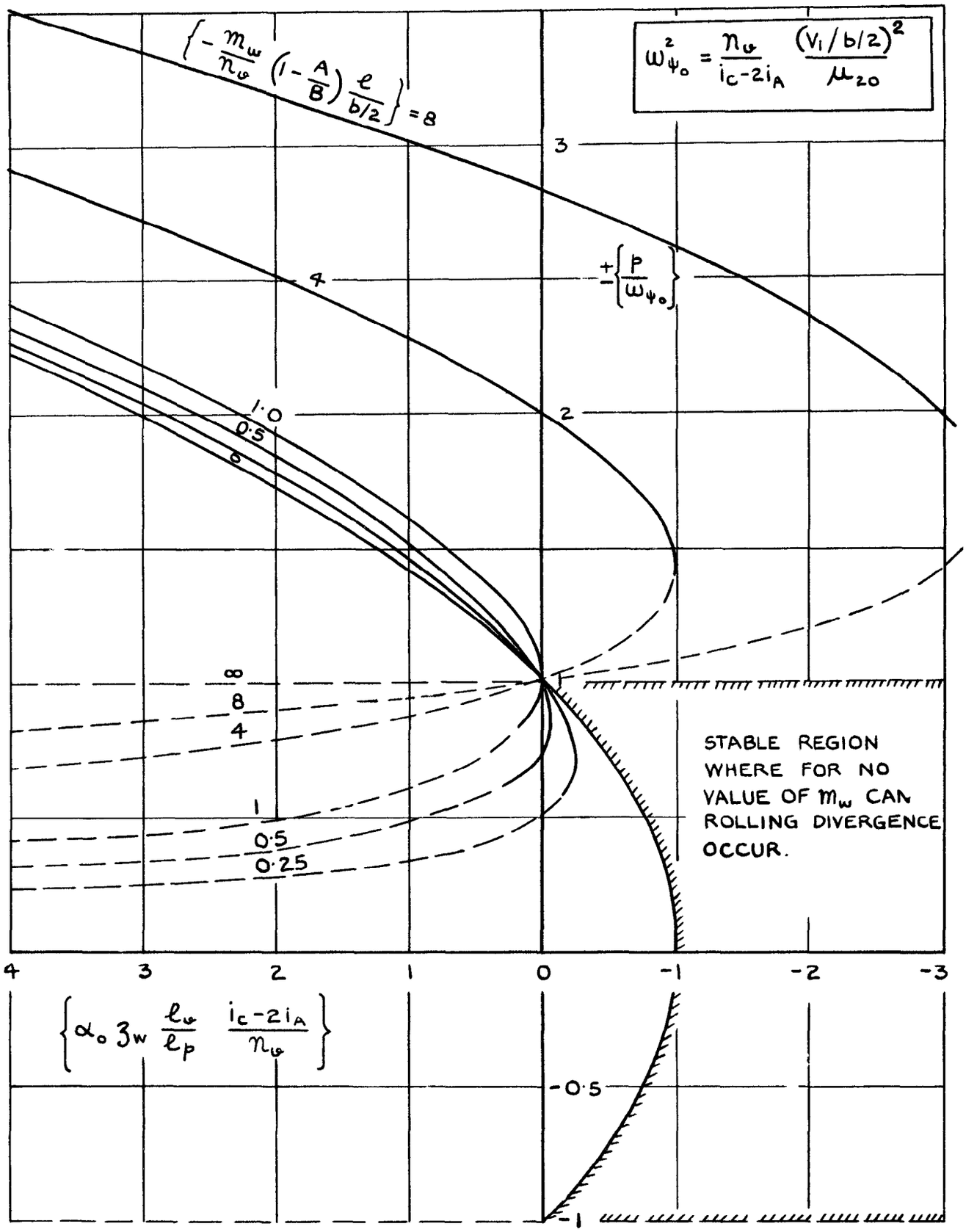

NOTE :- FULL LINES REPRESENT AUTOROTATIONAL STATES, THE DASHED BRANCHES OF THE CURVES REPRESENT NEUTRAL STABILITY.

FIG. 33. AUTOROTATIONAL RATES OF ROLL ($M_q=0$).

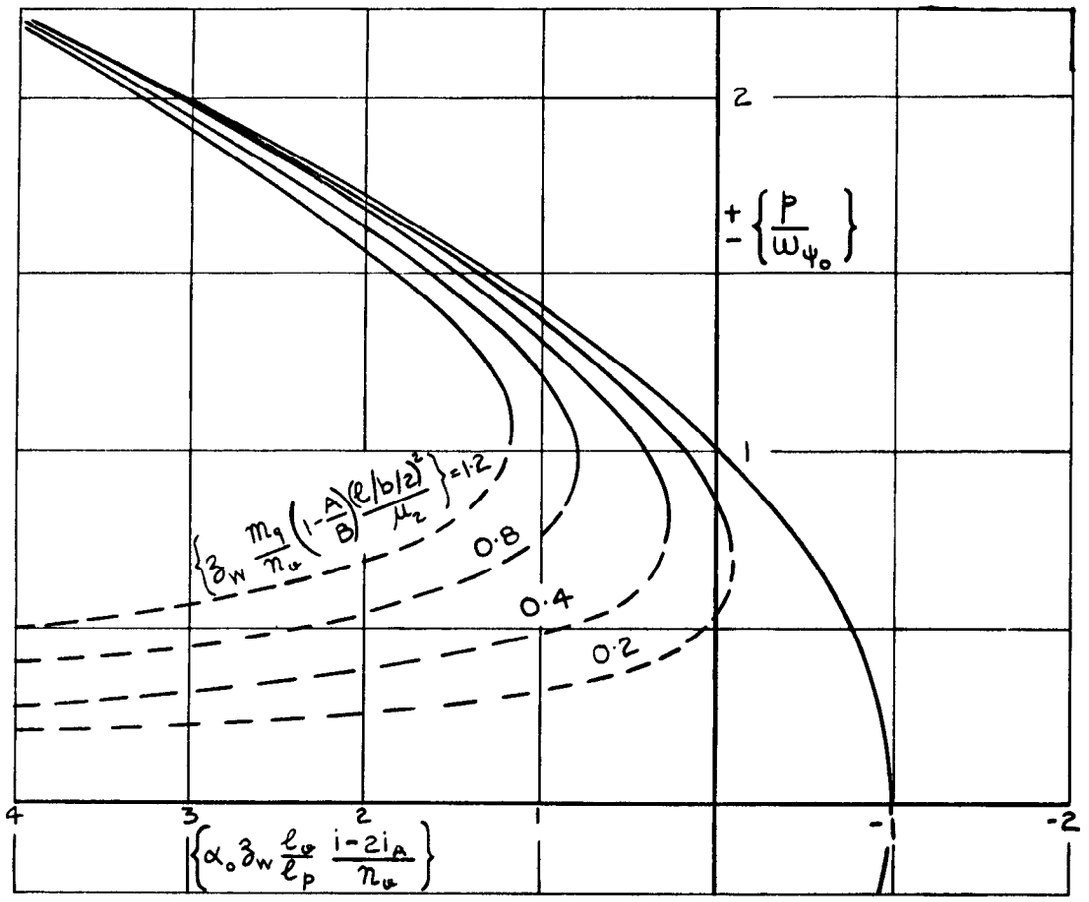

FIG. 34. EFFECT OF DAMPING IN PITCH m_q ON THE ROLL DIVERGENCE OF AN AIRCRAFT.

$$\left\{\frac{m_w}{n_v}\left(1-\frac{i_A}{i_B'}\right)\frac{\ell}{b/2}\right\}=0.$$

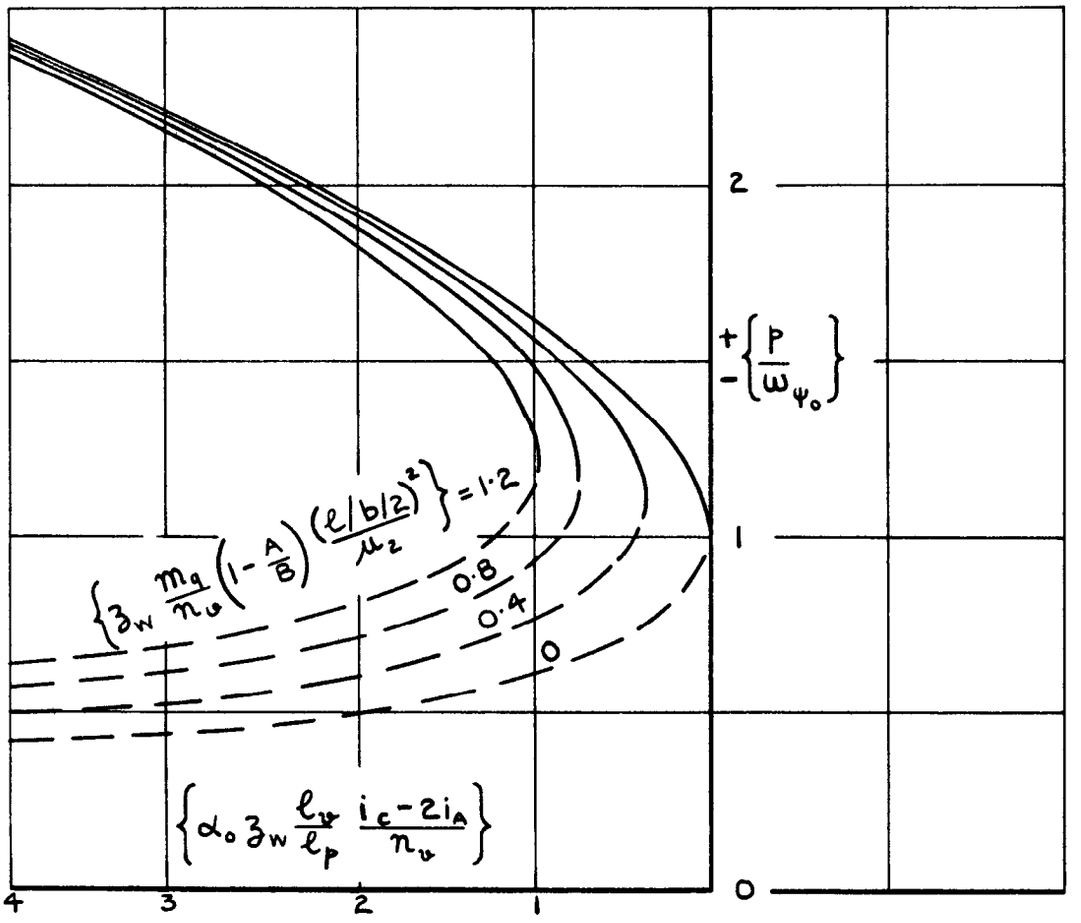

FIG. 35. EFFECT OF DAMPING IN PITCH ON THE ROLL DIVERGENCE OF AN AIRCRAFT.

$$\left\{\frac{m_w}{n_v}\left(1-\frac{i_A}{i_B'}\right)\frac{\ell}{b/2}\right\}=1.0.$$

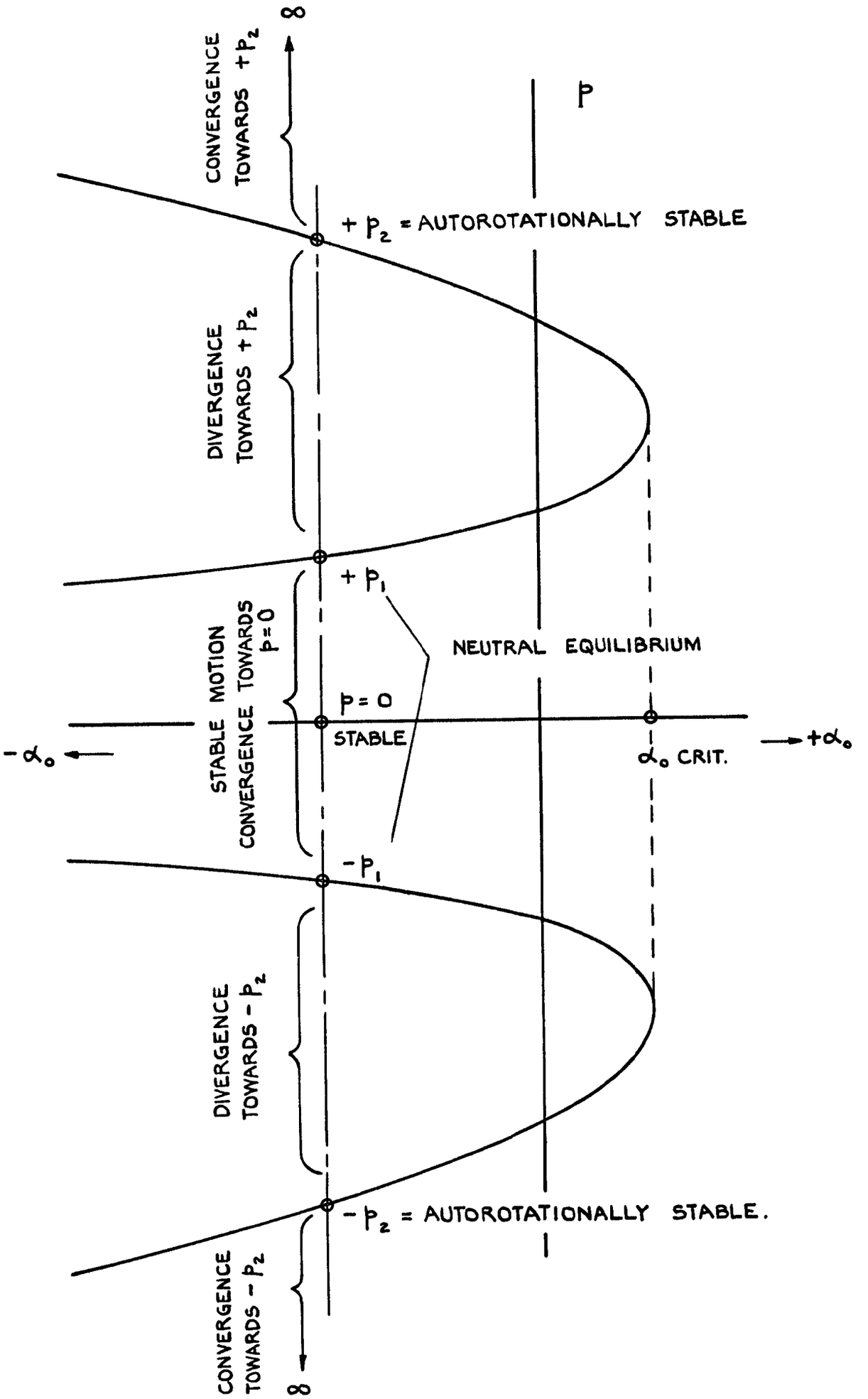

FIG.36. INTERPRETATION OF THE STABILITY BOUNDARIES OF THE ROLLING MOTION OF AN AIRCRAFT WITH INERTIA COUPLING PLOTTED IN FIG. 33 – 35.

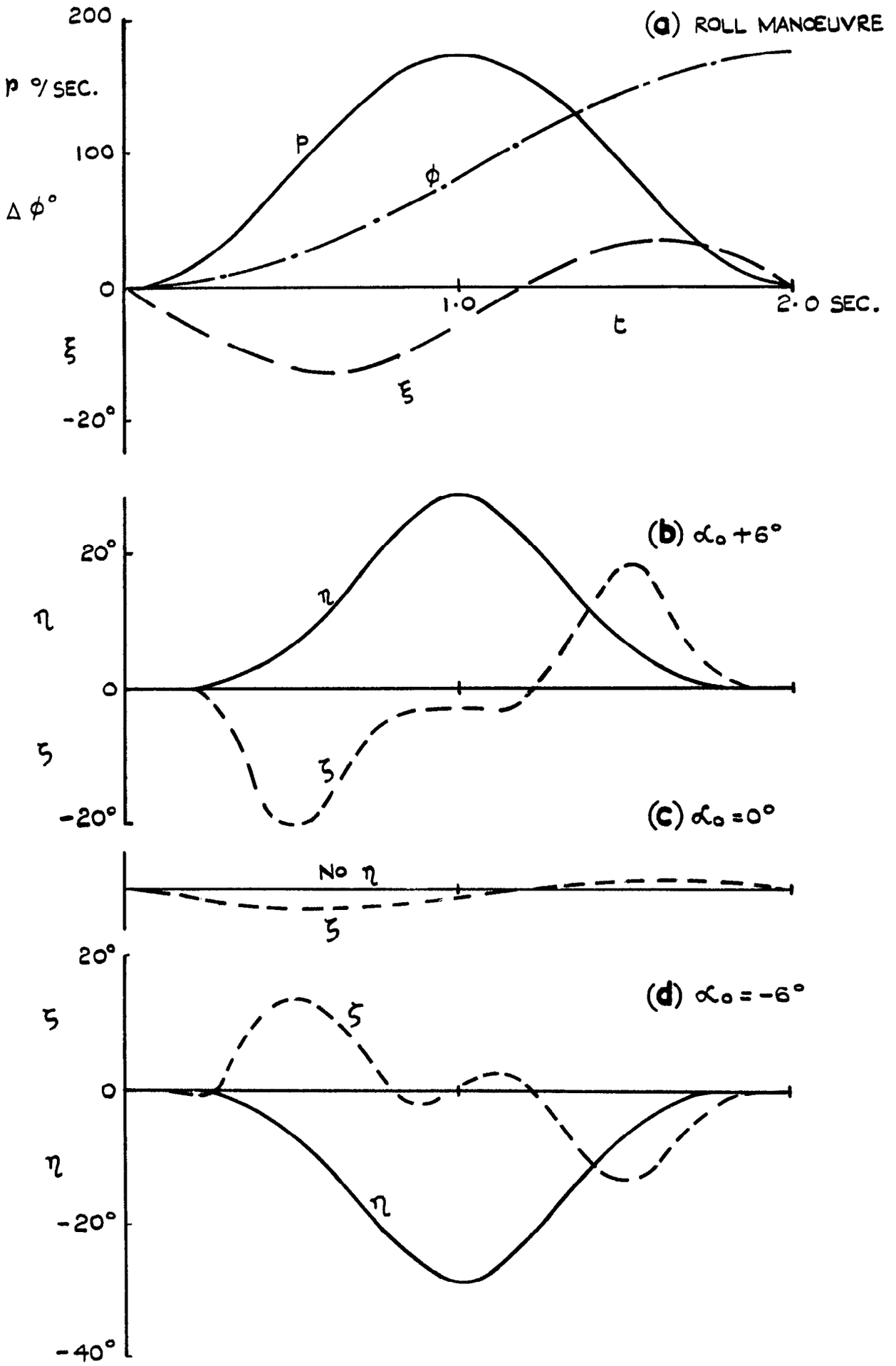

FIG. 37.(a-d) CONTROL CO-ORDINATION REQUIRED TO PERFORM THE ROLLING MANOEUVRE ILLUSTRATED IN (a) WITH $\Delta\alpha = \beta = 0$ THROUGHOUT.

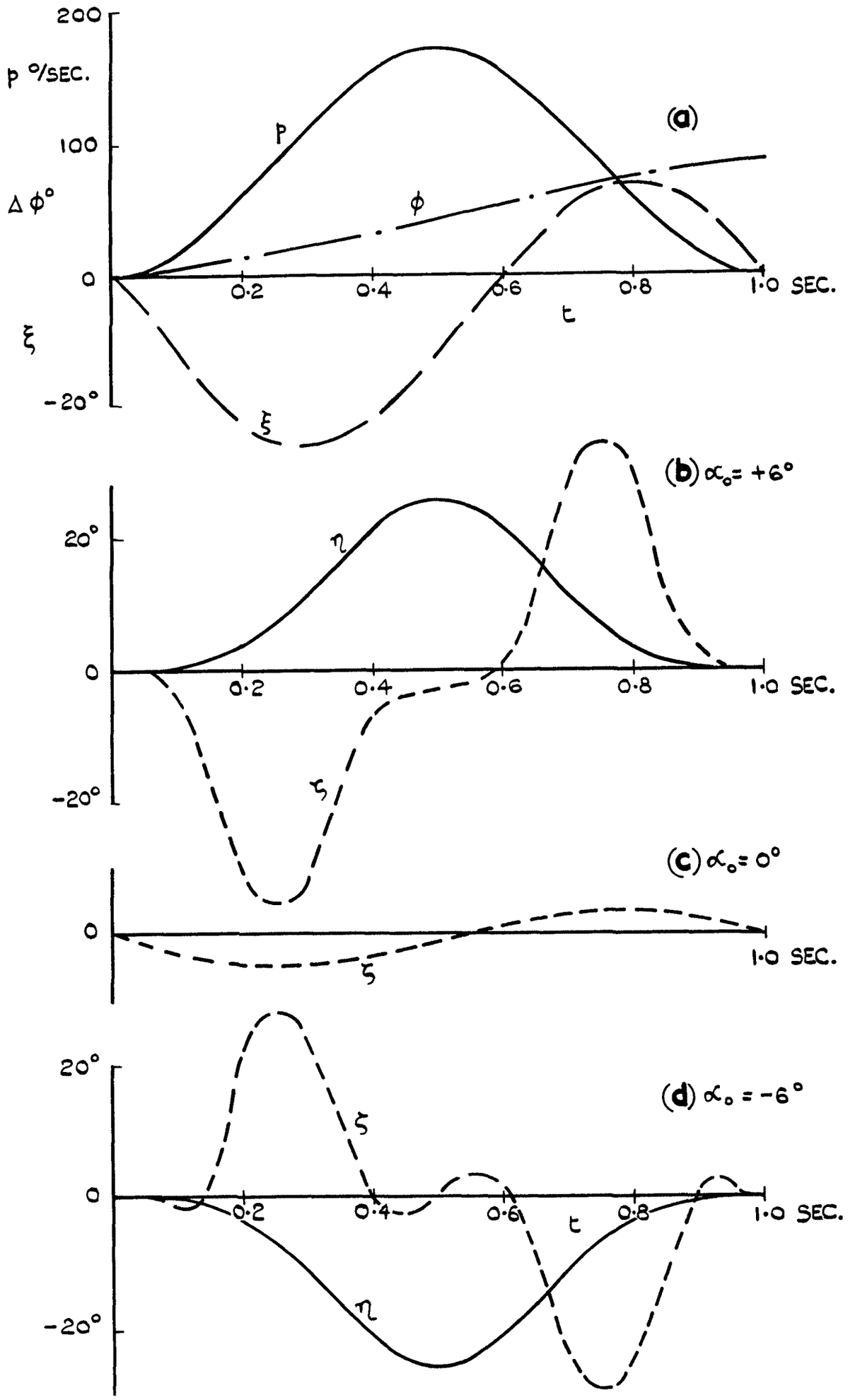

FIG.38(a-d) CONTROL CO-ORDINATION REQUIRED TO PERFORM THE ROLLING MANOEUVRE ILLUSTRATED IN (a) WITH $\Delta\alpha = \beta = 0$ THROUGHOUT.

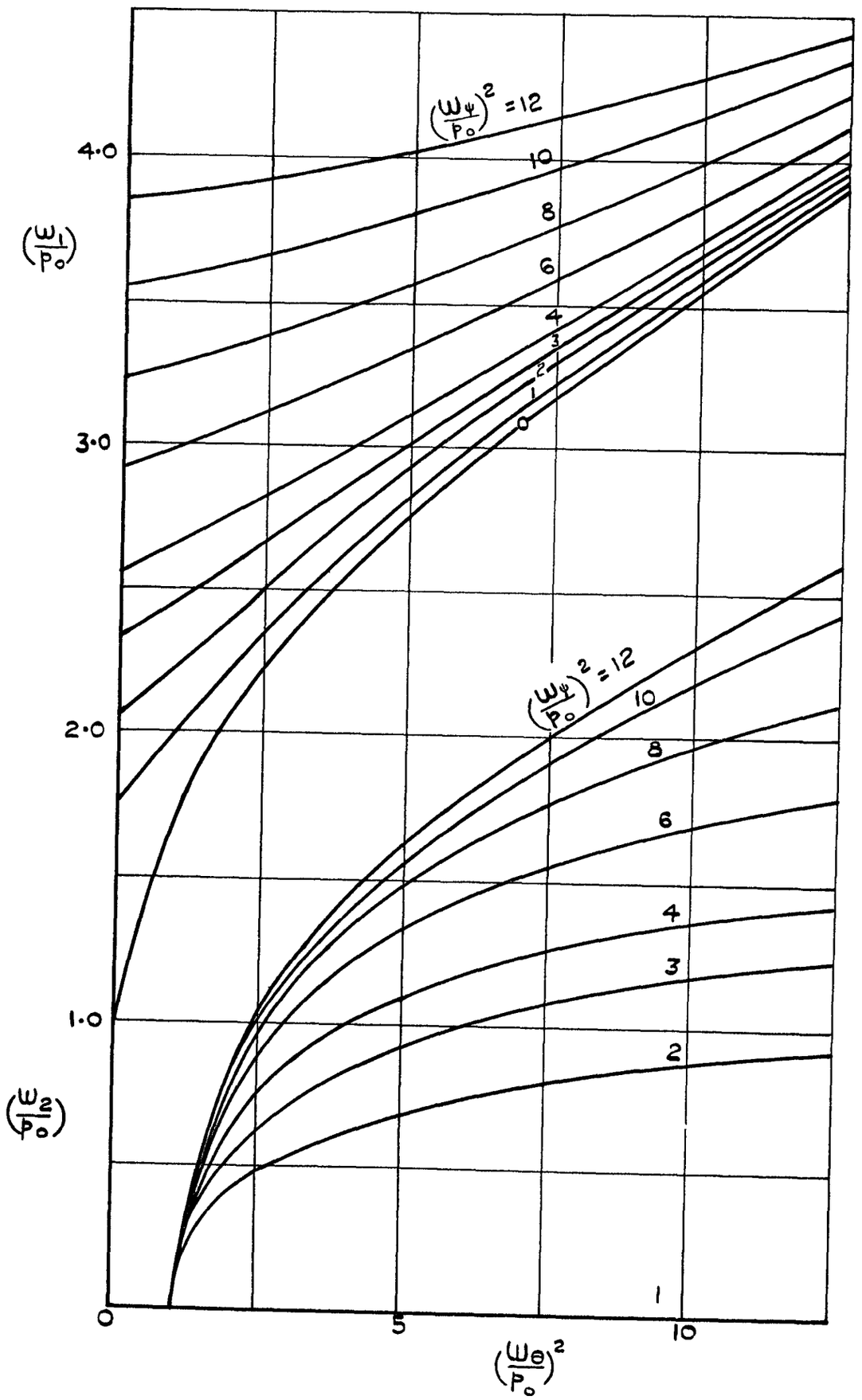

FIG. 39. FREQUENCIES OF THE OSCILLATORY MODE OF AN AIRCRAFT ROLLING WITH $p = p_0$ HAVING $A \ll B$.

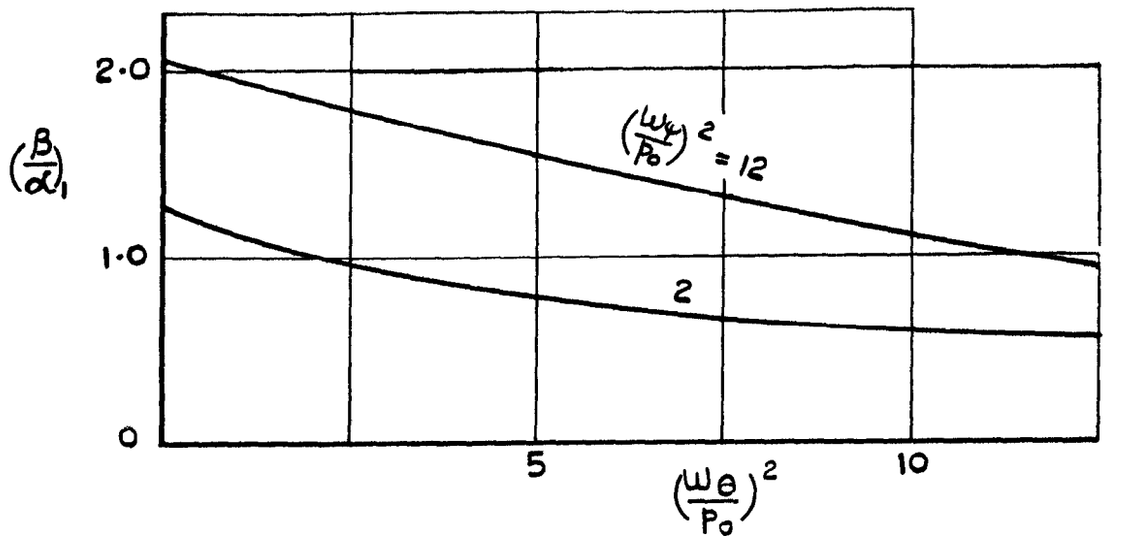

FIG. 40. AMPLITUDE RATIO β/α OF THE HIGH FREQUENCY OSCILLATION OF AN AIRCRAFT ROLLING WITH $p=p_0$ HAVING $A \ll B$.

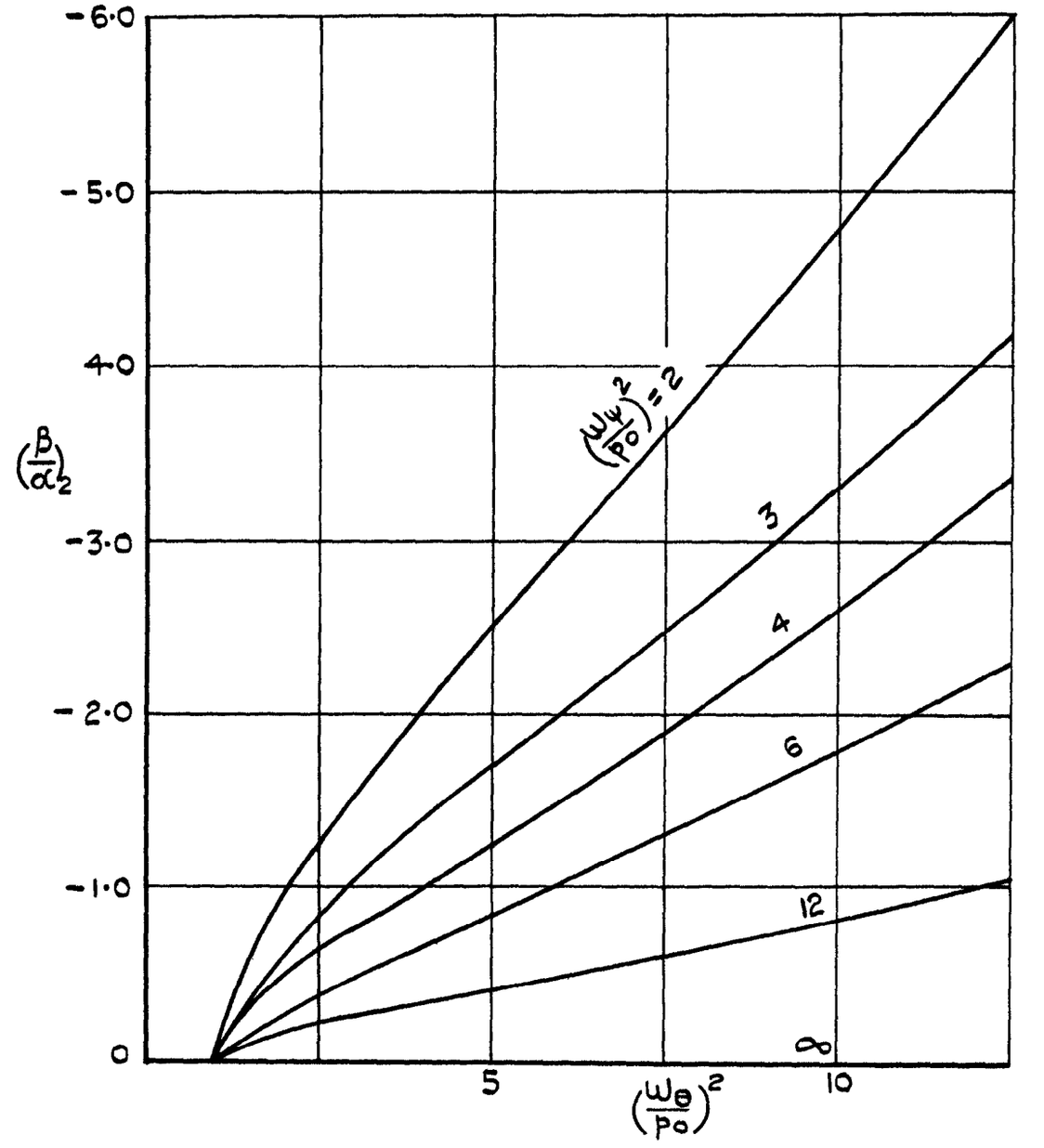

FIG. 41. AMPLITUDE RATIO β/α OF THE LOW FREQUENCY OSCILLATION OF AN AIRCRAFT ROLLING WITH $p=p_0$ HAVING $A \ll B$.

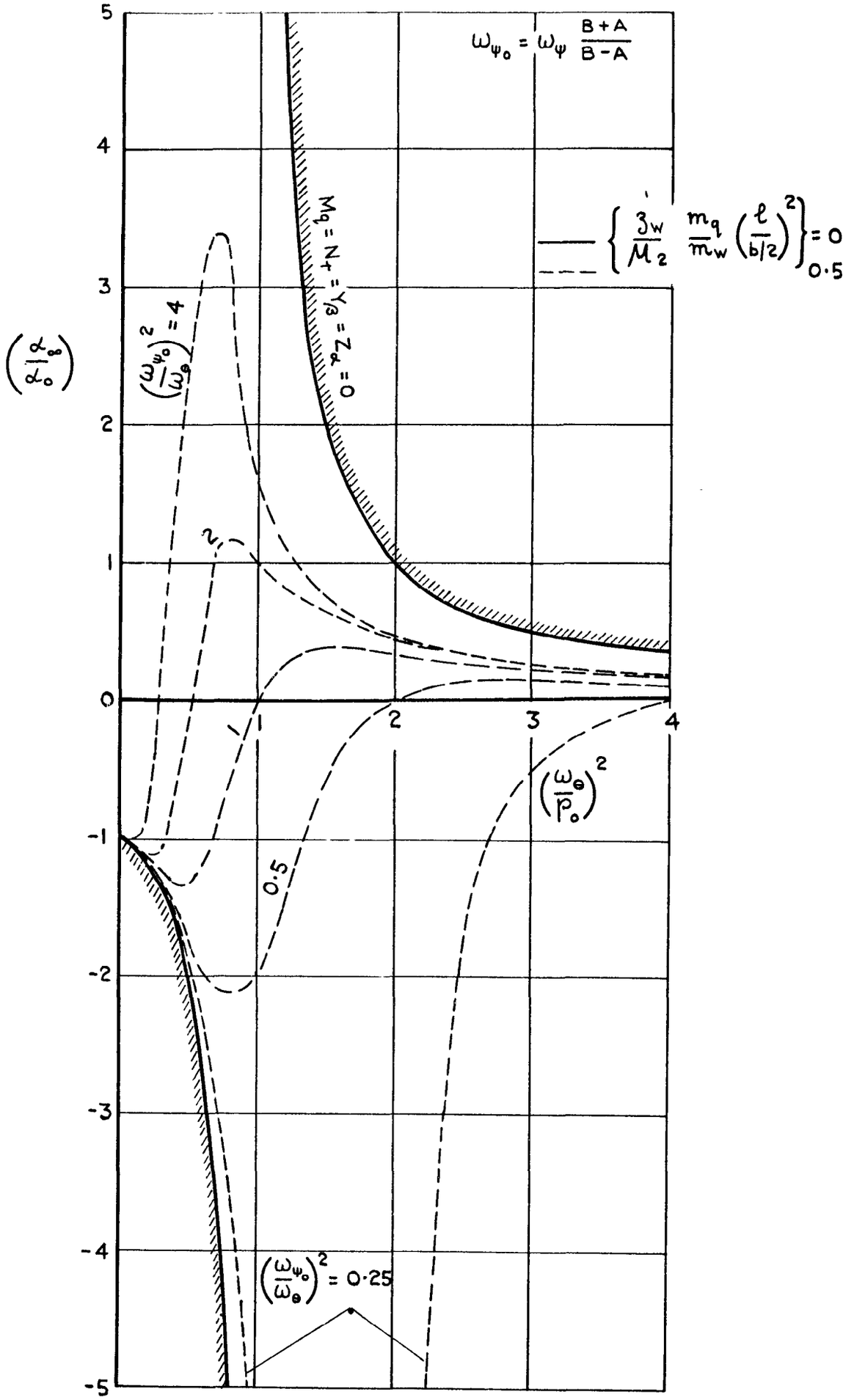

FIG. 42. INCIDENCE TRIM CHANGE IN α OF AN AIRCRAFT ROLLING WITH $p = p_0$, HAVING $A \ll B$

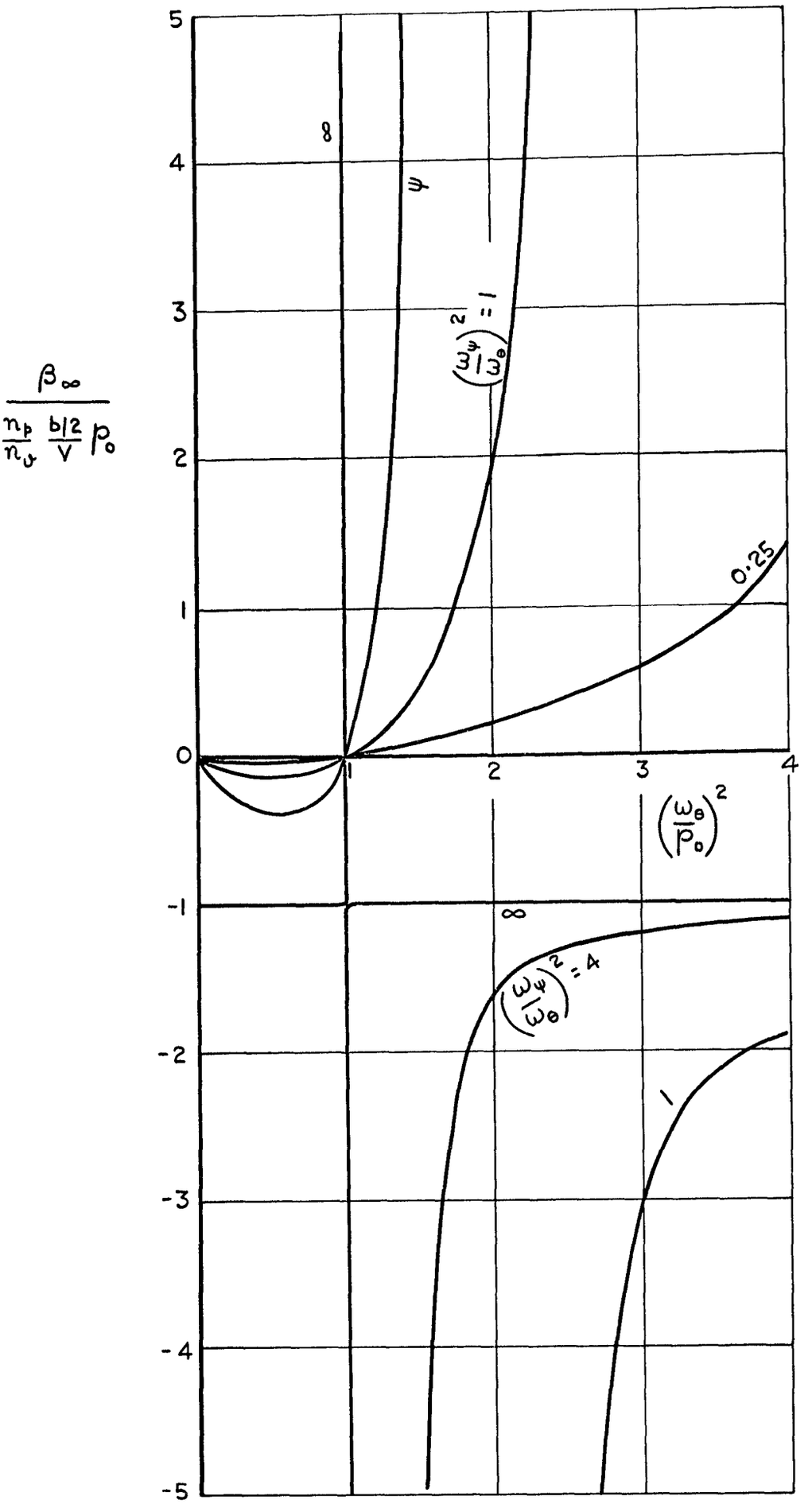

FIG. 43. TRIM CHANGE IN β OF AN AIRCRAFT ROLLING WITH $p = p_0$, IF $M_q = n_v = y_v = z_w = 0$.

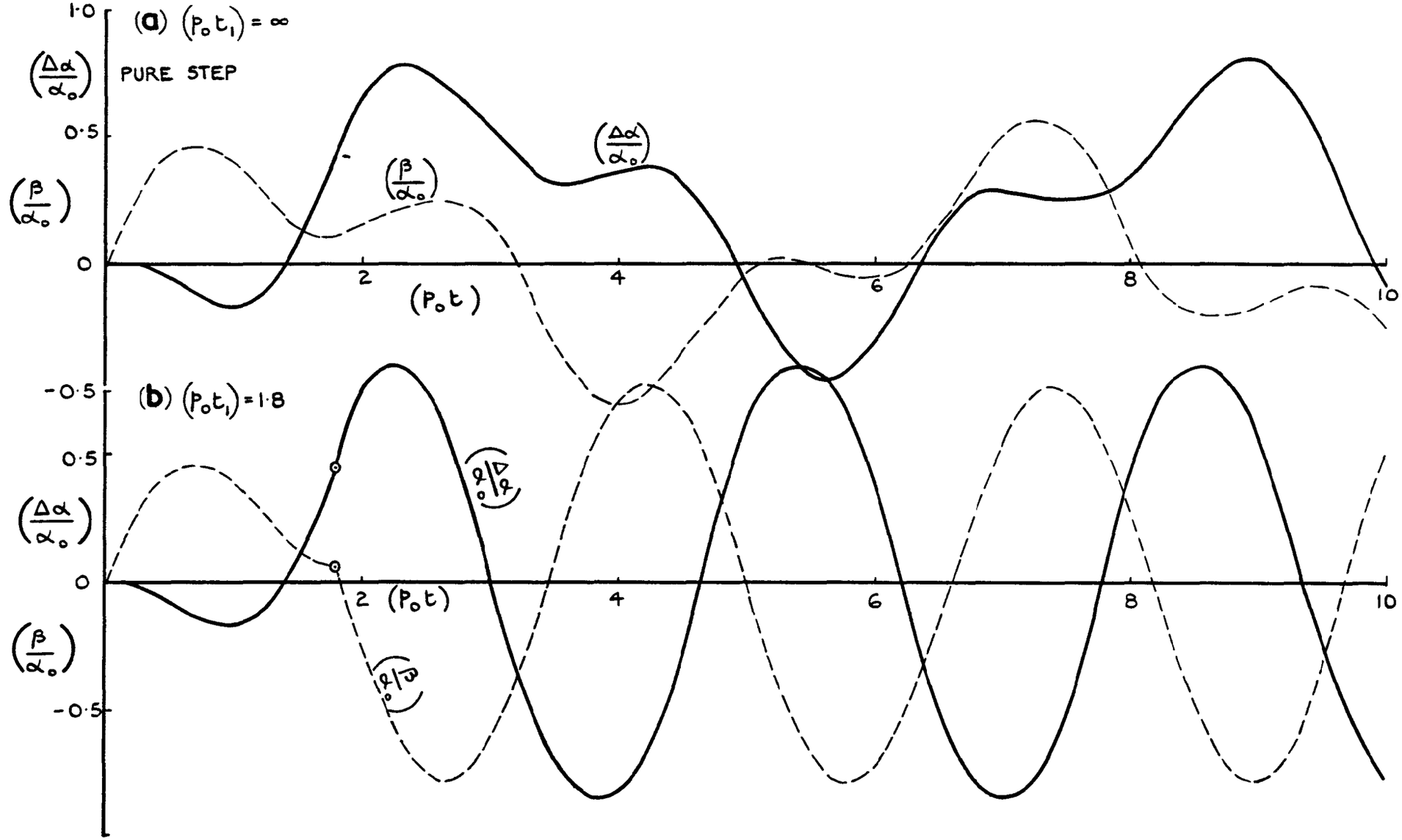

FIG.44(a & b). RESPONSE IN PITCH AND YAW TO A SQUARE WAVE-FUNCTION $p = p_0$ FOR $0 > t > t_1$.

$$\left[\left(\frac{\omega_\theta}{p_0}\right)^2 = \left(\frac{\omega_\psi}{p_0}\right)^2 = 4{\cdot}0. \quad \frac{A}{B} = 0{\cdot}25\right]$$

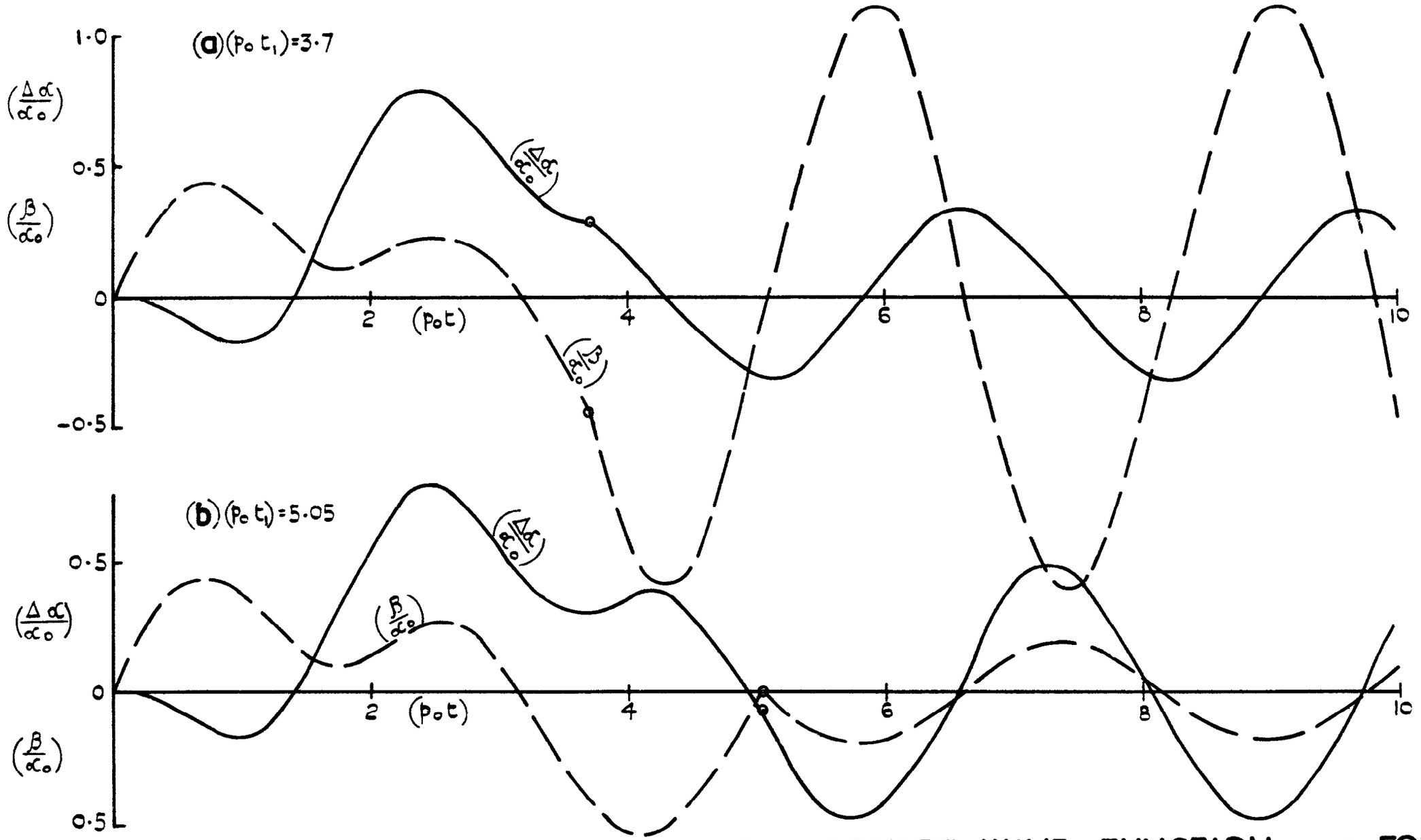

FIG.45(a & b) RESPONSE IN PITCH AND YAW TO A SQUARE WAVE-FUNCTION $p = p_o$ FOR $0 > t > t_1$ $\left[\left(\frac{\omega_\theta}{p_o}\right)^2 = \left(\frac{\omega_\psi}{p_o}\right)^2 = 4.0 \quad \frac{A}{B} = 0.25.\right]$

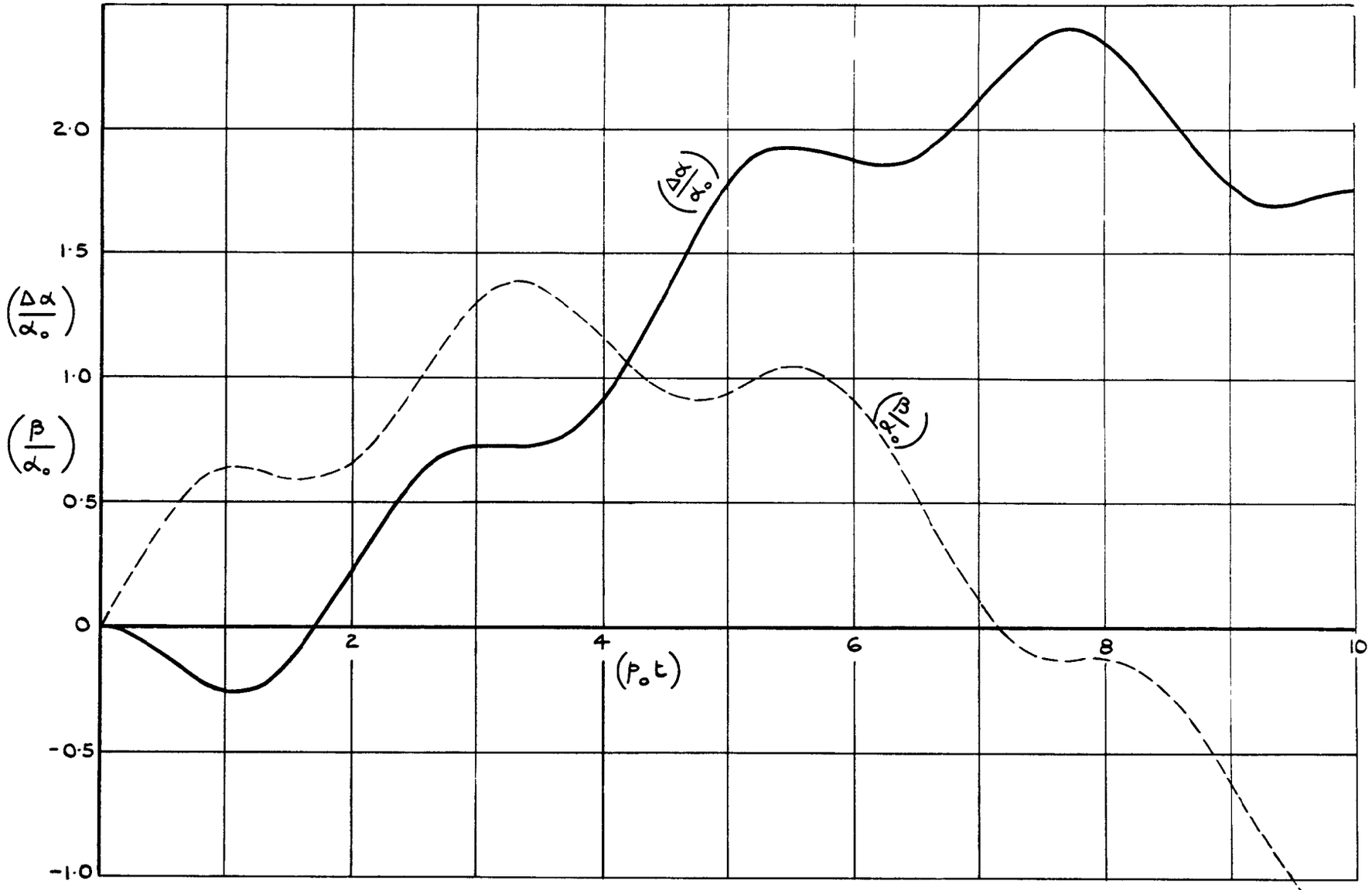

FIG. 46. RESPONSE IN PITCH AND YAW TO A STEP FUNCTION $p = p_0$ TO $t > 0$

$$\left(\frac{\omega_\theta}{p_0}\right)^2 = \left(\frac{\omega_\psi}{p_0}\right)^2 = 2{\cdot}0 \quad \frac{A}{B} = 0.$$

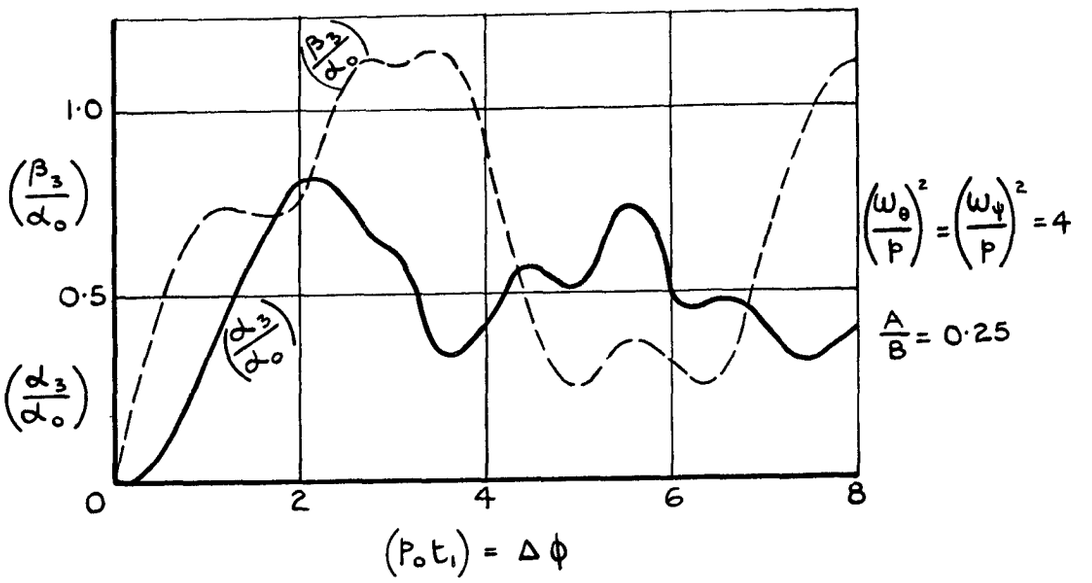

FIG. 47. AMPLITUDES OF THE RESIDUAL OSCILLATIONS IN PITCH AND YAW AFTER p_0 IS TERMINATED AT t_1 SECS. i.e. AFTER $\Delta\phi = p_0 t_1$ BANK ANGLE.

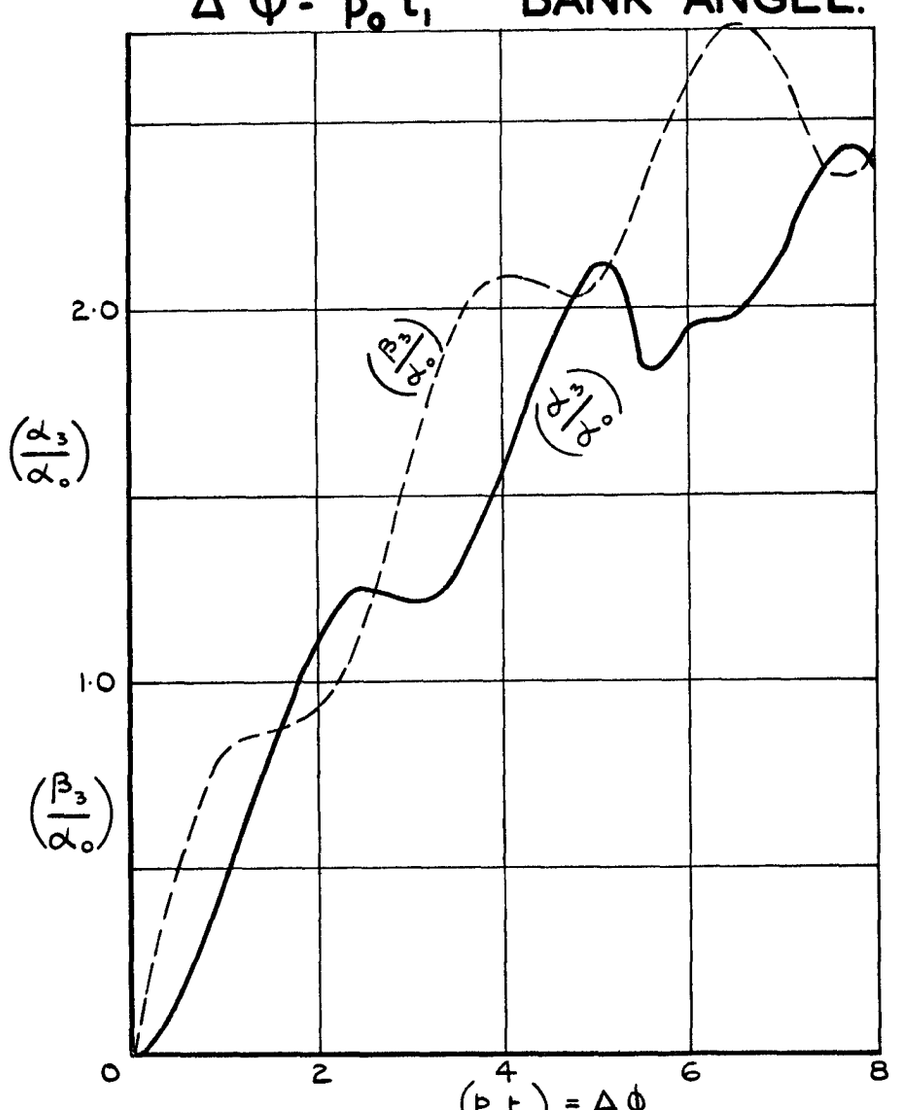

FIG. 48. AMPLITUDES OF THE RESIDUAL UNCOUPLED PITCHING & YAWING OSCILLATIONS AFTER p_0 IS TERMINATED AFTER t_1 SECS, i.e. AFTER $\Delta\phi = p_0 t_1$ $\left(\frac{\omega_\theta}{p}\right)^2 = \left(\frac{\omega_\psi}{p}\right)^2 = 2$ $\frac{A}{B} = 0$

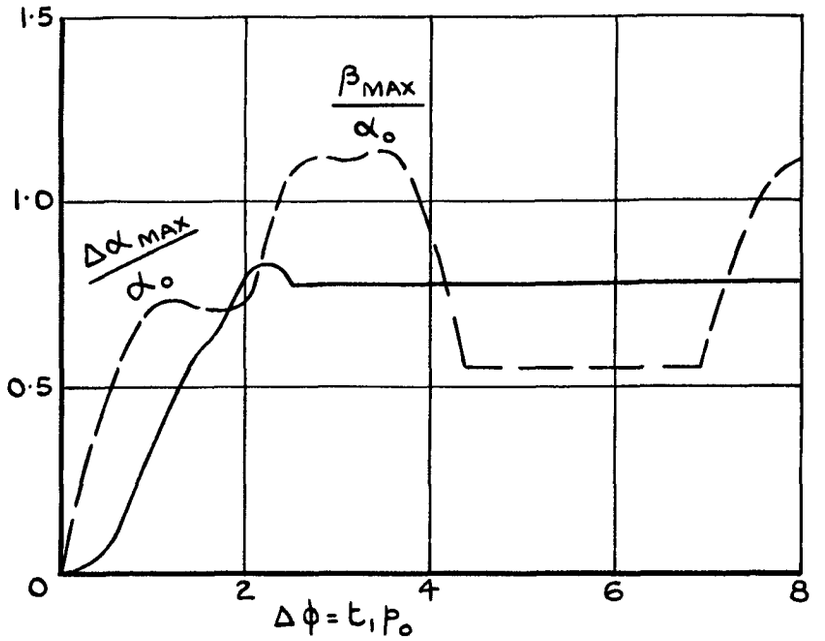

FIG.49. PEAK AMPLITUDES $\Delta\alpha_{MAX.}$ AND $\beta_{MAX.}$ IN RESPONSE TO A SQUARE WAVE $p_0(t)$ PLOTTED AGAINST $\Delta\phi$ (THEORECTICAL ANALYSIS)

$$\left[\left(\frac{\omega_\theta}{p_0}\right)^2 = \left(\frac{\omega_\psi}{p_0}\right)^2 = 4 \qquad \frac{A}{B} = 0{\cdot}25\right].$$

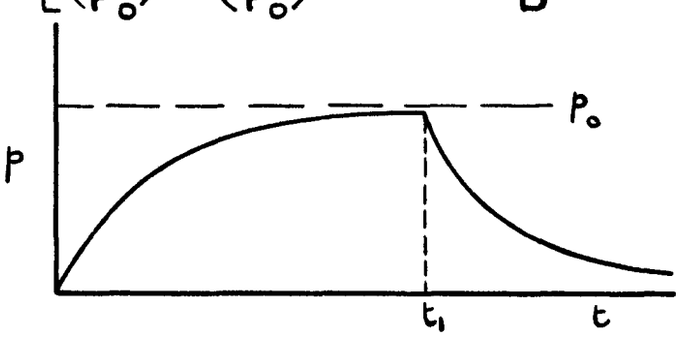

FIG.50. ROLLING MANOEUVRE SIMULATED FOR ANALYSIS IN FIG.51.

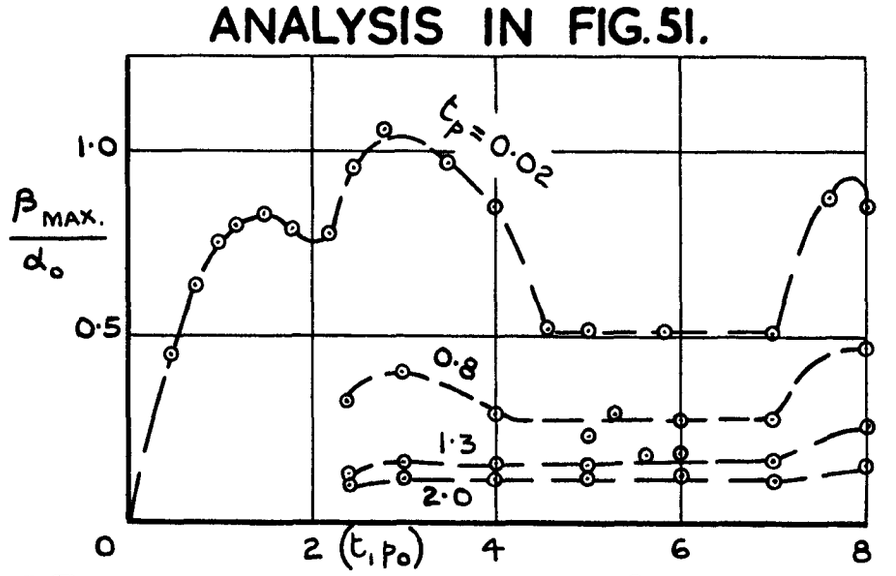

FIG.51. PEAK AMPLITUDES IN β IN RESPONSE TO THE SIMULATED MANOEUVRE ILLUSTRATED IN FIG. 50.

$$\left[\left(\frac{\omega_\theta}{p_0}\right)^2 = \left(\frac{\omega_\psi}{p_0}\right)^2 = 4 \quad \frac{A}{B} = 0{\cdot}25\right].$$

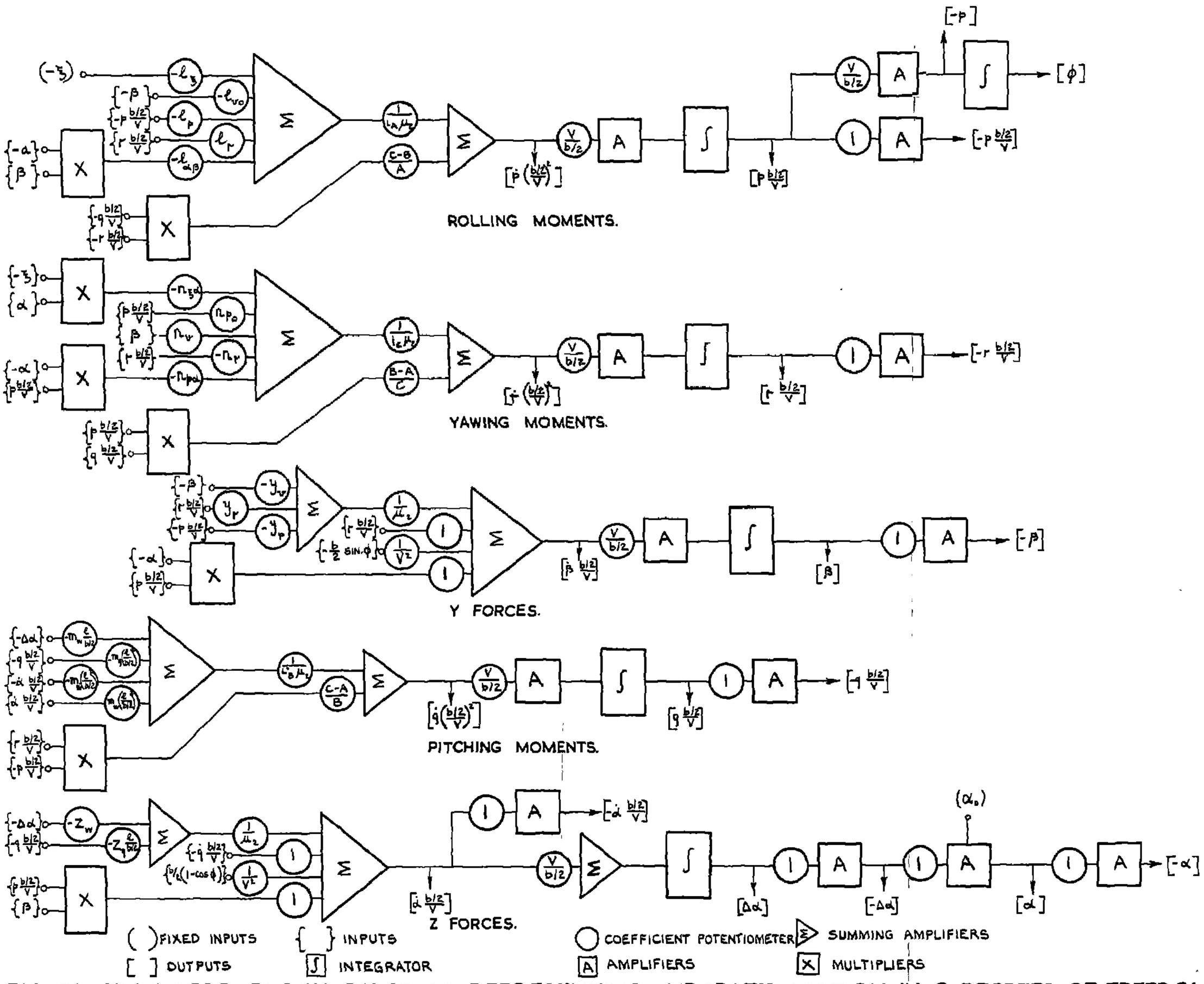

FIG. 52. SIMULATOR BLOCK DIAGRAM REPRESENTING AIRCRAFT MOTION IN 5 DEGREES OF FREEDOM IN PRINCIPAL INERTIA AXES. (SCALING FACTORS HAVE BEEN OMITTED FROM THIS GRAPH).

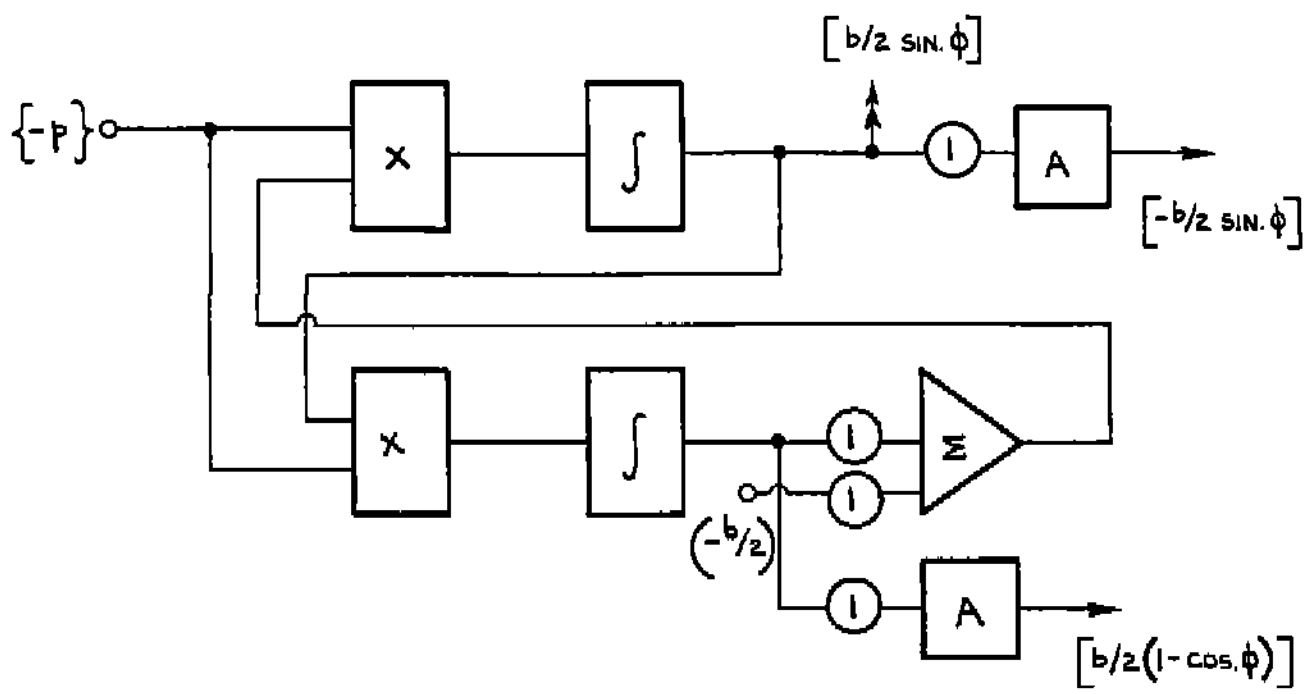

FIG. 53. SIMULATOR CIRCUIT TO COMPUTE SIN ϕ AND $(-\cos \phi)$.

SUGGESTED BY T.R. STRETTON

C.P. No. 435
(18,250)
A.R.C. Technical Report

Published by
HER MAJESTY'S STATIONERY OFFICE

To be purchased from
York House, Kingsway, London w.c.2
423 Oxford Street, London w.1
13A Castle Street, Edinburgh 2
109 St. Mary Street, Cardiff
39 King Street, Manchester 2
Tower Lane, Bristol 1
2 Edmund Street, Birmingham 3
80 Chichester Street, Belfast
or through any bookseller

Printed in Great Britain

S.O. Code No. 23-9011-35

C.P. No. 435